

**ATTACHMENT 3**

**GENE-0000-0018-3359-NP, "Technical Assessment, Quad Cities Unit 2  
Steam Dryer Failure – Determination of Root Cause  
and Extent of Condition," Revision 0, dated August 2003  
[NON-PROPRIETARY VERSION]**

GENE-0000-0018-3359-NP

Revision 0

Class I

DRF 0000-0018-1059

August 2003

## Technical Assessment

# Quad Cities Unit 2

### Steam Dryer Failure – Determination of Root Cause and Extent of Condition

**Principal Contributors:**

D.O. Henry  
L.K. Liu  
J. Lynch  
D.C. Pappone  
M.R. Patel  
S. Sundaram

**Approved:**  
R.M. Horn



## **INFORMATION NOTICE**

This is a non-proprietary version of the document GENE-0000-0018-3359-P, Revision 1, which has the proprietary information removed. Portions of the document that have been removed are indicated by an open and closed bracket as shown here [[ ]].

## **IMPORTANT NOTICE REGARDING CONTENTS OF THIS REPORT**

### **Please Read Carefully**

The only undertakings of the General Electric Company (GE) respecting information in this document are contained in the contract between Exelon Corp. and GE as amended to the date of transmittal of this document, and nothing contained in this document shall be construed as changing the contract. The use of this information by anyone other than Exelon Corp., or for any purpose other than that for which it is furnished by GE, is not authorized; and with respect to any unauthorized use, GE makes no representation or warranty, express or implied, and assumes no liability as to the completeness, accuracy, or usefulness of the information contained in this document, or that its use may not infringe privately owned rights.

## Table of Contents

1.	Introduction and Summary .....	9
2.	Root Cause Evaluation for QC2 Dryer Failure.....	10
2.1	Potential Root Causes .....	10
2.2	Event Timeline.....	11
2.3	Visual Observations .....	12
2.3.1	Outer Hood A (90 Degree Side) .....	12
2.3.2	Outer Hood F (270 Degree Side).....	14
2.4	Metallurgical Evaluation.....	16
2.4.1	Visual (Macroscopic) Evaluation .....	21
2.4.2	Sectioning, Chemistry and Tensile Testing .....	25
2.4.3	Scanning Electron Microscopy .....	26
2.4.4	Optical Metallography and Microhardness Testing.....	31
2.4.5	Discussion of Metallographic Examinations .....	32
2.4.6	Fatigue Crack Growth Behavior .....	34
2.5	Loading on Dryer.....	36
2.5.1	Design Basis.....	36
2.5.2	Loads Experienced by Dryer at EPU Conditions .....	37
2.5.2.1	Static and Low Frequency Loading (0-50 Hz) .....	38
2.5.2.2	50-130 Hertz Range .....	47
2.5.2.3	High Frequency Loading (130-230 Hz).....	47
2.5.2.4	Bistable Flow .....	47
2.5.2.5	Dryer Ring Vertical Motion.....	48
2.5.2.6	Transient PORV Loading .....	48
2.5.2.7	Operation in Degraded Condition.....	48
2.6	Dryer Structural Evaluation .....	49
2.6.1	Analysis model.....	49
2.6.2	Frequency Calculations.....	54
2.6.3	Flat Spectrum Analysis .....	57
2.6.4	Normal and Degraded Dryer Operation.....	62
2.6.5	Gravity Loading and Support Ring Vibrations .....	68
2.6.6	Effect of Interior Brackets .....	71
2.6.6.1	Normal Operation Pressure Load.....	71
2.6.6.2	PORV Loads .....	72
2.7	Root Cause Evaluation.....	84
2.7.1	Source of Low Frequency (0-50 Hz) Loading.....	91
2.7.1.1	Acoustic Circuit Analysis of Main Steam Lines.....	91
2.7.1.2	Frequency Content of MSL Vibration Data.....	94
2.7.1.3	Main Steam Line Component Frequencies.....	95
2.7.1.4	Finite Element Model Evaluation .....	96
2.8	Conclusion .....	96

3.	Extent of Condition.....	97
3.1	Reactor Internals Assessment .....	100
3.1.1	Flow Induced Vibration .....	100
3.1.1.1	Original Design Basis Evaluation of Instrumented Components .....	102
3.1.1.2	Reactor Internal Components in Steam and Feedwater Flow Path.....	108
3.1.1.3	Evaluation of Mitigating Features .....	127
3.1.1.4	Evaluation Conclusions .....	128
3.1.2	Reactor Internal Pressure Differences .....	129
3.2	Components in Steam Path External to the Reactor .....	130
3.2.1	Steamline Piping.....	130
3.2.1.1	Background.....	130
3.2.1.2	Testing Methodology/Process.....	130
3.2.1.3	Results.....	131
3.2.1.4	Additional Evaluations.....	131
3.2.2	Steamline Components .....	131
3.2.2.1	MSIVs.....	132
3.2.2.2	PORVs .....	133
3.2.2.3	Thermowells .....	133
3.2.2.4	HPCI/RCIC Isolation Valves.....	133
3.2.3	Conclusions.....	134
3.3	Extent of Condition Conclusions .....	134
4.	Dryer Repair Assessment.....	135
4.1	Hood Frequencies .....	136
4.2	Hood Stresses.....	138
4.3	Loss of Braces.....	144
5.	Assessment for Other Units .....	147
5.1	Significant Differences Between Units.....	147
5.2	Recommended Actions .....	148
5.2.1	Monitoring .....	148
5.2.2	Inspections .....	149
5.2.3	Repairs .....	149
6.	Conclusions.....	151
7.	References.....	152

## List of Tables

Table 2.2-1:	Event Timeline.....	11
Table 2.4-1:	Sample Descriptions, Examinations and Tests.....	17
Table 2.4-2:	Chemical Analysis Results.....	26
Table 2.4-3:	Tensile Test Results.....	26
Table 2.4-4:	Microhardness Test Data.....	31
Table 2.5-1:	Small Scale Test Data.....	44
Table 2.6-1:	Dryer Frequencies.....	54
Table 2.7-1:	Root Cause Evaluation Process Map.....	85
Table 3.1-1:	Riser Brace Designs.....	107

## List of Figures

Figure 2.3-1:	Fracture on Hood A (outside view) .....	12
Figure 2.3-2:	Fracture on Hood A (interior view) .....	13
Figure 2.3-3:	Fracture extends around the outer bracket (L).....	13
Figure 2.3-4:	Fracture extends down the vertical front hood (R).....	13
Figure 2.3-5:	Visual Characterization of the Fracture Along Hood A .....	14
Figure 2.3-6:	Indications in the Brackets where the Angled Brace was Joined to the Outer Hood Plates .....	16
Figure 2.4-1:	Dryer Failure and Crack Locations.....	18
Figure 2.4-2:	Hood Fracture Sample Locations.....	19
Figure 2.4-3:	Bracket to Hood and Brace Sample Locations .....	20
Figure 2.4-4:	Hood A Top Cover Fractures at Bracket Weld Area.....	21
Figure 2.4-5:	Middle Hood Area – Sample 2A .....	23
Figure 2.4-6:	Hood F Top Cover and Vertical Plate Cracks .....	25
Figure 2.4-7:	SEM of Sample 1A and 1B Cover Plate Fractures .....	28
Figure 2.4-8:	SEM of Sample 4 Cover Plate Fracture Surface.....	29
Figure 2.4-9:	SEM Traverse of Sample 4 Cover Plate Fracture Surface.....	30
Figure 2.4-10:	Optical Metallography .....	32
Figure 2.5-1:	Typical Pressure Spectrum – Reactor Test Data.....	38
Figure 2.5-2:	Pressure Field Across the Outer Hood.....	39
Figure 2.5-3:	Static Pressure Loading on Dryer Hoods.....	40
Figure 2.5-4:	Pressure Drum Locations in the U.S. Reactor .....	42
Figure 2.5-5:	Time History of Pressure in the U.S. Reactor.....	43
Figure 2.5-6:	Oscillating Pressures on Dryer Hoods .....	45
Figure 2.6-1:	Dryer Analysis Model – Support Structure .....	51
Figure 2.6-2:	Dryer Analysis Model – Dryer Banks and Hoods .....	52
Figure 2.6-3:	Dryer Analysis Model.....	53
Figure 2.6-4:	Boundary Conditions .....	55
Figure 2.6-5:	Mode Shapes: Dryer Vertical Plates .....	56
Figure 2.6-6:	Hood Vertical Plate Stress Distributions (0-50 Hz Load Spectrum) .....	58
Figure 2.6-7:	Hood Horizontal Plates Stress Distributions (0-50 Hz Load Spectrum) .....	59
Figure 2.6-8:	Dryer Middle Plate and Steam Dam Stress Distributions (0-50 Hz Load Spectrum) .....	60
Figure 2.6-9:	Dryer Stress Distribution (130-200 Hz Load Spectrum) .....	61
Figure 2.6-10:	Degraded Dryer Analysis Model and Pressure Load Application.....	63
Figure 2.6-11:	Degraded Dryer Stress Distribution: Inner Hood Vertical Plates .....	64
Figure 2.6-12:	Degraded Dryer Stress Distribution: Bottom and Top Plates.....	65
Figure 2.6-13:	Degraded Dryer Stress Distribution: Outer Hood Front Plate .....	66
Figure 2.6-14:	Degraded Dryer Stress Distribution: Steam Dam.....	67
Figure 2.6-15:	Deadweight Load: Support System Deflections and Stresses .....	69
Figure 2.6-16:	Deadweight Load: Base Plates and Hood Plates .....	70
Figure 2.6-17:	Addition of Brace Attachment Brackets in the Analysis Model.....	73

Figure 2.6-18:	Outer Hood Stress Intensities: Normal Operation Pressure Load .....	74
Figure 2.6-19:	Outer Hood Stress Components: Normal Operation Pressure Load.....	75
Figure 2.6-20:	Outer Hood Stress Components: Normal Operation Pressure Load (continued).....	76
Figure 2.6-21:	Outer Hood Stress Intensities Assuming Diagonal Brace Failure: Normal Operation Pressure Load .....	77
Figure 2.6-22:	Outer Hood Stress Components Assuming Diagonal Brace Failure: Normal Operation Pressure Load .....	78
Figure 2.6-23:	Outer Hood Stress Components Assuming Diagonal Brace Failure: Normal Operation Pressure Load (continued).....	79
Figure 2.6-24:	Normal Operation Pressure and PORV Loads.....	80
Figure 2.6-25:	Outer Hood Stress Intensities: Normal Operation Pressure and PORV Loads .....	81
Figure 2.6-26:	Outer Hood Stress Components: Normal Operation Pressure and PORV Loads .....	82
Figure 2.6-27:	Outer Hood Stress Components: Normal Operation Pressure and PORV Loads (continued).....	83
Figure 2.7-1:	Possible Crack Locations.....	86
Figure 2.7-2:	High Stress Locations For Various Root Causes.....	87
Figure 2.7-3:	Quad Cities Main Steam System .....	91
Figure 2.7-4:	Branch Line Scaling.....	93
Figure 2.7-5:	Acoustic Circuit Modeling Results.....	93
Figure 2.7-6:	MSL Vibration Frequency Content .....	95
Figure 3.1-1:	Major Reactor Internal Components.....	101
Figure 3.1-2:	Typical Feedwater Sparger .....	110
Figure 3.1-3:	Upper RPV Region Showing Dryer Guide Rod .....	112
Figure 3.1-4:	Dryer Guide Rod Azimuth Orientation.....	113
Figure 3.1-5:	Typical Shroud Head Guide Rod.....	115
Figure 3.1-6:	Top Head Nozzles.....	116
Figure 3.1-7:	Typical Steam Separator .....	121
Figure 3.1-8:	Typical Shroud Head Bolt .....	122
Figure 3.1-9:	Typical BWR/3/4/5 Internal Core Spray Piping.....	125
Figure 3.1-10:	Quad Cities 2 Water Level Instrument Nozzle .....	126
Figure 4.1-1:	Repaired Hood: Frequencies.....	137
Figure 4.2-1:	Repaired Hood Plate Stresses: Normal Operation Pressure Load .....	139
Figure 4.2-2:	Repaired Component Stresses: Normal Operation Pressure Load .....	140
Figure 4.2-3:	Repaired Hood Plate Stresses: PORV and Normal Operation Pressure Loads .....	141
Figure 4.2-4:	Repaired Component Stresses: PORV and Normal Operation Pressure Loads .....	142
Figure 4.2-5:	Stress Reduction With Repair: Normal Operation Pressure Load.....	143
Figure 4.3-1:	Effect of Vertical Braces on the Dryer Vane Support Structure: Deadweight Load .....	145

**Figure 4.3-2: Effect of Vertical Braces on the Dryer Vane Support Structure: Pressure Load.....146**

## **Quad Cities 2 Steam Dryer Failure Determination of Root Cause and Extent of Condition**

### **1. Introduction and Summary**

In May of 2003, Quad Cities Unit 2 experienced a significant increase in steam moisture content while operating at extended power uprate (EPU) conditions. Inspection of the steam dryer in June 2003 lead to the conclusion that the increase in steam moisture content was due to significant through-wall cracking, deformation, and failure of the outer bank hood on the 90° side of the dryer. In addition, the outer bank hood on the 270° side was cracked and several internal braces and tie bars had failed.

This report documents the root cause evaluation for the dryer failure. The other components in reactor and steam flow path were also evaluated in light of the dryer failure to determine if there were similar vulnerabilities to the failure mechanisms postulated for the dryer. As part of the root cause evaluation, a detailed evaluation was performed in order to more thoroughly understand the pressure loads acting on the dryer. Since the dryer repair design preceded this evaluation, the dryer repair design was assessed against the static and dynamic loads developed in this evaluation in order to confirm the adequacy of the repair.

The cause of the dryer failure is postulated to be high cycle fatigue resulting from low frequency pressure loading on the outer hoods during normal operation. The pressure loading is thought to be amplified by the geometric configuration of the main steamlines. The cracks in the hoods and braces are most likely to have been initiated during steady-state EPU power operation. The cracks continued to grow until the transient pressure loads from the stuck open relief valve and subsequent manual valve openings opened the cracks through-wall, leading to the increased steam moisture content. The previous cover plate failure in 2002 subjected the dryer structure on the 90° side to significant additional loading.

The reactor internal components and components in the steam flow path were also evaluated in light of the dryer failures. Since the cause of the dryer failures was attributed to high cycle fatigue, detailed evaluations were performed for these components to determine their susceptibility to flow induced vibrations at EPU conditions. These evaluations concluded that the previous EPU component analyses remain valid and that Quad Cities 2 can operate at EPU conditions without exciting the key internal components above their established vibration criteria limits.

The adequacy of the dryer and the dryer hood repair design was evaluated for the static and dynamic loads developed during this root cause evaluation. Based on the results of

this evaluation, the dryer and the dryer hood repairs were determined to be adequate for EPU operation.

## 2. Root Cause Evaluation for QC2 Dryer Failure

The primary purpose of this evaluation is to determine the most likely root cause of the steam dryer failure at Quad Cities 2. The evaluation reviewed the timeline of plant operation including operation at EPU conditions for significant events that may have caused or contributed to the dryer failure. The visual and metallurgical evidence was reviewed in order to determine the failure mechanism and, to the extent possible, the failure sequence. Realistic static and dynamic loadings on the dryer were calculated in order to determine the stresses experienced by the dryer. As an alternate approach for estimating the loading experienced by the dryer, the stress required to cause the outer hood failure by fatigue was calculated based on the ASME fatigue curves. A finite element analysis was performed in order to determine the stresses resulting from the applied loads. The observed evidence and analytical results were then evaluated in order to determine the most probable root cause of the dryer failure.

### 2.1 Potential Root Causes

The root cause evaluation considered the following credible potential root causes for the observed dryer failure:

- Material and fabrication issues
  - Weld defects
  - Poor quality plate material
- Thermal fatigue
- Fatigue due to pre-EPU operation
- Intergranular stress corrosion cracking (IGSCC)
- Dryer support ring deflection
- Bi-stable flow
- Damage from 2002 cover plate failure
- Transient loading due to power operated relief valve (PORV) operation
- Pressure loading from increased steam flow at EPU conditions
  - Flow induced vibration (FIV) at low frequency (0-50 Hz)
  - Flow induced vibration (FIV) at medium frequency (50-130 Hz)
  - Flow induced vibration (FIV) at high frequency (130-230 Hz)

The event timeline identified events that may have caused mechanical overloading. The visual and metallurgical examinations provided information for evaluation of indications of fatigue or IGSCC cracking. The loads evaluation provided the forcing functions for the static and dynamic loads. These loads were then used to determine the stresses

experienced by the dryer. The results from these evaluations were then used to determine the most probable root cause for the observed dryer hood failure.

## 2.2 Event Timeline

The following table shows a summary of the potentially significant events that have occurred at Quad Cities 2 during extended power uprate operation:

**Table 2.2-1: Event Timeline**

<b>Date</b>	<b>Event</b>
March 2002	Full EPU power first achieved
June 7, 2002	Increased steam moisture content (cover plate failure)
June 20, 2002	Power reduction
July 11-28, 2002	Shutdown for cover plate failure
July 28, 2002 – April 14, 2003	EPU power operation with normal steam moisture content
April 15, 2003	Steam moisture content >0.05% (attributed to local core peaking)
April 16, 2003	Stuck open PORV transient event and subsequent shutdown for valve replacement
April 20-22, 2003	Plant Restart
April 20, 2003	PORV testing (2 cycles)
April 22 – May 8, 2003	EPU power operation
May 6, 2003	Increased steam moisture content*
May 8-11, 2003	Shutdown for additional PORV replacement
May 14-19, 2003	EPU power operation with increased steam moisture content (~0.23%)
May 28, 2003	Maximum steam moisture content (>0.35%), power reduction to pre-EPU power level
June 10, 2003	Shutdown for hood failure

\* First steam moisture content measurement following PORV event

Transient or impact loads during the cover plate failure in 2002 may have played a role in the failure of the dryer hood. PORV event may have overstressed hood structure and initiated or exacerbated cracking.

## 2.3 Visual Observations

GE Reactor services conducted remote visual examinations (VT-1 and VT-3) in support of a forced outage of Quad Cities Unit 2 during June 12 through June 14, 2003 to assess the condition of the Steam Dryer. Structural damage as a result of fracture was evident on Dryer Hood A and indications were noted in several tie bars on the top of the Dryer. A linear indication noted on Dryer Hood F was later evaluated as a superficial scratch (NRI) after power wire brushing. Several internal braces in Hood A were fractured and had become detached. In Hood F, one internal vertical brace was fractured, and linear indications were observed on two internal bracket to hood weld areas and base metal. No other relevant indications were noted.

### 2.3.1 Outer Hood A (90 Degree Side)

Initially, a partial examination of the dryer was performed before its removal from the vessel. The partial examination revealed significant structural damage on Dryer Hood A on the 90° side of the dryer. Figure 2.3-1 displays the damage from the outer front surface.



**Figure 2.3-1: Fracture on Hood A (outside view)**



**Figure 2.3-2: Fracture on Hood A (interior view)**

The fracture on Dryer Hood A extended over approximately  $\frac{3}{4}$  of the hood length. When the dryer was removed from the vessel, additional remote examinations were conducted from both the Dryer exterior and interior. Figure 2.3-2 shows the damage on the 180° side from underneath.

The fracture extended from its major opening in the middle of the dryer hood toward the 0° and 180° sides on the top of the hood around two interior welded structural brackets before continuing down the vertical sides, shown in Figures 2.3-3 and 2.3-4.



**Figure 2.3-3: Fracture extends around the outer bracket (L)**  
**Figure 2.3-4: Fracture extends down the vertical front hood (R)**

The top of the hood is joined to its vertical face by a corner weld. The major opening of the fracture in the middle of the hood was located in the area of that welded joint. The visible major fracture surfaces appeared relatively flat with some ductile shear near the

edges of the fracture faces, characteristic of fatigue. No beach marks were visible, but they were likely to be obscured by the oxide on the fracture surfaces. The visible fracture faces did not appear faceted, as would be characteristic of intergranular stress corrosion cracking (IGSCC). The shear area on the exterior surface shown in Figure 2.3-5, suggests initiation on the interior dryer surface and propagation to the exterior surface in this area.

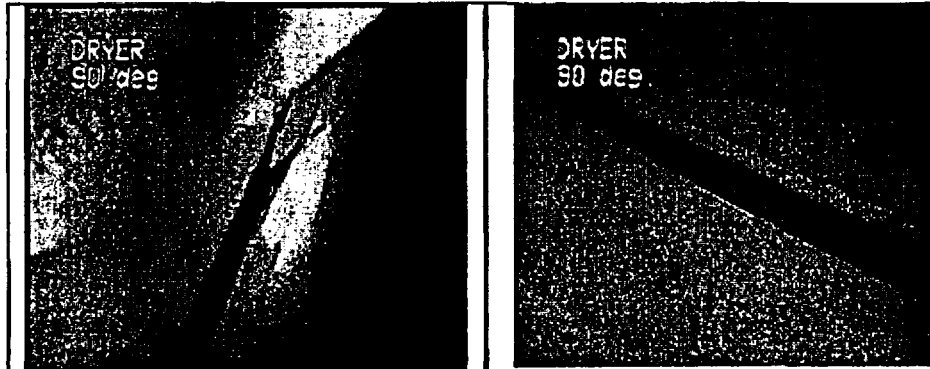


**Figure 2.3-5: Visual Characterization of the Fracture Along Hood A**  
Photograph from interior and the top surface respectively

Based on the remote visual examination the location of fracture initiation could not be determined; however, the likely areas appeared to be the toes of the welds on the interior brackets and the weld root or weld toe in the joint between the horizontal top and vertical face of the hood near the major opening of the fracture. The fracture may have had multiple initiation sites. As the crack moved away from the interior brackets toward the sides of the hood, the direction of crack propagation changed from the top to the vertical face. This suggested that this cracking occurred in the advanced stages of the fracture when structural integrity on the top of the dryer was lost and the stress distribution in the hood had changed to favor propagation down the vertical face. The direction of crack propagation appeared to follow the stress distribution, around concentrations at the internal bracket welds, and in the later stages down the vertical face of the dryer. The crack did not follow the weld heat affected zone, as would be characteristic of IGSCC. The cause of the fracture appeared to have been fatigue based on the results of the remote visual examination. This was supported by the overall appearance of the fracture and the appearance of the fracture surfaces. The specific location of crack initiation could not be determined, but the fracture surface suggested that initiation had occurred on the interior dryer surface without any characteristics of IGSCC.

### 2.3.2 Outer Hood F (270 Degree Side)

Visual inspections were also conducted on the opposite side of the dryer with emphasis on Hood F. These inspections included the outer surfaces as well as the inner surfaces of the outer hood and the angled and vertical braces. Crack indications were found in several of the structures. On the interior of the hood, indications were observed on both

diagonal bracket to hood welds, extending into the base metal. The interior vertical brace on the 180° side of the unit was fractured on the upper end. No missing pieces or parts were observed. Figure 2.3-6 details the crack indications at the 0 and 180 degree stiffeners that were present on the interior of the outer hood. These indications were observed at the junction of the bracket to the vertical plate of the Hood F. The other end of the bracket could not be inspected due to the presence of air bubbles. These locations were chosen for additional metallographic evaluation.

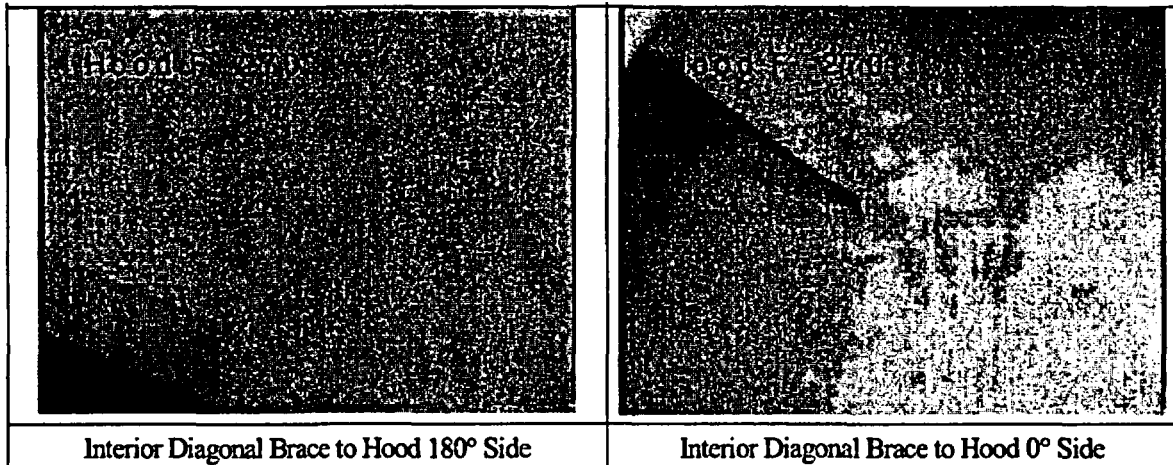


**Figure 2.3-6: Indications in the Brackets where the Angled Brace was Joined to the Outer Hood Plates**

## 2.4 Metallurgical Evaluation

Eight dryer samples were sent to Vallecitos Nuclear Center (VNC) for evaluation. The evaluation included the following examinations and tests:

- Visual Macroscopic Examination
- Fractography, Scanning Electron Microscopy (SEM)
- Optical Metallography
- Micro-Hardness Testing (MHT)
- Tensile Testing
- Chemical Analysis

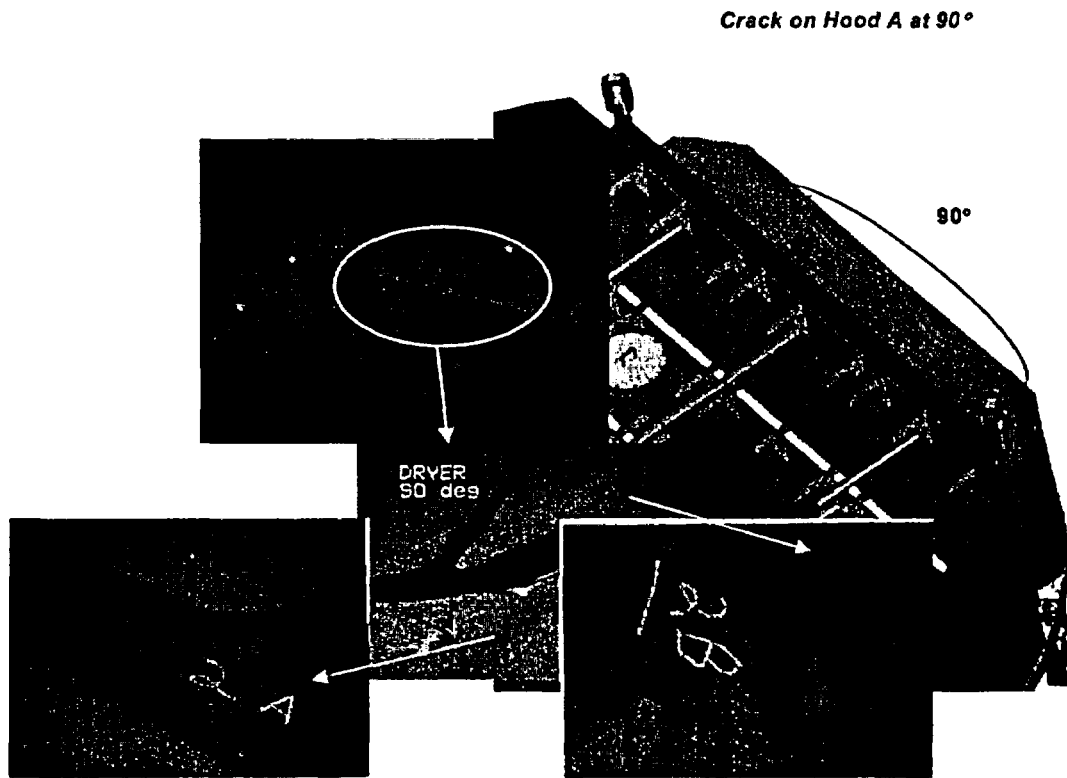
All the samples were examined in the hot cell prior to decontamination. Subsequently, selected samples were decontaminated for further examination and testing.

Table 2.4-1 shows a summary of the samples identifying the examinations and tests conducted. Figures 2.4-1, 2.4-2 and 2.4-3 illustrate the samples and their locations in the steam dryer.

**Table 2.4-1: Sample Descriptions, Examinations and Tests**

Sample	Description	Macro	SEM	Optical Met.	MHT	Tensile	Chem
1A	Hood A (90°) Bracket to Hood (top) - 180° side	x	x	x	x		EDS
1B	Hood A (90°) Bracket to Hood (top) - 0° side	x	x				
2A	Hood A (90°) Segment from mid-Hood (mate to 2B) with top and vertical face	x	x	x	x	x	Chem EDS
2B	Hood A (90°) Segment from mid-Hood (mate to 2A) with top and vertical face	x					
3A	Hood A (90°) Vertical brace with portion of angle brace attached, 180° side	x					
3B1	Hood A (90°) top half of angle brace from the 0° side	x					
3B2	Hood A (90°) bottom half of angle brace from the 0° side	x					
4	270 Deg Bracket to Hood with top and vertical face sections, 180 degree side	x	x	x	x		





**Figure 2.4-2: Hood Fracture Sample Locations**

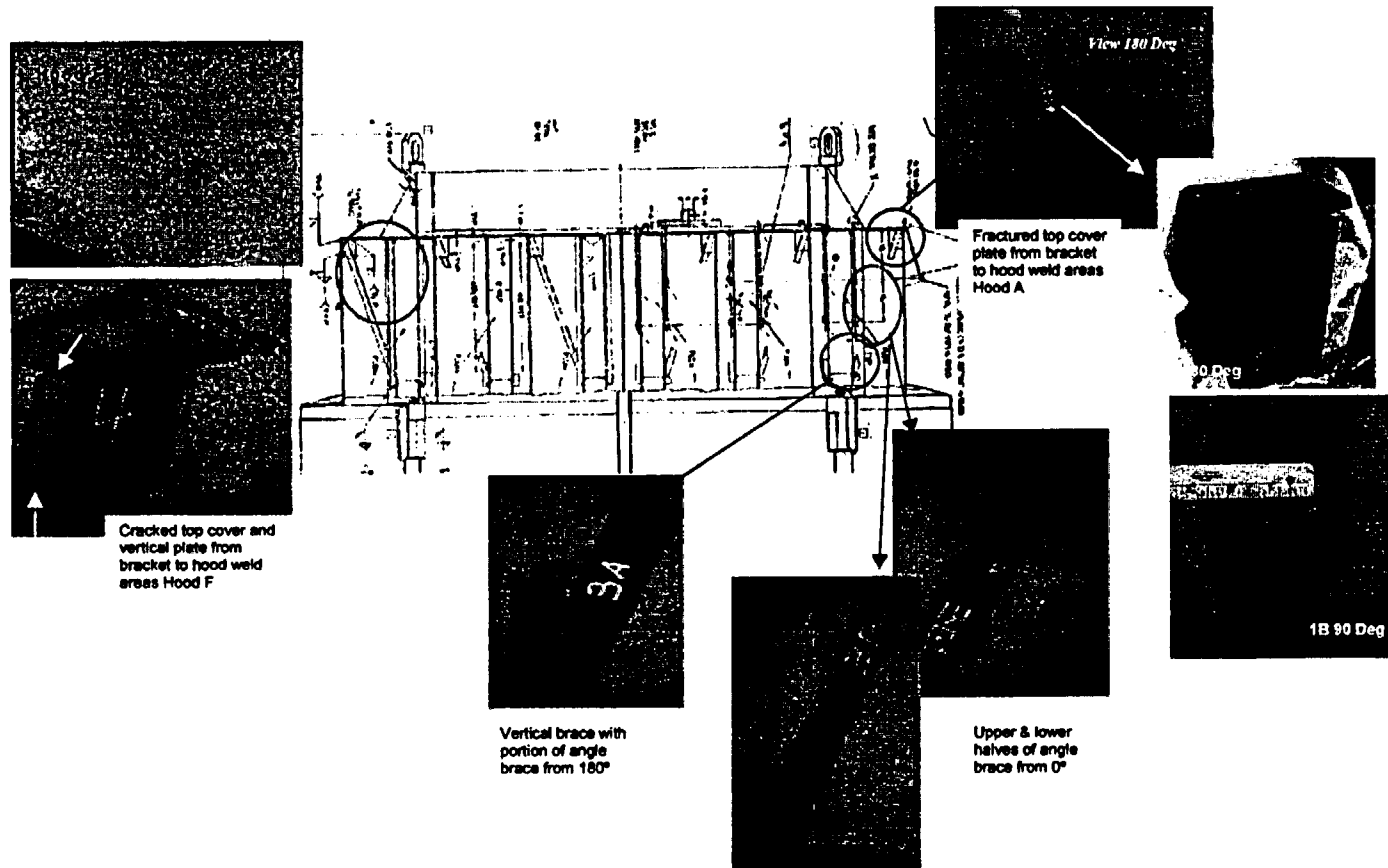
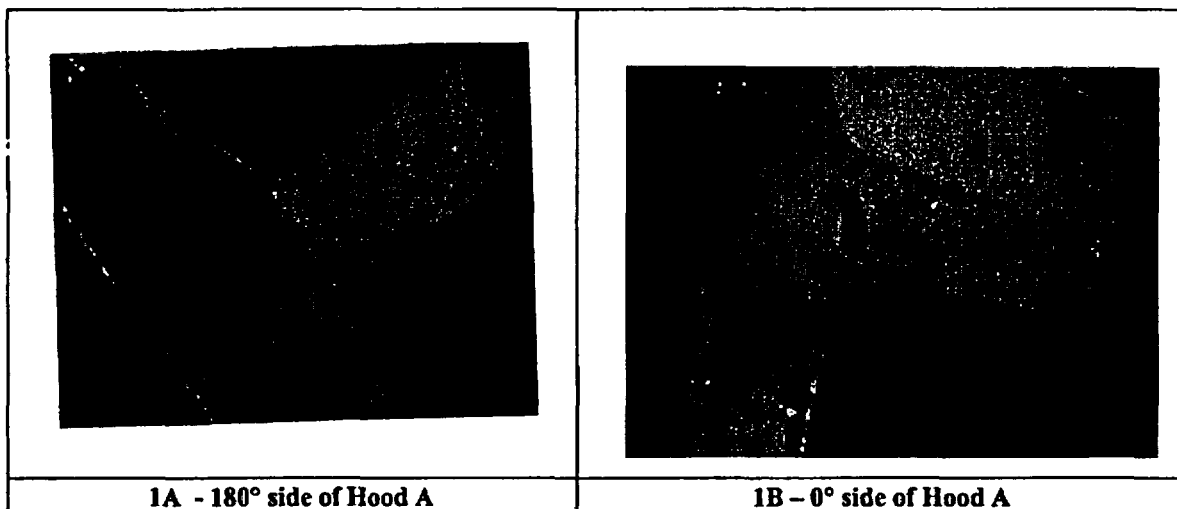


Figure 2.4-3: Bracket to Hood and Brace Sample Locations

### 2.4.1 Visual (Macroscopic) Evaluation

All 8 steam dryer samples were remotely examined in the as-received condition at between 1X and 4X magnification. The outer surfaces of all samples were coated with a predominantly gray oxide layer typical for long-term exposure of stainless steel in the BWR environment. The first two samples, 1A and 1B, were determined to correspond to the 180° side of Hood A and to the 0° side of Hood A respectively, Figure 2.4-4.



**Figure 2.4-4: Hood A Top Cover Fractures at Bracket Weld Area**

A clear beach mark pattern was observed on sample 1A. Beach marks are indicative of a progressive cracking mechanism and are especially typical of fatigue fractures. The beach mark pattern indicated crack initiation at the fillet weld toe on the cover plate.

The fracture of sample 1B showed initiation at the toe of the weld on the bracket. The sample 1B fracture progressed through the weld before propagating into the cover plate. Since the bracket to cover plate weld is only a fillet as required by the drawing and not a full penetration weld, the fracture exposed the unwelded portion of the end of the bracket plate which appears as a dark parting line area in the photo of the fracture face in Figure 2.4-4. The radial markings on the 1B fracture surface shows propagation into the cover plate from the bracket side weld toe on both sides of the bracket plate. The fracture face does show lines of directional propagation consistent with fatigue, but the formation of a classic beach mark pattern was disturbed because the cracking propagated through the fillet prior to entering the cover plate.

On both the 1A and 1B samples the fracture surfaces were angled toward the initiation area at the welds relative to the cover plate surface and became perpendicular to the cover plate surface as the crack front moved away from the weld. The appearance of the fracture surface and remaining ligament prior to final failure shows that the crack front

propagated away from the welds along the cover plate for a considerable distance prior to breaking through the outside surface of the plate. No significant deformation or necking indicating overload was apparent on either sample. The remaining ligament prior to final failure was approximately 0.03 inches on both samples.

Sample 2A and 2B were taken from the mid plate fracture area on Hood A where the cracking from the 0° and 180° brackets converged at the hood top cover to vertical face weld (weld H2). This area represented the largest displacement of fracture surfaces with the fracture at that point proceeding in multiple directions propagating down the vertical face.

As shown Figure 2.4-5, Sample 2A as viewed from the inside surface of the dryer, revealed that the corner weld of the cover plate to vertical face was back-welded on the root side. Examination of Area 3 shows that cracking propagated through the weld, but did not initiate at or in the weld. As the cracking progressed down the vertical face of the weld it changed direction (Area 2) and propagated horizontally.

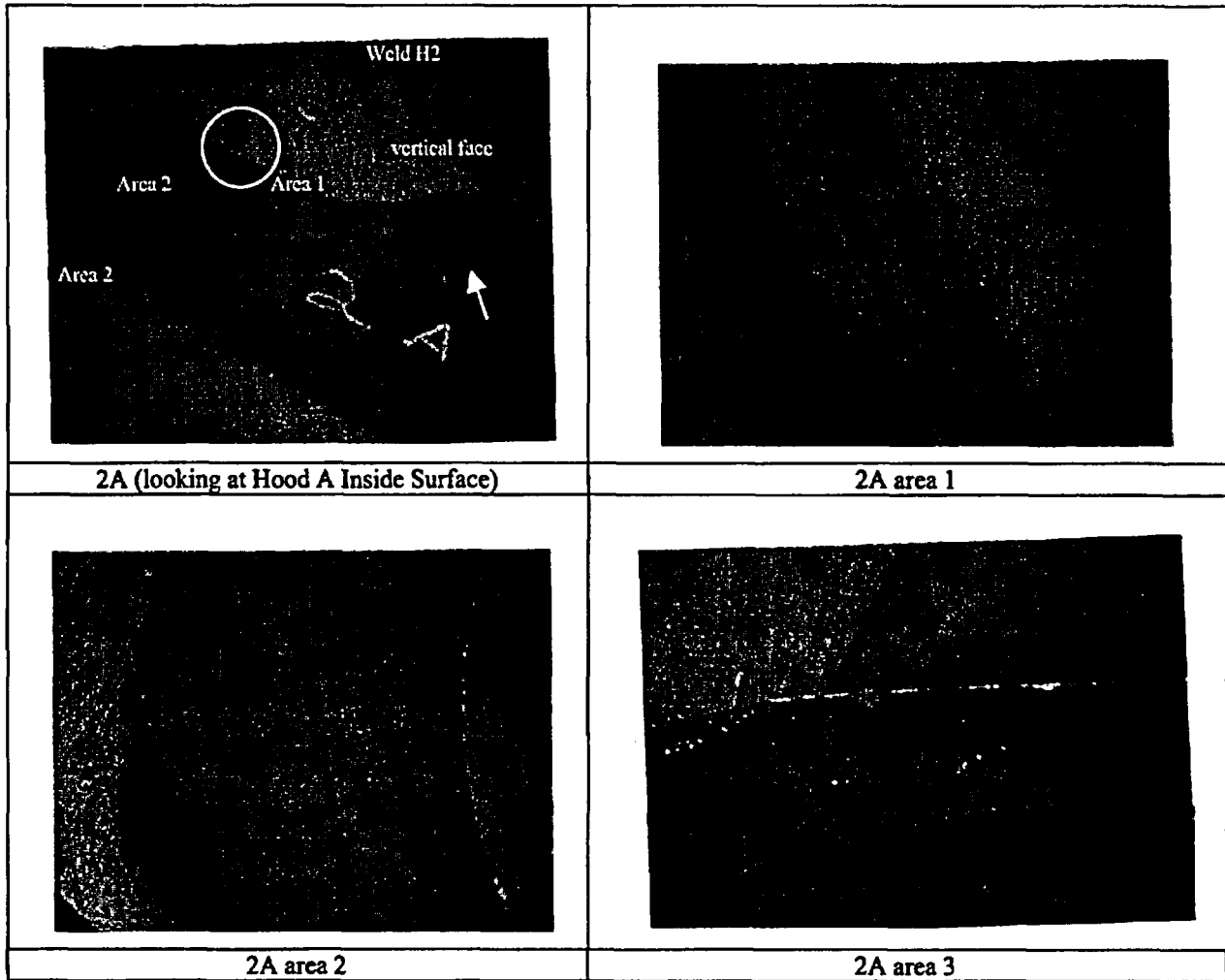


**Figure 2.4-5: Middle Hood Area – Sample 2A**

The fracture surfaces of brace samples, 3A, 3B1 and 3B2 and the brace remnants on samples 1A and 1B were also assessed.

Sample 4, taken from Hood F (from the 180° side of the dryer based on the IVVI report) contained two cracks. As shown in Figure 2.4-6, this piece contained two cracks: one crack at the end of the bracket on the vertical face and one at the bracket to top cover plate location (denoted by the arrows in Figure 2.4-6). The vertical face crack (4B) had been cut through the middle close to the bracket and the fracture surface was exposed and damaged during removal. Both the crack and intact hood cover crack 4C were opened

for evaluation. The exposed fracture face of sample 4B was relatively flat and consistent in appearance with fatigue. The crack had propagated through the weld similar to 1B, but the fracture surface was too damaged to yield additional information. The fracture surface of sample 4C contained clear beach marks, indicating fatigue initiation at the bracket similar to 1A. The remaining ligament thickness on sample 4C was approximately 0.1 inch.

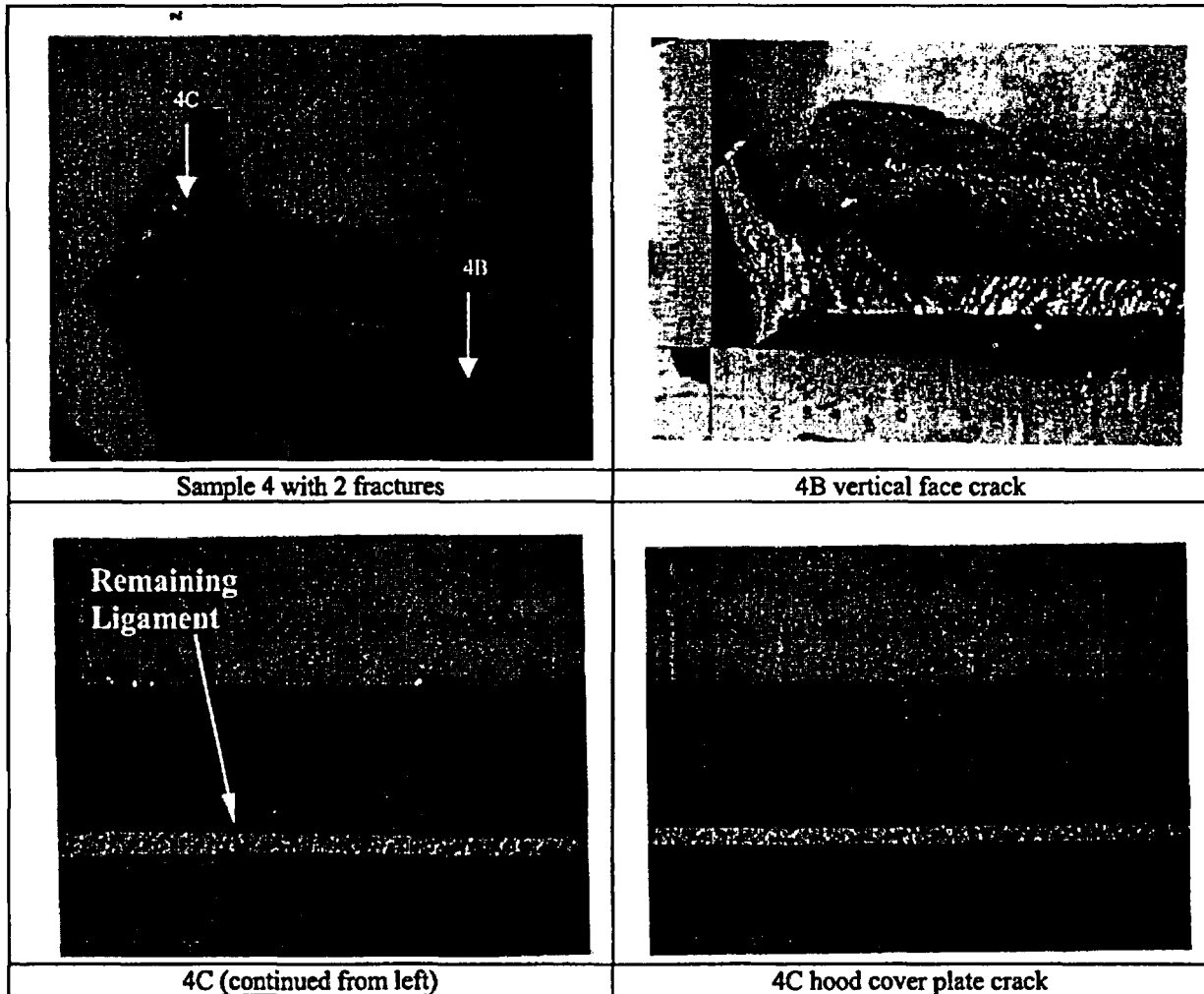


**Figure 2.4-6: Hood F Top Cover and Vertical Plate Cracks**

### 2.4.2 Sectioning, Chemistry and Tensile Testing

Samples 1A, 1B, 2A, and 4C were sectioned for detailed evaluation. The samples were removed using vertical and horizontal band saws. Samples were removed for fractography, optical metallography and microhardness testing, chemical analysis, and tensile testing. The results of these tests are described in the following paragraphs.

Two samples of cover plate material were removed from sample 2A for chemical analysis by a Spectra Span DCP (Direct Coupled Plasma) system. As shown in Table 2.4-2, the results established the chemistry of the material to be consistent with 304 stainless steel, the specified material for the dryer.

**Table 2.4-2: Chemical Analysis Results**

[[


]]

EDS, a semi-quantitative chemical analysis method, was also applied to samples of the Hood A top cover plate, vertical face plate, and weld metal. The results indicated the material composition to be consistent with Type 304 stainless steel wrought material and Type 308 weld metal.

Two sub-sized tensile specimens were machined from the cover plate material obtained from sample 2A. Table 2.4-3 shows that the material met the requirements for ASTM A-240 Type 304 material.

**Table 2.4-3: Tensile Test Results**

[[


]]

**2.4.3 Scanning Electron Microscopy**

Fracture faces from Samples 1A, 1B, 2A, and 4C were evaluated with scanning electron microscopy after cleaning to remove the oxide from the fracture surface. Figure 2.4-7 shows directional lines consistent with the direction of crack propagation at low magnification on samples 1A and 1B; Examination of the samples at higher magnification did not reveal fatigue striations or other significant features. The crack from sample 2A near the end of the crack that propagated from the Hood A cover plate into the vertical face was opened to reveal the fracture surface. Figure 2.4-7 shows that

the 2A crack fracture consisted of two primary planes at the plate surfaces joined by an intermediate plane. Some directional lines were observed, but overall there appeared to have been relative movement resulting in smearing on the fracture surface and no striations or other detail features could be identified.

The fracture surface 4C (Hood F cover plate) was better preserved than that of 1A or 1B because the crack had not opened during service. Examination of 4C did reveal fatigue striations in two locations, Areas 1 and 2 as shown in Figure 2.4-8, with spacing measured to be from approximately 0.3 to 2 microns. A low magnification SEM traverse of the fracture surface is shown in Figure 2.4-9.

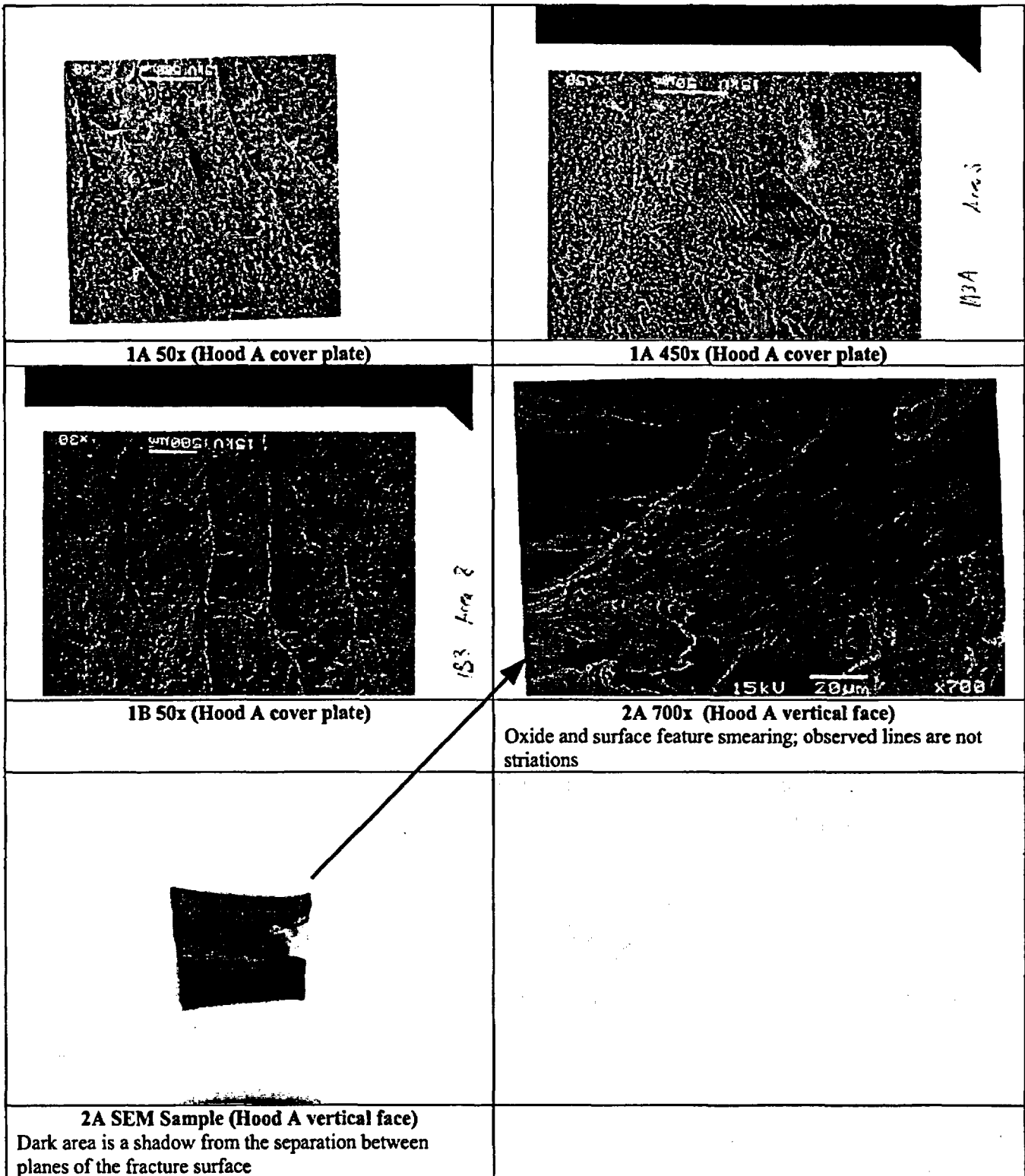


Figure 2.4-7: SEM of Sample 1A and 1B Cover Plate Fractures

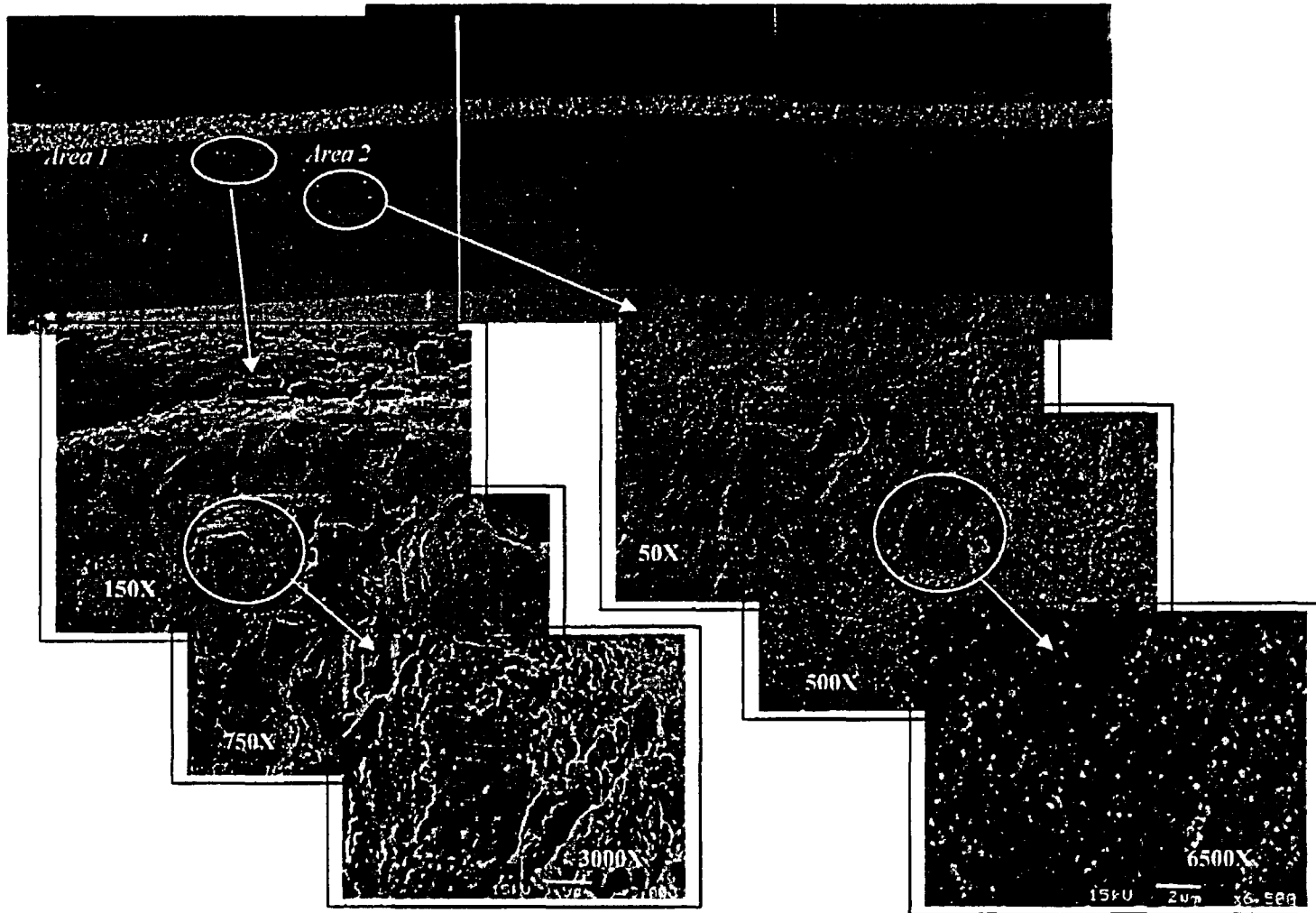
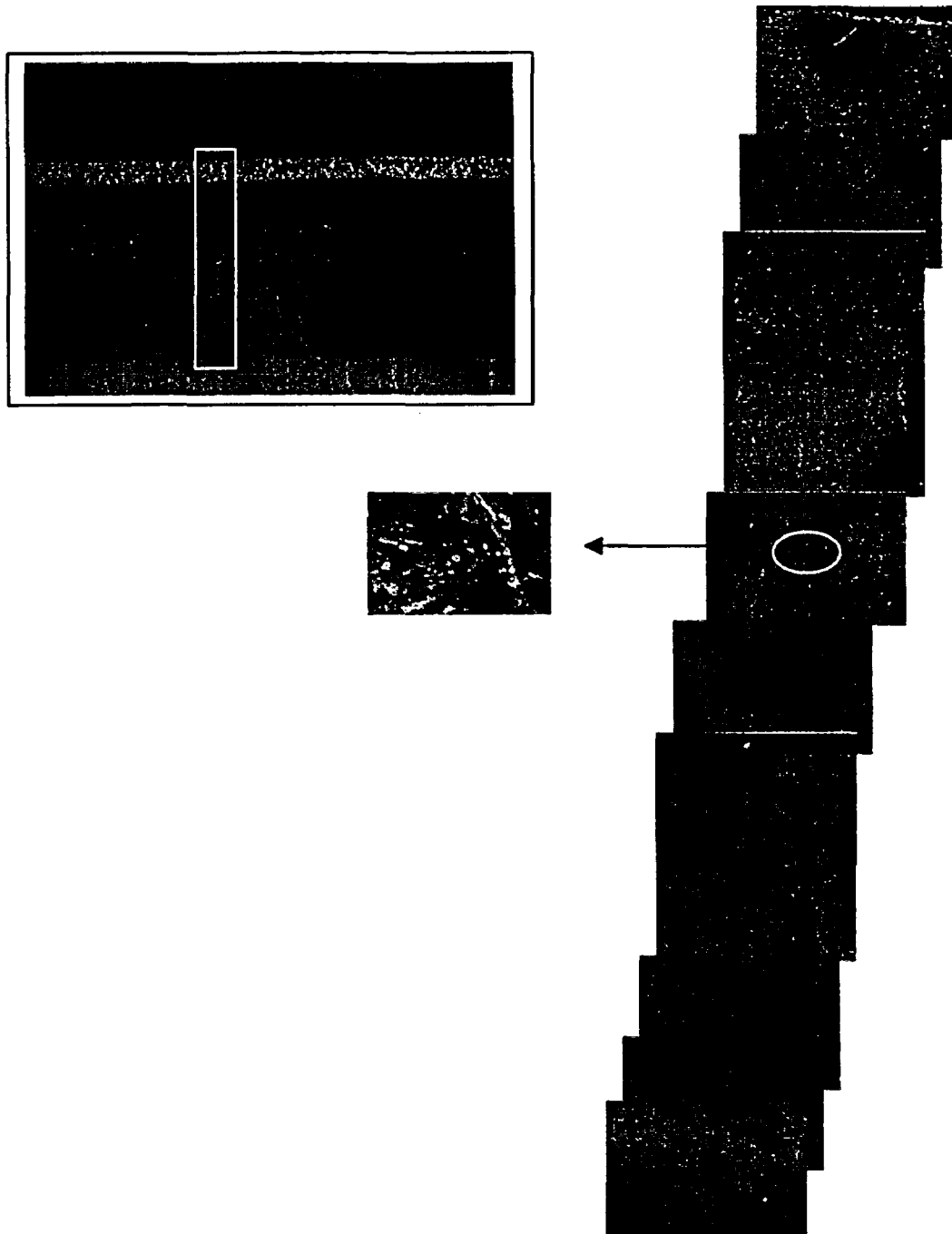


Figure 2.4-8: SEM of Sample 4 Cover Plate Fracture Surface



**Figure 2.4-9: SEM Traverse of Sample 4 Cover Plate Fracture Surface**

**2.4.4 Optical Metallography and Microhardness Testing**

Specimens from samples 1A, 2A, and 4C were polished and etched for metallographic examination. The microstructure was representative of Type 304 stainless steel as expected. The observed ASTM grain size at 100x was 3 to 5. As shown in Figure 2.4-10, cracking in all the samples was consistently transgranular. Some areas exhibited ditching at the grain boundaries, indicating isolated spots of sensitization, but no evidence of intergranular stress corrosion cracking associated with these areas was observed. Microhardness measurements were performed using a Knoop indenter with a 500 gram load on the optical metallographic specimens from samples 1A, 2A, and 4C. Surface hardness was slightly higher than the average in samples 1A and 2A which is not unusual for rolled plate (Table 2.4-4). Overall, the hardness was as expected for Type 304 plate.

**Table 2.4-4: Microhardness Test Data**

[[


]]

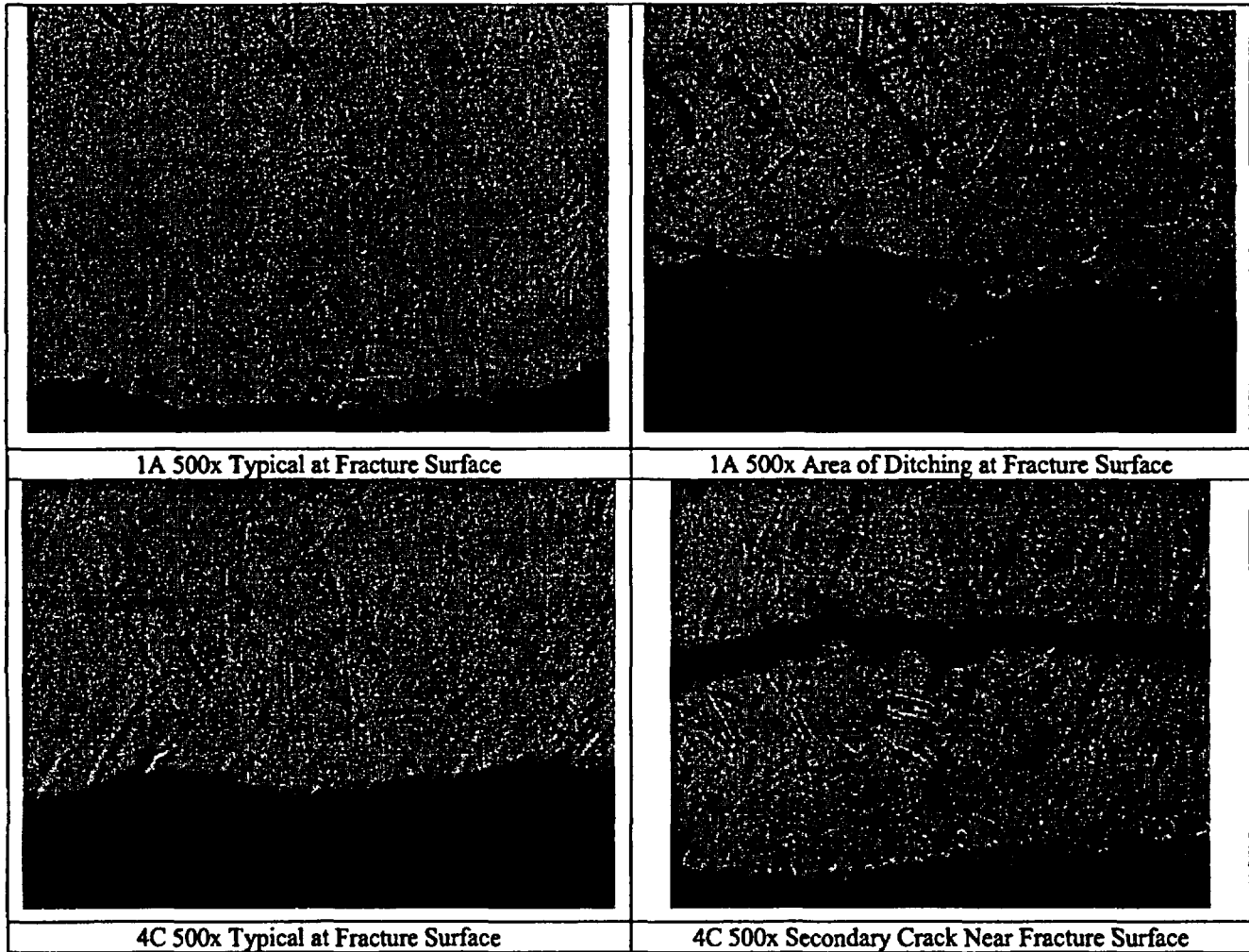


**Figure 2.4-10: Optical Metallography**

#### **2.4.5 Discussion of Metallographic Examinations**

As described previously, a metallurgical evaluation was performed to assess the failure mechanisms for the QC2 dryer. Based on examination of the samples and the site IVVI examination, the following conditions were observed:

Hood A 0° Side: Top cover plate fracture and detached angle brace

Hood A 180° Side: Top cover plate fracture, detached angle and vertical braces

Hood F 0° Side: Vertical face plate crack

Hood F 180° Side: Top and vertical face plate cracks, cracked vertical brace

The large scale cracking on the Hood A cover plate, which led to the steam moisture content increase, initiated on the interior surface at both bracket cover plate welds and propagated a considerable distance before breaking through the remaining ligament to the outside surface. The cracking propagated toward the hood mid-section from the bracket areas on both sides, converged, and propagated down the vertical face of the dryer opening a large fracture area. On the ends of Hood A, cracking also propagated some distance in the cover plate, and eventually changed direction and propagated into the vertical face plate.

SEM examination conducted on samples from both Hood A and Hood F showed the fracture appearance was consistent with a mechanical fatigue mechanism. "Beach marks" were observed on the fracture surface emanating from the weld, and surface features indicating the propagation direction ("river patterns") were also noted. Examination of the fracture surfaces indicate that the cracking initiated in the toe of the weld to the brackets and propagated laterally in both directions. On the F Hood sample, striations with spacing of approximately 0.3-2 $\mu$ m were found, consistent with a high cycle fatigue mechanism.

Quantitative chemical and EDS tests show that the failed cover plate material was Type 304 stainless steel, as specified in the original drawings. The failed material in general meets ASTM A 240, Type 304 requirements for ultimate and yield strength, elongation, and hardness (based on microhardness results).

Cover plate cracking in all cases was determined to initiate at the toe of the weld joining the cover plate to the bracket attached to the angle brace. No welding flaws, such as undercut, were observed; the fracture initiation occurred at the location of the stress concentration caused by the weld joint of the bracket to the cover plate, specifically at the weld toes. The weld joint between the horizontal and vertical hood plates was back-welded and played no role in crack initiation. The fracture surface appearance shows the damage mechanism causing the cracks was mechanical fatigue, with the presence of striations revealed by the SEM on the Hood F sample adding further confirmation of high cycle fatigue. No evidence of intergranular stress corrosion cracking (IGSCC) was observed. The overall observations were supported by evaluation of the samples from both Hood A and Hood F.

In addition, it was noted on Hood F that cracking, either on the vertical hood face or the hood top cover, was present even when the vertical and angle braces were structurally sound. Thus, initiation of hood cracking was not necessarily dependent on initiation of cracking in the angle braces based on the Hood F observations.

Irregular multi-planed fracture surfaces were observed on the ends of some braces indicating non-uniform loading near the time of final failure which could be attributed to the loss of integrity in the cover plate as hood cracking propagated, as well as the detachment of opposite ends of the angle and vertical braces.

Where the vertical brace was damaged or missing, the damage to the hood was more severe, i.e., the IVVI reports indicate the crack on the 180° Side of Hood F was longer than the crack on the 0° side and the crack opening and extent observed on the 180° side of Hood A was wider and longer, respectively, than the crack on the 0° side.

Based on the evaluation the following conclusions were reached:

- The cause of Steam Dryer Hood A failure was high cycle fatigue.
- Cracking in Steam Dryer Hood F was also caused by high cycle fatigue.
- The fractures initiated at the weld toes joining brackets to the interior surface of the hood.
- Crack initiation was a function of stress concentration near the toe of the weld, but not associated with welding flaws.
- Initiation of cracking in the vertical face plate was not dependent on initiation of cracking in the vertical and angle braces. It is possible that cracking in the hood may precede cracking in the vertical and angle braces.
- No material deficiencies were identified.
- No evidence of IGSCC was observed.

#### **2.4.6 Fatigue Crack Growth Behavior**

The conclusions of the metallurgical exam established that the cracking extended in the lengthwise direction significantly without penetrating through wall. As a result of these observations, an effort was made to assess the fatigue crack growth, based on the several surface crack geometries obtained from the metallurgical examination of the 270 degree side of the cracked steam dryer. This fracture mechanics assessment is based on a combination of NASA Technical Paper 1578 and Appendix C of ASME Section XI. The stresses used in this assessment were obtained from the analyses presented in Section 2.6.

The stress intensity range ( $\Delta K$ ) values for a given crack geometry and the applied bending loading were calculated based on the technical approach outlined in a NASA Technical Paper 1578. The fatigue crack growth rate per cycle was calculated using the relationships given in Appendix C of ASME Section XI. The fatigue crack growth relationship from the Code included the effects of R-ratio to account for the effects of the weld residual stresses.

The inputs were the following:

- (1) The crack geometries were obtained from the metallurgical evidence obtained from the cracked steam dryer sections.
- (2) The loading was obtained from a stress analysis conducted on the steam dryer model with a unit internal pressure of 1.0 psi.

[[

]]

*270 degree side*

For the lengthening direction (along the inner surface), the  $\Delta K$  was found to increase as the crack grew longer. The rates were predicted to be on the order of  $1E-6$  in/cycle. Likewise, the  $\Delta K$  was found to decrease in the through plate direction as 'a' approached the thin remaining ligament of 0.1 inches. The crack growth rates in the through thickness direction were predicted to slow significantly to rates below  $1E-7$  in/cycle. These predictions for the growth were also consistent with final crack shape.

From a review of the above results, the following observations could be made:

- 1) Crack growth rates per cycle would only be comparable at the surface and the deepest point when the crack was shallow in depth (<50% of the plate thickness).
- 2) As the crack got deeper, the crack growth rate at the deepest point would be predicted to be at least one order of magnitude smaller than the rate at the surface.
- 3) These predicted rates are consistent with the metallurgical findings (Reference 2.4-1).

*90 degree side*

This fracture mechanics approach was also used to evaluate the crack growth on the 90 degree side outer top hood where the crack was much longer and where the failure

occurred. In addition, the remaining ligament to only 0.03 inches compared to 0.1 inch observed on the 270 degree side. The evaluation established that the significantly higher stresses that were associated with operation after the cover plate degradation occurred would increase  $\Delta K$  leading to much higher growth rates. These rates, in turn, would produce the longer crack lengths and the deeper crack (>90% of the thickness) consistent with the much smaller remaining ligament.

The calculated crack growth rates would predict the shape of the cracks found on both the 270 and the 90 degree sides of the dryer. Therefore, the above conclusions from the fracture mechanics crack growth rate evaluation are consistent with the metallurgical results for both sides of the dryer.

## **2.5 Loading on Dryer**

This section describes the static and dynamic loads acting on dryer that may have contributed to the hood failure. The magnitude and frequency content of each load acting on dryer was determined. These loads were then used as input to structural evaluation for determining the stresses acting on the hood.

### **2.5.1 Design Basis**

The steam dryer is a non-safety component. The dryer is required to maintain structural integrity during design basis events (i.e., not generate loose parts that can prevent safety components from fulfilling their safety function during the event). The design basis for the dryer includes the normal operating condition as well as the faulted Main Steam Line Break (MSLB) pressure loading condition, including weight and seismic loads. However, the existing design basis documentation for the dryer addressed primarily the MSLB pressure differential loading as the limiting case, based on the criteria of total structural collapse or loose parts. The dryer is not an ASME code component. However, in the design basis analysis, while the ASME Section III code was utilized for the normal condition, the faulted condition was evaluated based on collapse criteria. Bounding differential pressure values were established for the critical components required to maintain structural integrity without gross collapse. The RIPD for the Quad Cities Unit 2 MSLB event in the EPU condition was bounded by the collapse pressure limits established in the design basis analysis (Reference 2.5-1).

Subsequently, the Quad Cities 2 steam dryer was modified to include perforated inserts in the dryer outlet plenum. As part of this modification, a detailed finite element stress analysis of the dryer assembly was performed and qualified to the applicable ASME code stress limits.

## **2.5.2 Loads Experienced by Dryer at EPU Conditions**

The loads experienced by the steam dryer during EPU conditions were:

- Static pressure drop loads
- Low frequency loading (0-50 Hz range)
- Mid range frequency loading (50-130Hz range)
- High frequency loading (130-230 Hz range)
- Bistable flow
- Dryer ring vertical motion
- Transient PORV loads
- Dynamic loads associated with operating in a degraded condition following the 2002 cover plate failure

Figure 2.5-1 shows a typical pressure spectrum from an operating reactor. These loads are discussed in detail in the following sections.

[[

**Figure 2.5-1: Typical Pressure Spectrum – Reactor Test Data**

]]

#### **2.5.2.1 Static and Low Frequency Loading (0-50 Hz)**

This range of frequencies includes the static flow pressure drop loads and low frequency turbulent pressure loads. Several sources of information were used to determine the dryer loading in this range of frequencies:

1. Quad Cities 2 CFD analysis (static loads)
2. Pressure data measured in the dryer region at other reactors
3. Quad Cities 2 small-scale test data
4. Loads inferred from the observed cracking

### **2.5.2.1.1 Static Pressure Drop Loads**

A CFD analysis was performed to determine the steady-state flow pressure drop loads for Quad Cities. The pressure drop across the outer hood is composed of two parts; the overall dryer pressure drop, and a pressure drop caused by the high local velocities between the dryer outer hood and the reactor vessel. The velocity is high in this region because of the relatively small area through which the steam flows as it approaches the MSL nozzles. The pressure field on the outside of the outer hood is shown in Figure 2.5-2. Figure 2.5-3 shows computed pressure drops across various sections of the dryer.

[[

**Figure 2.5-2: Pressure Field Across the Outer Hood**

]]

[[

]]

**Figure 2.5-3: Static Pressure Loading on Dryer Hoods**

#### **2.5.2.1.2 Low Frequency Loading (0-50 Hz)**

Several approaches were used to assess the magnitude of the low frequency loads experienced by the Quad Cities 2 dryer. These included loads inferred from observed cracking, scale model tests and measured plant data at other reactors. Each of these approaches is described below.

Pressure Data Measured in the Dryer at Other Reactors

The pressure data was measured at one U.S. plant and two foreign plants. In the U.S. plant, the pressure was measured by pressure drums that used strain gages. The pressure drums were calibrated in the laboratory before installation at the plant. The pressure was measured in the middle of the cover plates of the outer bank hood in the 90° and 270° azimuth (Figure 2.5-4). In the two foreign reactors the pressure sensors were located below the dryer ring, on the skirt and drain channels. For the QC2 event, it was considered more appropriate to use the pressure measurements from the U.S. reactor since the pressure sensor location was in the region of interest.

For the U.S. plant, data was taken at various power levels at steady state conditions. Data was also taken during valve closure transients. [[

]]The data at the instrumented plants showed that the low frequency vibrations vary approximately as the square of the steam flow velocity. [[

]] Thus, this scaling was based on the observed behavior of the measured low frequency signals at the tested plants.

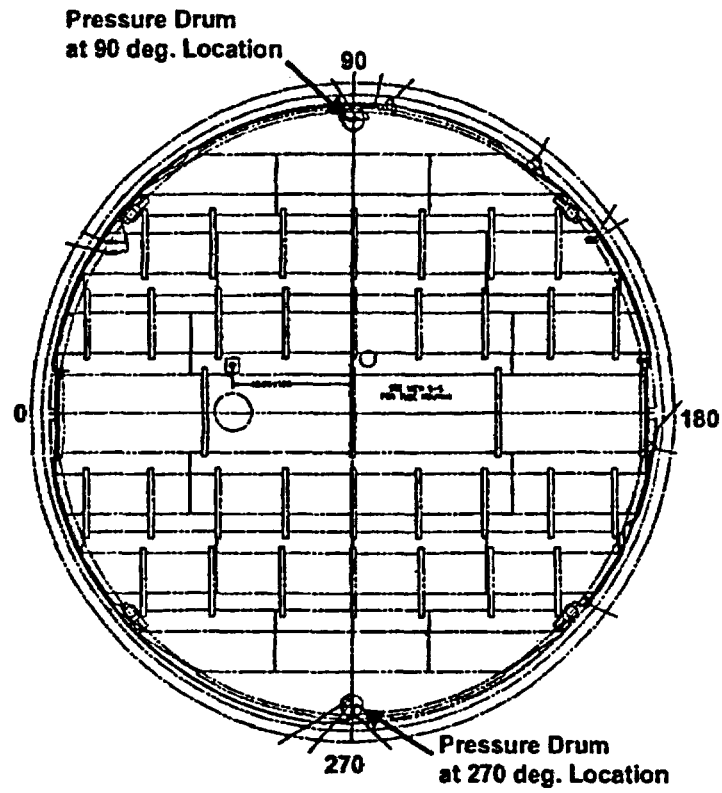


**Figure 2.5-4: Pressure Drum Locations in the U.S. Reactor**

[[

**Figure 2.5-5: Time History of Pressure in the U.S. Reactor**

]]

Quad Cities 2 Small Scale Test Data

Tests at about 1/17 scale in air, [[ ]], were performed for Quad Cities 2 at equivalent EPU conditions. The dryer, vessel and steam dome, with the MSL piping, were included in the model. The scaled low-frequency pressure results on various sections of the dryer are presented in the table below.

**Table 2.5-1: Small Scale Test Data**

[[


]]

The oscillating pressure values arrived at by scaled testing, at the cover plate [[ ]], are in the range of those determined by scaling from the actual U.S. plant at the same location. Because the plant pressure values at this dryer location agree reasonably well with the pressure values from the test model at the same location, the oscillating pressure at another location, the top of the inner hood, is scaled using the ratio of values from the test model. [[

]]The graphical representation of the oscillating pressures on the dryer hoods is shown in Figure 2.5-6. The loading on the finite element model was based on this pressure distribution.

[[

]]

**Figure 2.5-6: Oscillating Pressures on Dryer Hoods**

**Loads Inferred from Observed Cracking**

The stress required to cause the outer hood failure by fatigue was calculated based on the ASME fatigue curves. The fatigue calculation provides an alternate approach for estimating the loading experienced by the dryer. Two calculations were performed; a conservative estimate and a realistic estimate.

***Conservative estimate***

The natural frequency of the outer hood vertical plate is [[

]]

[[

.

1.

]]

2. [[

]].

#### **2.5.2.2 50-130 Hertz Range**

Based on the U.S. plant data, there is negligible pressure loading in this range of frequencies. This range of frequencies is also fairly quiescent in both the Quad Cities 2 MSL accelerometer data and the small-scale test model data. In any case, finite element spectrum analysis in this frequency range showed small stresses in the dryer.

#### **2.5.2.3 High Frequency Loading (130-230 Hz)**

Acoustic loading is the loading from standing waves that may be generated in the reactor and in the main steam lines that communicate with the outer hood region. [[

]]Based on plant measurements and scale model tests, the frequency content of the loading is in the 130-230 Hz range. Quad Cities 2 MSL accelerometer data also shows response at about 160 Hertz at QC2. However, the pressure oscillations with frequencies in this range are generally not significant because the dryer components (except the ¼" cover plate which was replaced with a ½" cover plate) do not have fundamental natural frequencies in this range. With the replacement of the lower cover plate in 2002, the QC2 dryer no longer has any sub-components in this range of frequencies, which would be excited by this loading. In the absence of dryer components with first mode frequency in this range, the loading produces small stresses. This was confirmed in whole-dryer frequency analyses and spectrum analyses with a 130-230 Hz flat spectrum load. Plant data, as well as the results from small scale testing, show that there are no significant pressure peaks above 230 Hz.

#### **2.5.2.4 Bistable Flow**

[[

]]

#### **2.5.2.5 Dryer Ring Vertical Motion**

The dryer ring is supported by the RPV on four support brackets and is free to flex between the supports. [[

]] Based on the average velocity through the dryer, the amplitudes at Quad Cities 2 are bounded by the reactor where the measurements were taken. [[

]] Because the forces vary with the square of the mass flux, the loads at Quad Cities would be about three fourths of those at the U.S. reactor. Static analyses under deadweight loading were performed to calculate the stresses resulting from this motion. The stresses were well below the endurance limit. The dryer component frequencies are well above the dryer ring motion frequency and hence little amplification from the ring motion will be present.

#### **2.5.2.6 Transient PORV Loading**

The PORV loads produce a transient pressure pulse on the outer bank hood vertical plates with the pressure distribution centered at the steam line with the valve. A PORV opening causes a rapid increase in the flow rate in the associated MSL. The flow rate increases rapidly enough to cause a decompression wave to travel back from the PORV into the reactor vessel, where it then spreads out into the vessel. [[

]]

#### **2.5.2.7 Operation in Degraded Condition**

The dryer was operated in a degraded condition for some period of time during the 2002 cover plate failure event. The dryer may have experienced several types of dynamic loading as the cover plate failure event progressed. These loadings are qualitatively discussed below.

After the cover plate to the outer hood weld cracked but before an opening occurred, the outer vertical hood may have been unsupported at the bottom. The pressure drop across the dryer face causes high stresses due to the large plate surface area. However, if a large portion of the vertical hood plate is not connected to the horizontal cover plate, the pressure drop is taken across a weakened structure, which increases the stresses in the plate and remaining welds.

After a portion of the horizontal cover plate was displaced, there is the potential for flow-induced vibration and flutter as the steam flows past the unsupported vertical outer hood plate. Since the unsupported span is long (nearly 11 feet), the vibration and flutter would cause high bending stresses at the top and sides of the outer hood.

For some period of time, the horizontal cover plate was evidently attached to the vertical hood plate by a plastic hinge at the bottom of the vertical plate. There was evidence of significant wear in the stand-off and in a portion of the cover plate where a groove about 1" by about ½" was worn away. The hinge loading and plate impact would result in additional stresses in the outer hood.

It is difficult to perform detailed analysis of the dryer stress conditions under these various stages of loadings. However, a finite element analysis of the dryer in the first loading condition (with the hood vertical plate free at the bottom) shows significantly higher stresses [[ ]] in the outer hood as compared to normal operation (see Section 2.6.4).

## **2.6 Dryer Structural Evaluation**

Stress analyses were performed to correlate the failure locations with the dryer structural response to the loads discussed in Section 2.5. Stress analyses were also performed to better understand the stresses at the locations where cracking was found for use in assessing crack propagation as discussed in section 2.4.6. Analyses were performed for:

1. Frequency calculations.
2. Dryer response to flat spectrum loading in the (0-200 Hz) excitation ranges.
3. Dryer response to normal operation flow loads due to low frequency (0-50 Hz).
  - a. Degraded dryer operation during the 2002 cover plate failure.
  - b. Dryer operation after installation of the ½-inch cover plate.
4. Dead weight load and dryer support ring fluctuations
5. Pressure load corresponding to PORV event.
6. Effect of the interior brackets (5 inch x 7 inch) with and without the postulated failure of diagonal braces.

Based on the analyses, low frequency loads in the 0-50 Hz were identified to have the potential to produce cracking at the diagonal brace attachments to the outer hood plates. The operation with failed cover plate during 2002 and the PORV events could have also played a role in the process.

### **2.6.1 Analysis model**

Finite element analyses of the dryer were performed using the ANSYS finite element Code (Version 6.1 running under the Windows 2000 operating system). The analysis

model shown in Figures 2.6-1, 2.6-2, and 2.6-3 included the dryer support ring with the cross-beams, base-plate, drain troughs, dryer hoods, and the steam dam above the dryer with its support gussets, all modeled with shell elements. The dryer vane bundles and perforated inserts were modeled as plates with sufficient stiffness for them not to interact with lower vibration modes of the dryer structure. The hood support braces and tie-bars were modeled as rectangular beams with section area and modulus equal to the section properties of the 2" × 2" × 3/8" angle irons.

The initial analysis model did not include the brackets attaching the diagonal angle irons to the hood vertical and horizontal plates. Effect of the brackets was investigated using expanded analysis model discussed in Section 2.6.7.

[[

**Figure 2.6-1: Dryer Analysis Model – Support Structure**

]]

[[

**Figure 2.6-2: Dryer Analysis Model – Dryer Banks and Hoods**

]]

[[

**Figure 2.6-3: Dryer Analysis Model**

]]

### 2.6.2 Frequency Calculations

Frequency calculations were performed with the dryer supported from the RPV dryer support brackets. The support was modeled by fixing all degrees of freedom at the dryer holddown interface (Figure 2.6-4).

The calculated component frequencies are listed in Table 2.6-1 and the representative mode shapes are shown in Figure 2.6-5.

**Table 2.6-1: Dryer Frequencies**

[[	

[[

]]

Thus, the acoustic loads in the 50 – 230 Hz range need not be considered in the root cause investigation. ]]

[[

]]

**Figure 2.6-4: Boundary Conditions**

[[

**Figure 2.6-5: Mode Shapes: Dryer Vertical Plates**

]]

### 2.6.3 Flat Spectrum Analysis

Flat spectrum analyses were performed 1) to identify maximum stress locations for the loads in the flow turbulence range (0-50 Hz), and 2) to confirm the conclusion from the frequency calculations that the higher frequency (50-200 Hz) excitations do not affect the dryer components after having replaced the ¼-inch cover plate by the ½-inch cover plate.

#### 0-50 Hz

A uniform spectrum of dynamic loads over the 0-50 Hz frequency range was applied at all the pressure bearing surfaces. The stress distributions due the applied loading are shown in Figures 2.6-6, 2.6-7 and 2.6-8. The largest stresses are calculated at the horizontal welds connecting the hood vertical plates and top plates at locations where the diagonal braces are connected to the hood plates. The second largest stresses occur at the middle regions of the horizontal welds connecting the hood vertical plates and the bottom cover plates. These stress calculations are based on the uniform spectral loads applied throughout the dryer and need to be adjusted for the pressure distributions in the dryer. However, the analyses point out that the most vulnerable dryer locations are at the horizontal welds of the of the dryer hood vertical and top plates, and the stresses from 0-50 Hz excitations are significantly higher than the stresses from 50-200 Hz excitations discussed in the next paragraphs.

#### 50-130 Hz

A uniform spectrum of dynamic loads over 50-130 Hz frequency range was applied at all the pressure bearing surfaces. The calculated dryer peak stresses were small [[ ]] compared to stresses from the 0-50 Hz flat spectrum.

#### 130-200 Hz

A uniform spectrum of dynamic load over the 130-200 Hz frequency range was applied at all the pressure bearing surfaces. The stress distribution due the applied loading is shown in Figure 2.6-9. The calculated dryer stresses [[ ]] are insignificant compared to stresses from 0-50 Hz flat spectrum loads confirming the frequency analysis results that the acoustic loads in the 130 – 200 Hz range need not be considered in the root cause investigation.

[[

**Figure 2.6-6: Hood Vertical Plate Stress Distributions (0-50 Hz Load Spectrum)**

]]

[[

Figure 2.6-7: Hood Horizontal Plates Stress Distributions (0-50 Hz Load Spectrum) ]]

[[

**Figure 2.6-8: Dryer Middle Plate and Steam Dam Stress Distributions (0-50 Hz Load Spectrum)** ]]

[[

**Figure 2.6-9: Dryer Stress Distribution (130-200 Hz Load Spectrum)**

]]

#### **2.6.4 Normal and Degraded Dryer Operation**

Analyses were performed to investigate the effects of degraded operation during 2002 when the dryer operated for several weeks with a damaged front hood cover plate on the 90-degree side. The analysis model was modified by removing the cover plate on the 90-degree side from the model. The modified analysis model is shown in Figure 2.6-10.

The normal operation flow turbulence loads calculated in Section 2.5 were applied to the analysis model as shown in Figure 2.6-10. [[

]]The loads were applied as static loads with the results used with a dynamic amplification factor when necessary.

Analysis results are shown in Figures 2.6-11 through 2.6-14. The results are shown for the dryer side with cover plate removed and the dryer side with the ¼-inch cover plate replaced by the ½-inch cover plate. Thus, the side with intact cover plate represents the dryer just before the current hood failure.

As shown in the analysis results, the removal of the cover plate affects only the dryer components in the outer hood regions. Specifically, high stresses are calculated at the bottom of the hood front plate vertical welds and at the diagonal brace attachment at the top edge of the hood front plate. [[

]]

The analyses indicate that the brace attachment location will continue to accumulate fatigue usage after the repair but the vertical weld stresses will be well below endurance limit with no further damage accumulation. Also, the cover plate failure would have decreased the pressure loads compared to the loads used in the analyses. Therefore, the stress levels and resulting fatigue usage may not be as high as indicated by the analysis results. Thus, the degraded cover plate operation may have increased fatigue usage at the top horizontal weld of the 90-degree outer bank hood but would not produce a fatigue failure in the rest of the dryer.

[[

**Figure 2.6-10: Degraded Dryer Analysis Model and Pressure Load Application**

]]

[[

**Figure 2.6-11: Degraded Dryer Stress Distribution: Inner Hood Vertical Plates** ]]

[[

**Figure 2.6-12: Degraded Dryer Stress Distribution: Bottom and Top Plates**

]]

[[

]]

**Figure 2.6-13: Degraded Dryer Stress Distribution: Outer Hood Front Plate**

[[

]]

**Figure 2.6-14: Degraded Dryer Stress Distribution: Steam Dam**

### 2.6.5 Gravity Loading and Support Ring Vibrations

Based on plant experience, the support ring may have a vertical vibratory motion of [[ ]]. Static analyses under deadweight loading were performed to estimate the stresses resulting from this motion. The dryer components are isolated from the support ring frequency. Therefore, there should be little load amplification and the stresses from the ring motion can be obtained from the deadweight stresses using deflection ratios.

Analyses were performed for an equivalent 1-g acceleration load. The analysis results are shown in Figures 2.6-15 and 2.6-16. The ring displacement from deadweight is calculated to be [[ ]] (Figure 2.6-16). Therefore, the stresses from the ring vibrations can be obtained from the stresses shown in figure using a multiplying factor of [[ ]]. The stresses are well within the ASME Code stress limit.

[[

]]

**Figure 2.6-15: Deadweight Load: Support System Deflections and Stresses**

[[

**Figure 2.6-16: Deadweight Load: Base Plates and Hood Plates**

]]

## 2.6.6 Effect of Interior Brackets

Analyses described in Sections 2.6.2 through 2.6.5 identified the flow turbulence loads as having the potential to cause fatigue crack initiation at the diagonal brace attachments to the outer hood. More detailed analyses were performed for this region to support crack initiation and crack growth analyses described in Section 2.4. Specifically, the dryer analysis model was modified to include the 5" x 7" welding brackets used to attach the braces to the hood plates.

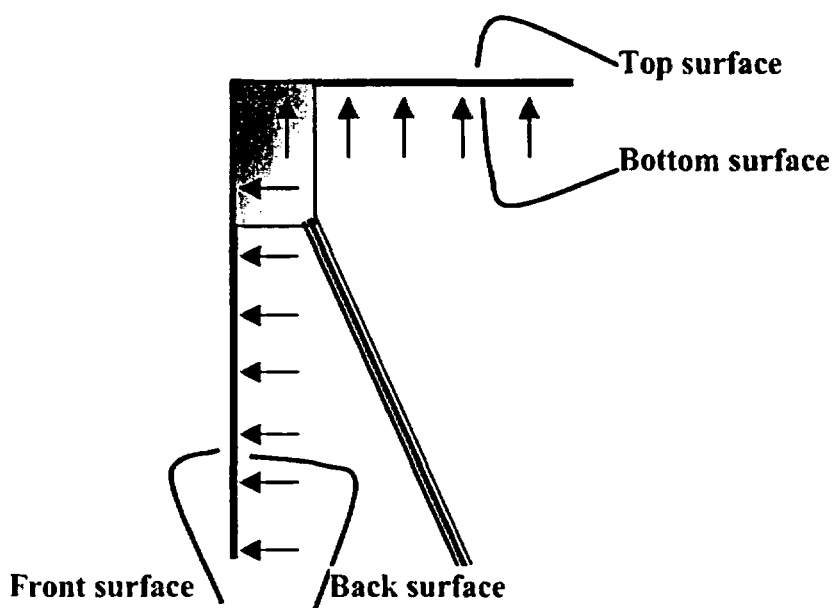


Figure 2.6-17 shows the modifications in the analysis model. The modified analysis model was used to calculate outer hood stresses for the normal operation pressure loads and the PORV event loads. The loads were applied as static loads with the results used with a dynamic amplification factor when necessary.

### 2.6.6.1 Normal Operation Pressure Load

The normal operation flow turbulence loads calculated in Section 2.5 were applied to the modified analysis model as shown in Figures 2.6-10. Inclusion of the attachment brackets in the analysis model shifts the high stress location from the horizontal weld between the hood front and top plates to the two bracket corners away from the plate weld. The relative peak stresses at the vertical plate/bracket corner and the top plate/bracket corner would depend on the presence/absence of the diagonal brace. Analyses were performed with and without the braces to help understand the role of a failed brace on gross plate failure.

Analysis results are shown in Figures 2.6-18 through 2.6-23. Highest stresses in the unfailed configuration occur at the junctions of the hood plates with the brackets connecting the diagonal braces as shown in Figures 2.6-18, 2.6-19 and 2.6-20. The stresses are bending stresses with tensile stresses on the bottom surface of the top plate

and the back surface of the vertical plate. [[

]]Dynamic stress amplification of these statically calculated stresses together with residual stresses and added stress concentrations at specific weld geometries could initiate fatigue cracks at these locations which can then grow with time. The SX-components of stresses in the top plate as shown in Figure 2.6-19 for the un-failed brace configuration are used for crack growth calculations presented in Section 2.4.6.

Figures 2.6-21, 2.6-22, and 2.6-23 show that failure of a diagonal brace would redistribute the stresses so that the top plate would have a higher peak stress compared to the vertical plate. Such a stress redistribution will also occur in the case of a partial failure of the brace connection to the bracket. Thus, crack initiation can equally occur at the connection with the top plate or the vertical plate depending on the relative extent of cracking at the bracket connections to the top plate, front plate and the diagonal brace.

#### 2.6.6.2 PORV Loads

Pressure loads from the PORV opening event were superposed on the normal pressure distribution on the outer hood front plate. The loads were applied in one of the main-steam line region on one of the outer hoods as shown in Figure 2.6-24. The stresses calculated for the PORV events are shown in Figures 2.6-25 through 2.6-27.

The actual effects of the PORV induced loads and the subsequent shutdown and startup are uncertain. However, it is clear that following these events, the steam moisture content increased significantly. This was attributed to a large opening on the 90 degree side of the dryer. Based on the failure analysis, the fatigue crack had extended a significant length from the initiating locations at both bracket locations prior to the steam moisture content increase. The added applied loads from the PORV event were calculated and used to determine the Sx components of the stress for the top outer hood plate. [[

]]The overall stress state was one of bending along with a net tensile membrane stress. Based on the metallurgical assessment, the final ductile ligament on the failed side of the dryer was approximately no more than 0.03 inches in thickness. By scaling the stresses to account for the reduced ligament, the PORV event increased the statically calculated bending and membrane stresses to failure levels. The bending stress itself would lead to measurable surface plasticity. This would in turn lead to further fatigue damage or failure. The average calculated membrane stress also led to a large predicted increase in the net section stress. This load in conjunction with dynamic load factors due to the rapid pressure loading and the presence of a discontinuity or reduced local thickness, would increase the stress beyond the flow stress, producing through-wall cracking, particularly in the vicinity of the B-side bracket region. Knowing that the fatigue crack was of substantial length and that these PORV events led to some through-wall penetration of the subsurface crack, subsequent lengthening of the crack to achieve a large opening would take place in a short time.

[[

]]

**Figure 2.6-17: Addition of Brace Attachment Brackets in the Analysis Model**

[[

]]

**Figure 2.6-18: Outer Hood Stress Intensities: Normal Operation Pressure Load**

[[

Figure 2.6-19: Outer Hood Stress Components: Normal Operation Pressure Load ]]

[[

**Figure 2.6-20: Outer Hood Stress Components: Normal Operation Pressure Load** ]]  
**(continued)**

[[

**Figure 2.6-21: Outer Hood Stress Intensities Assuming Diagonal Brace Failure:  
Normal Operation Pressure Load** ]]

[[

Figure 2.6-22: Outer Hood Stress Components Assuming Diagonal Brace Failure: Normal Operation Pressure Load ]]

[[

Figure 2.6-23: Outer Hood Stress Components Assuming Diagonal Brace Failure:  
Normal Operation Pressure Load (continued) ]]

[[

]]

**Figure 2.6-24: Normal Operation Pressure and PORV Loads**

[[

**Figure 2.6-25: Outer Hood Stress Intensities: Normal Operation Pressure and  
PORV Loads** ]]

[[

Figure 2.6-26: Outer Hood Stress Components: Normal Operation Pressure and PORV Loads ]]

[[

Figure 2.6-27: Outer Hood Stress Components: Normal Operation Pressure and  
PORV Loads (continued) ]]

## 2.7 Root Cause Evaluation

The potential root causes identified in Section 2.1 were:

- Material and fabrication issues
  - Weld defects
  - Poor quality plate material
- Thermal fatigue
- Fatigue due to pre-EPU operation
- Intergranular stress corrosion cracking (IGSCC)
- Dryer support ring deflection
- Bi-stable flow
- Damage from 2002 cover plate failure
- Transient loading due to power operated relief valve (PORV) operation
- Pressure loading from increased steam flow at EPU conditions
  - Flow induced vibration (FIV) at low frequency (0-50 Hz)
  - Flow induced vibration (FIV) at medium frequency (50-130 Hz)
  - Flow induced vibration (FIV) at high frequency (130-230 Hz)

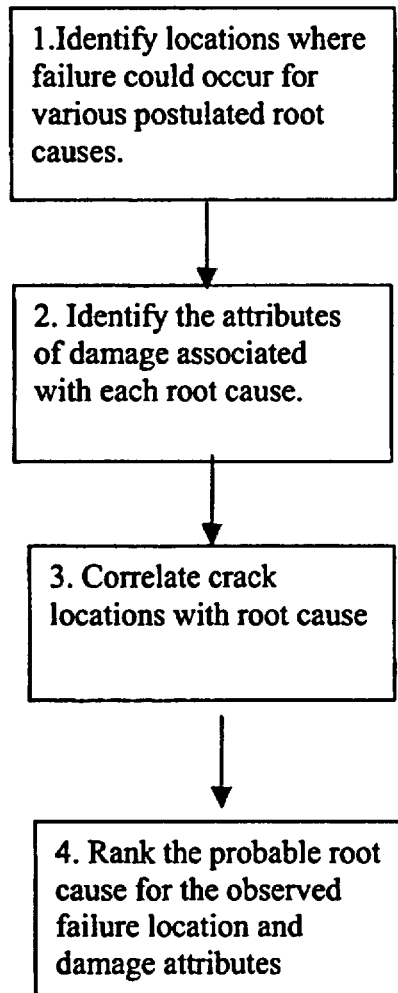
The visual examinations and metallurgical analyses in Sections 2.3 and 2.4 concluded that the failure was due to high cycle fatigue. These analyses eliminated the material and fabrication issues as potential causes. These analyses also eliminated IGSCC as a potential cause.

The dryer is in the steam region in the vessel where the temperature is constant during normal operation. Since the dryer does not experience rapid temperature oscillations, thermal fatigue was also eliminated as a potential cause.

Fatigue due to pre-EPU operation is unlikely, given the long operating time at pre-EPU conditions without failure. Since both the 2002 and the 2003 failures occurred at EPU conditions over a relatively short period, the fatigue most likely occurred during EPU operation.

Prior to the actual inspection and subsequent metallurgical analyses, a root cause assessment was undertaken to postulate all factors and locations that could lead to steam moisture content increase. This assessment made use of the process flow map given below (Figure 2.7-1). It led to a prioritization of the factors as given in Table 2.7-1.

**Table 2.7-1: Root Cause Evaluation Process Map**



Step 1. Identify locations where failure would occur for various postulated root causes.

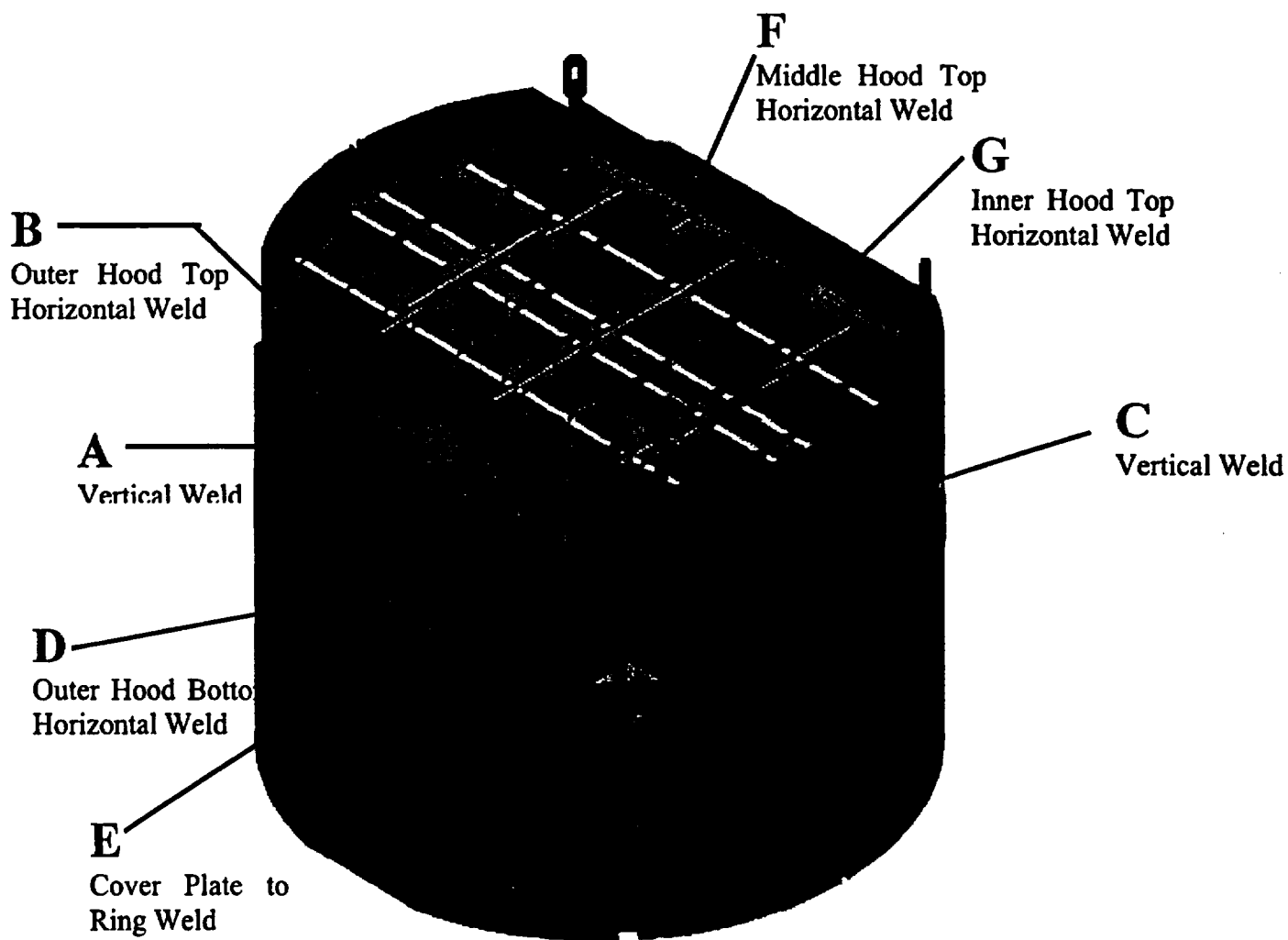
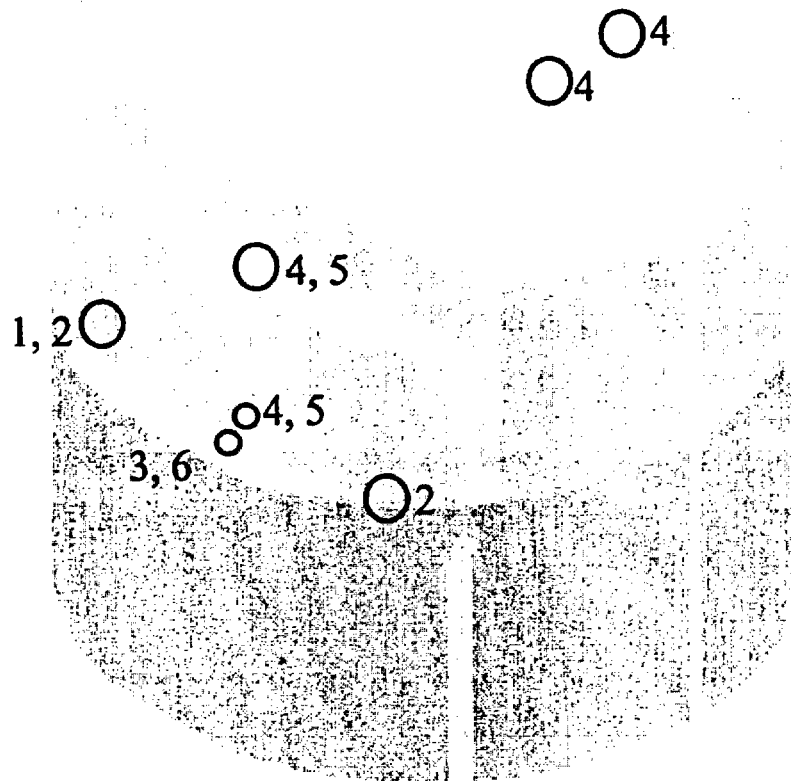


Figure 2.7-1: Possible Crack Locations



**Figure 2.7-2: High Stress Locations For Various Root Causes**

Root Cause Number	Root Cause
1	Transient (PORV)
2	Degraded Dryer Operation with cracked cover plate
3	Acoustic Loading (High Frequency)
4	Low Frequency (0-50 Hz)
5	Bi-stable flow
6	Dryer Ring Vertical Motion

Step 2. Study the attributes of damage associated with each root cause

Attributes of damage

1. Crack length
2. Location
3. Evidence of fatigue
4. Ductile tearing
5. Original Weld Quality
6. Health of surrounding material
7. Signs of impact loading
8. Discoloration
9. Loose parts

Root Cause Number	High Stress Location (See Figure 2.7-2)	High Displacement Location	Failure Mode Appearance	Additional Features	Crack Length	Carryover Symptoms
1	Corner of A and D	Yes (denting)	Ductile + Fatigue (vertical seam)	Pizza Size in-line with MSL (pushed in or out)	Long	Jump
2	Corner of A and D; Corner of C and D	NA	Fatigue	Need to confirm Initiation location was bottom	Long	Slow or Jump
3	E at center	NA	Fatigue	Unexpected	Moderate	Slow or Jump
4	D at center	NA	Fatigue		Moderate	Slow or Jump
5	B at Center	NA	Fatigue	Static, unexpected	Short	Slow increase
6	E at Center					

Step 3. Correlate crack locations with root cause

Observed Location	Possible Root Cause	Primary cause ranking
A <sub>bottom</sub>	1, 2	2
B	4, 5	4
C <sub>bottom</sub>	2	2
D	4, 5	4
E	3, 6	3
A+B <sub>bottom</sub>	1, 2, 4, 5	4
A+B <sub>top</sub>	4, 5	4
C+D	2, 4, 5	4
A+D	1, 2, 4, 5	4
D+E	2, 3, 4, 5, 6	3
A+B+C	4, 5	4
A+C+D	1, 2, 4, 5	2
F, G	4	4

Step 4. Rank the probable root cause for the observed failure location and damage attributes

Root Cause Number	Root Cause	Probability
1	Transient (PORV)	Contributing Factor
2	Degraded Dryer Operation with cracked cover plate	Contributing Factor
3	Acoustic Loading (High Frequency)	Low
4	Low Frequency	High
5	Bi-stable flow	Low
6	Dryer Ring Vertical Motion	Low

With this early assessment as a basis, it was possible to use the information from the visual examination to develop the first elements of the root cause. Given that the cracking location was found to be the top outer hood plate (Location B), the primary factors would be expected to be the low frequency loading in combination with the loading during the 2002 time when the cover plate was degraded. Using the more detailed information from the metallurgical examination in Section 2.4, it was possible to confirm that the failure was due to high cycle fatigue. Based on the loads evaluation in Section 2.5, low frequency pressure loading is the most likely source of the loading that caused the fatigue failure. The observed crack initiation locations and crack growth trajectories correlate well with stress distributions calculated in Section 2.6. The additional understanding gained from comparing the crack growth in the Hood A side with the observed cracks in the Hood F side of the dryer substantiates the conclusion that operation with the degraded cover plate in 2002 was a major contributing factor. As described in Section 2.6.6.1, a diagonal brace failure would have increased the stresses on the top plate; this may account for the cracking observed on the top of Hood A. The PORV loading evaluation in Section 2.6.6.2 shows that the additional loading during the PORV events was sufficient to fail a substantial length of the top surface ligament associated with a long subsurface fatigue crack. Upon re-start, the cracking would progress much faster leading to a large opening and the observed increase in steam moisture content.

### 2.7.1 Source of Low Frequency (0-50 Hz) Loading

In Section 2.5.2.1.2 of this report it was concluded that the likely source of the of the low frequency oscillations is the MSLs. To get a better understanding of the source of low frequency loading three independent evaluations were conducted:

- Acoustic Circuit Analysis of the Main Steam Lines
- Analysis of the frequency content of the Quad Cities MSL Vibration Data
- Calculation of the most likely main steam line component frequencies

#### 2.7.1.1 Acoustic Circuit Analysis of Main Steam Lines

Acoustic circuit analysis uses analytical techniques similar to finite element modeling to model fluid systems to identify potential sources of low frequency pressure waves, acoustic drivers, nominal vibration frequencies and the transfer functions.

The Quad Cities main steam lines system (Figure 2.7-3) was modeled.

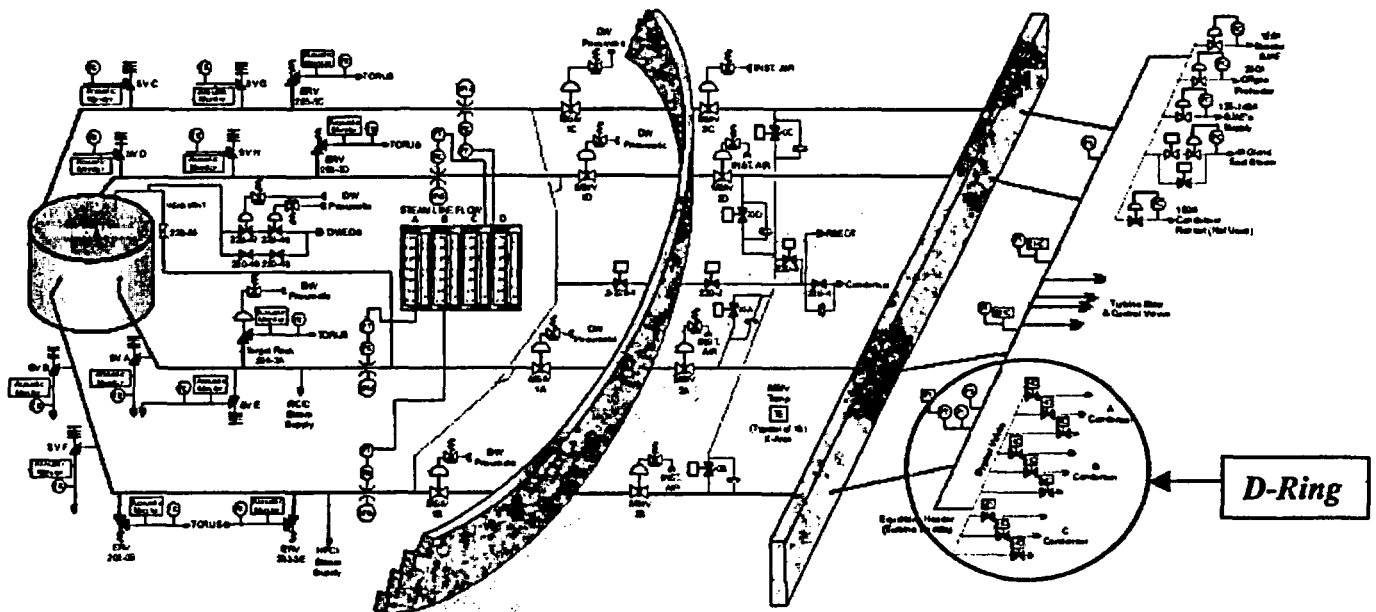


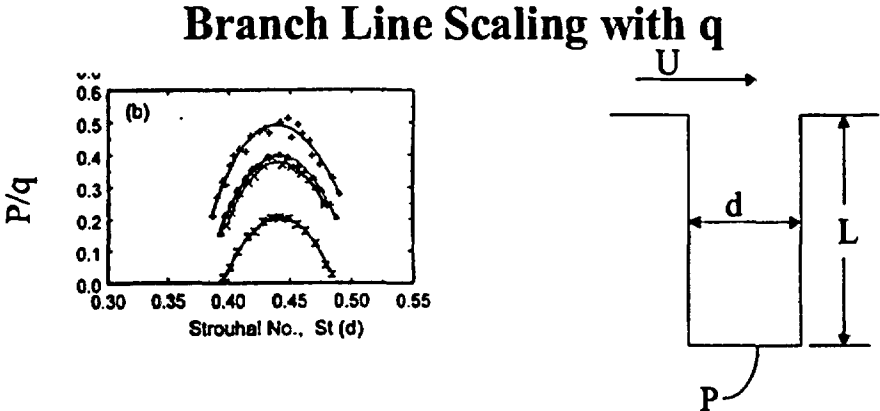
Figure 2.7-3: Quad Cities Main Steam System

The Model inputs were as follows:

- Reactor Vessel Steam Volume – 6,635 cubic feet
- Reactor Pressure - 1,050 psig

- Steam Acoustic Speed – 1,600 ft/sec
- Frequency Range Analyzed – 0 to 130 Hz
- MSL Steam Velocities – 205 ft/sec
- As-build and Design Drawings for Quad Cities MSL

The Acoustic Circuit Analysis uses the Strouhal number and branch line opening shape to determine acoustic response (Figure 2.7-4).



**Acoustic Modeling Results**

The results show that the most likely component to produce low frequency pressure oscillations in the 0-50 Hz range is the MSL D-ring or equalizing header [[  
]]It should be noted that the results are within  
a 10% frequency band. The results are shown below in Figure 2.7-5.

[[

**Figure 2.7-5: Acoustic Circuit Modeling Results**

]]

### **2.7.1.2 Frequency Content of MSL Vibration Data**

As a check of the acoustic circuit analysis a review of the frequency content of the Quad Cities MSL Vibration data was conducted. The results show that the main frequencies for Quad Cities Unit 2 in the 0-50 Hz range are as follows:

[[

]]

The results for both Quad Cities Units 1 and 2 are shown in Figure 2.7-6. The results are fairly consistent with Acoustic Circuit Analysis evaluations with the addition of [[ ]] as a possible frequency to be considered.

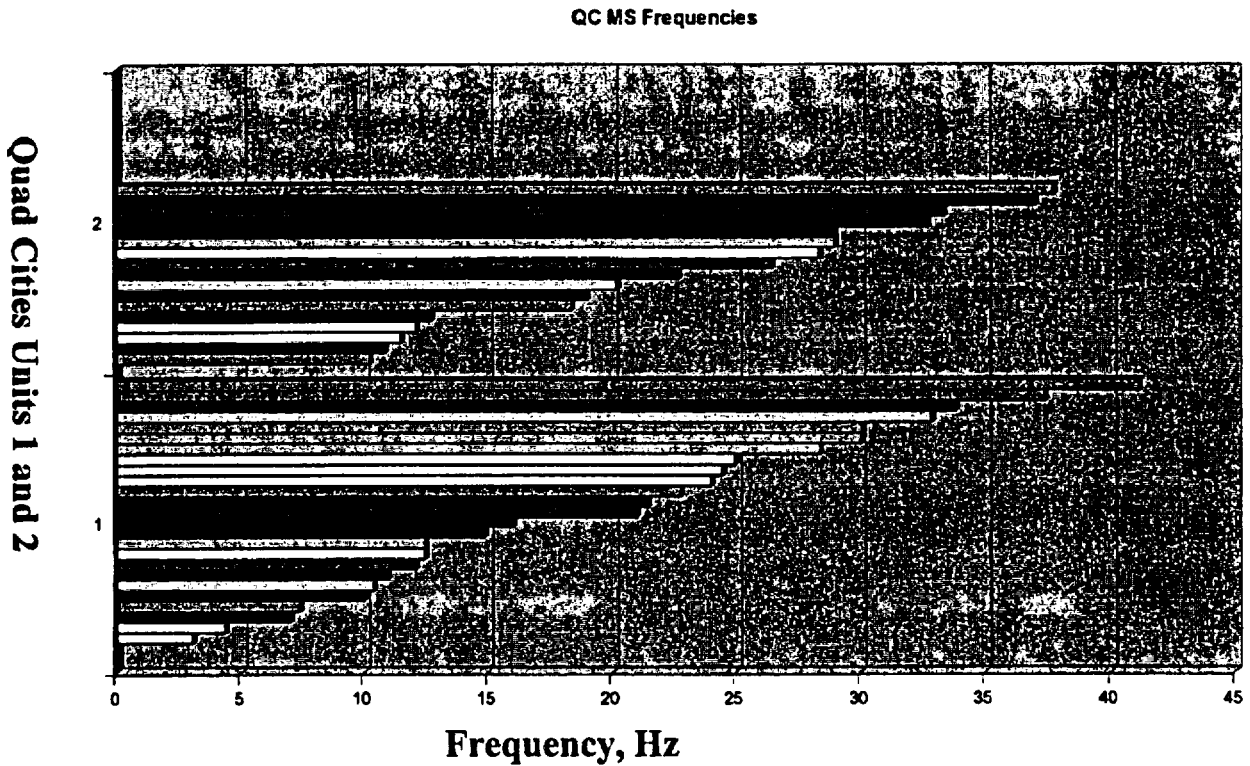


**Figure 2.7-6: MSL Vibration Frequency Content**

### **2.7.1.3 Main Steam Line Component Frequencies**

A further step to validate the acoustic model was to calculate the natural frequencies of the most likely MSL component that possibly could contribute to the observed Quad Cities Unit 2 frequencies. The results are as follows and appear to be consistent with acoustical circuit analysis and Quad Cities 2 observed MSL frequencies:

[[

]]

#### **2.7.1.4 Finite Element Model Evaluation**

To validate that the dryer structural response for the most likely loading frequency, a finite element model was run with a [[ ]]dynamic load. This evaluation included the possible variability in plate and uncertainty in the acoustic modeling.

The result of this evaluation produced almost identical results as the 0-50 Hz flat spectrum analysis shown in Section 2.6 of this report.

### **2.8 Conclusion**

The cause of the dryer failure is postulated to be high cycle fatigue resulting from low frequency pressure loading on the outer hoods during normal operation. The pressure loading is thought to be amplified by the geometric configuration of the main steamlines. The cracks in the hoods and braces are most likely to have been initiated during steady-state EPU power operation. The cracks continued to grow until the transient pressure loads from the stuck open relief valve and subsequent manual valve openings opened the cracks through-wall, leading to the increased steam moisture content. The previous cover plate failure in 2002 subjected the dryer structure on the 90° side to significant additional loading. The most likely sources of the low frequency pressure oscillations are the MSL D-ring in a frequency range from [[ ]].

### **3. Extent of Condition**

The EPU evaluations for components in the steam and feedwater flow path were reviewed in light of the dynamic loading experienced by the dryer. The review included reactor internals, main steamline piping, and main steamline components. The components in the steam and feedwater flow paths were screened for the effect of EPU changes on the components. Consideration was given to the lessons learned from the dryer root cause evaluation. The significant operating condition changes for EPU are:

- Increased steam flow
- Increased feedwater flow
- Higher feedwater temperature
- Increased recirculation pump vane passing frequency
- Increased steam carryunder

Since low frequency acoustic loading was identified as the root cause of dryer failure, these reviews focused on the component response to flow induced vibrations and, where applicable, acoustic vibrations. The CFD results indicated that the flow velocity over the surface could increase the pressure difference across the component; therefore, the screening also considered potential changes to the reactor internal pressure difference loading. The screening also included components in the steam and feedwater flow path for which the original EPU evaluations had concluded there was no significant impact due to EPU conditions. The results of the screening matrix are shown below.





The screening identified components where further analyses would be useful in strengthening the EPU evaluations in light of the experienced gained from the root cause evaluation. Since the root cause for the dryer failure was determined to be high cycle fatigue from loads experienced during normal operation, these additional evaluations only considered normal operating conditions. The duration of transient and accident conditions is too short to accumulate the type of fatigue observed in the dryer failure. Section 3.1 documents the reactor internals assessment. Section 3.2 documents the assessment for the steamline components.

### **3.1 Reactor Internals Assessment**

This assessment addressed all the major internals in the reactor vessel, including all the components in the feedwater and steam flow paths. The location of components is shown in Figure 3.1-1. These reviews focused on the component response to flow induced vibrations. The CFD flow evaluation identified increased reactor internal pressure differences (RIPD) in some locations of the dryer due to the flow field over the dryer hoods. Therefore, this assessment also reviewed the RIPD load definitions for the reactor internals for similar situations where the RIPD load definitions could potentially be higher based on a more detailed consideration of the flow field.

#### **3.1.1 Flow Induced Vibration**

Quad Cities 2 has a BWR/3 reactor with 251-inch diameter vessel. In accordance with GE policy and later NRC Regulatory Guide 1.20, the first plant of a given type (prototype plant) is extensively instrumented and tested for vibration. Dresden 2 is the prototype plant for BWR/3 251 plants. The reactor internal components of Dresden 2 were extensively instrumented and data was collected at various core flows along two rod lines. Due to the differences in jet pump riser brace designs, the Dresden 3 and Quad Cities 1 and 2 reactors were also instrumented. This assessment is based on measurements obtained during the in-reactor vibration tests conducted at all the plants. Measured data and operating experience from other plants were also used when necessary.

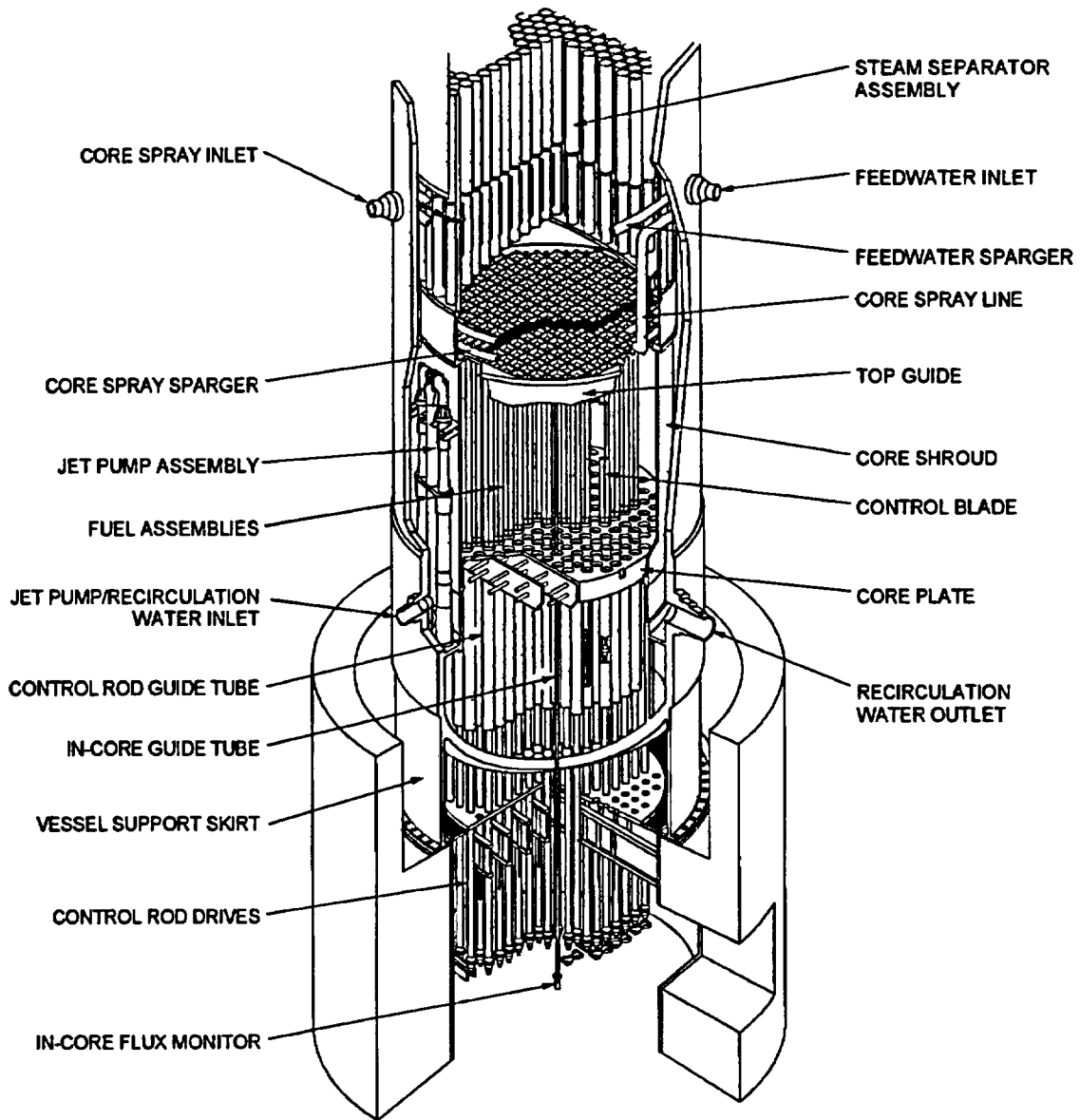


Figure 3.1-1: Major Reactor Internal Components

The components that were identified as being susceptible to flow-induced vibration in the original design basis for BWR/3 251 size plants, components which encountered problems in the field due to flow-induced vibrations (FIV), and new mitigation components added subsequent to the original design, were considered in the original evaluation. Subsequently all the components in the steam flow path and feedwater flow path were considered in the evaluation. The critical components affected by flow-induced vibration were originally identified and instrumented in the original design basis. The following major components which were instrumented at the prototype plant were evaluated for balanced flow conditions in the power uprate region: shroud, shroud head and separator assembly, jet pumps, control rod guide tubes, in-core guide tubes and fuel channels. In addition, the steam dryer and the jet pump sensing lines (JPSL) were also evaluated. The steam dryer is a non-safety related component. The JPSL is not affected by power uprate but by increased recirculation pump speed. These two components were evaluated as they have encountered problems in the field due to flow-induced vibrations. There is no plant specific measurement data on these two components. The steam dryer was evaluated using the test results from a domestic BWR and two foreign BWRs. The jet pump sensing lines were evaluated using the test results from GE's High Flow Hydraulic Facility.

This section is divided into two parts: (a) Original evaluation based on instrumented components in the original design basis including components affected by Recirculation pump vane passing frequency and (b) Subsequent evaluation of components in the steam and feedwater path.

### **3.1.1.1 Original Design Basis Evaluation of Instrumented Components**

The objective of this evaluation was as follows: For those safety related reactor internal components that are affected by power uprate, extrapolate the maximum vibratory stresses in the EPU region from existing vibration data and assess whether or not they are within the acceptance criteria. Output from the reactor internals vibration evaluation is used in PUSAR Section 3.3.5. In addition, a separate evaluation is made for components affected by recirculation pump vane passing frequency (VPF).

In order to monitor the vibration amplitudes during reactor operation, strain gages, accelerometers and displacement transducers (which can withstand the reactor operating temperature and pressure) were installed on selected reactor internal components in the Dresden/Quad Cities (D/QC) reactors prior to startup. The sensors' responses in the form of varying voltage were recorded on magnetic tapes and displayed on paper charts. The results and conclusions in reports [Refs. 3.1-3 to 3.1-5] were derived from a detailed post-test analysis of the taped information. In the data analysis subsequent to the field tests, the measured vibration amplitudes at dominant frequencies were compared to the allowable limits derived from the natural vibration modes of the component. For each vibration frequency, the location of the highest stress was identified and the allowable

vibration limits for all the gage locations were established from the corresponding analytical mode shape. The vibration limits were determined by setting the maximum zero to peak stress amplitude of the mode to 10,000 psi, including the effects of stress concentration. This stress limit used for Type 304 steels of BWR internals is lower than the most conservative value allowed by the current ASME Section III design codes for the same material [Ref. 3.1-6]. The ASME value is 13,600 psi for service in excess of  $10^{11}$  cycles.

Vibration measurements were made during pre-operational, pre-critical and power operational conditions. Data were collected for several core flow rates, power levels (rod lines), and for balanced, unbalanced and transient flow conditions.

The D/QC reactor internals vibration measurement reports [Refs. 3.1-3 to 3.1-5] were first reviewed to determine which components were likely to have significant vibration in the EPU region. The vibration data of the components chosen for further evaluation were analyzed at balanced flow test conditions at the 75% and 100% rod lines to determine the expected vibration response in the power uprate region. The vibration amplitudes at various frequencies at these two test points were extrapolated to 2957 MWt thermal power and 108% core flow. The extrapolated vibration amplitude response at EPU condition was compared with the acceptance criteria to obtain the percent criteria for each mode. The percent criteria for all modes were absolute summed. The extrapolated vibration peak amplitude responses in the power uprate region were compared with the GE vibration acceptance criterion.

The evaluation results at the uprated condition for each of the components identified are presented below. The sensor locations and test results referred to below pertain to the startup tests conducted at D/QC.

Core Shroud: Displacement gages D1, D2, D3 and D4 were installed at Dresden-2 to measure shroud tangential motion. At Dresden-3, displacement gage D3 was installed to measure radial motion while velocity sensors V1, V2 were installed to measure the tangential motion at the top of the shroud. At QC1, accelerometers A1, A2 and displacement gage D3 were installed to measure shroud tangential motion. At QC2, displacement sensors D1, D2, and D3 were installed to measure shroud radial motion.

[[  
]]Because of the low level of vibrations, there is no concern for vibration under power uprate conditions.

Shroud Head and Separator Assembly: At Dresden-2, velocity sensors V1, V2, V3, and V4 were installed at the separator to measure tangential motion. [[  
]].

To assess whether or not the separator flow induced vibrations are acceptable during power uprate, it is necessary to determine how the excitation mechanisms change during

power uprate. There are basically two sources of excitation, namely, flow turbulence and the periodic forces generated by the swirling motion of the flow through the separators. The magnitudes of the turbulence excitation change with the square of the separator velocity. Because there are no distinct peaks or valleys in the turbulence excitation spectrum, the separator, shroud head, and shroud assembly will vibrate at the structural system natural frequencies. Since the structural natural frequencies are not changed by higher steam flow rates, the vibration frequency will be the same irrespective of the power level. The higher steam flow rates corresponding to 117.8% of original licensed core thermal power only results in higher vibration amplitudes at the structural natural frequencies.

For the periodic excitation forces, the magnitude increases with the square of the velocity while the forcing frequency increases linearly with the flow velocity. Examination of the response spectrum of the shroud/separator sensors shows that there is insignificant response at the calculated periodic forcing frequency [[ ]]. Thus, it can be concluded that the shroud/separator vibration is mainly from flow turbulence. The above conclusion is used to determine the shroud/separator vibration amplitudes.

Separator flow velocity calculations show an increase of the maximum velocity by about [[ ]] for the EPU condition as compared to the rated condition. Since the vibration amplitudes are expected to increase by the square of the separator inlet flow velocity, the vibration amplitudes are expected to increase [[ ]]. Since the maximum vibration amplitude reached during startup testing of the D/QC plant was no more than [[ ]] of the acceptance criteria, it can be readily concluded that shroud separator vibration amplitudes during power uprate will be within the acceptance criteria.

Control Rod Guide Tube (CRGT): At Dresden-2, Strain gages SG-9, SG-10, and SG-12, were installed to measure axial strain on the CRGT. There were no sensors at Dresden-3, QC1 and QC2 plants. For the control rod guide tubes, the maximum axial vibration strains under any flow condition, are less than [[ ]] of the acceptance criteria. Thus, the strains are very low. Since the vibration amplitudes in this region are mainly a function of core flow, the stresses are expected to remain well within the 100% acceptance criteria under power uprate conditions.

In-Core Guide Tube (ICGT): At Dresden-2, strain gages SG-13, SG-14, and SG-16 were installed at two ICGT's to measure the axial strain resulting from bending of the ICGT. There were no sensors on the ICGT at D3, QC1, or QC2.

For the ICGT, the maximum axial vibration strains of ICGT's, under any flow condition, are less than [[ ]] of the acceptance criteria. Since the vibrations in this region are mainly a function of core flow, the responses at power uprate conditions are expected to remain well within the 100% acceptance criteria.

**Jet Pump Assembly:** A total of 8 sensors, which included 2 displacement sensors and 6 strain gages were installed on selected jet pumps during Dresden-3 start up testing. The displacement sensors measured the vibration of the jet pump elbow, and the strain gages mounted on the upper and lower riser braces (thin and thick riser braces) measured the riser pipe motion.

For balanced flow conditions, test point H-11 at ~75% rod line and 100 % core flow, and test point H-34 at ~100% rod line and 97.9% core flow were used to extrapolate to uprated region (2957 MWt). This yielded a predicted maximum response of less than [[ ]] of the acceptance criteria except during possible D2 riser brace resonance with the vane passing frequency (VPF) of the recirculation pump.

**Fuel Assembly:** Three strain gages were installed on D2 fuel channels to measure axial dynamic strains. [[

]]The strain gage sensors failed before power ascension. However, test results from power tests at other plants show that the fuel channel vibrations are less than [[ ]] of the criteria during power operation also. Hence, based on the pre-critical test results from D2 and the power test results from other plants, vibration responses at power uprate conditions are expected to be well within the 100% acceptance criteria.

[[

]]

**Jet Pump Sensing Line:** The analysis of jet pump sensing line (JPSL) concerns and effects of increased pump speeds are described in SIL 420 and SIL 551. In 1987 GE determined that the JPSLs are susceptible to failure due to vane passing frequency effects. Sensing lines are connected to the jet pump diffusers to measure pump flow. There have been instances where either the sensing line has broken or the weld that attaches the line to the diffuser has broken. These failures were attributed to fatigue when the vane passing frequency of the recirculation pump coincides with the natural frequency of the sensing line. Broken sensing lines are detectable and do not require prompt shutdown of the reactor. In order to detect disassembly of a jet pump, at least one jet pump sensing line for each pair on a riser must be intact. Core flow measurement

accuracy is also affected by loss of a sensing line but usually the impact on the accuracy is small for one or two broken lines.

At D/QC, the recirculation pumps have six vanes. [[  
]]. A detailed dynamic analysis was performed to find the natural frequencies of the JPSLs under water.

Although prior inspections have shown no sensing line cracking (with the exception of QC1 JPSL #7, which failed for other reasons), D2, D3, QC1 and QC2 units have some potential for resonance in the current operating speed range. Operating at higher pump speed will move the VPF away from the natural frequencies of some JPSL's and closer into the second mode natural frequencies of other JPSL's. JPSL's 1/11, 2/12, 3/13, and 10/20 have the potential for resonance with the VPF of the recirculation pumps. JPSL clamps have already been installed at Quad Cities 2 to mitigate this problem.

JPSL cracking does have economic impact, but does not directly affect safety. Failure of a sensing line can be detected and thus no specific consideration of the sensing line is necessary from a plant safety viewpoint.

Jet Pump Riser Brace: With EPU, the drive flow increase needed to overcome the increased core pressure drop may require a small increase in recirculation pump speed and hence the VPF. An increased VPF may cause it to become closer to the second natural frequencies of the riser braces. It may also cause the VPF to become further from the second natural frequencies of the riser braces. Due to hydrodynamic coupling, the second mode of the riser brace leaves is an in-phase mode and therefore easier to excite than the first out-of-phase mode. If the VPF does become closer to the natural frequencies, the vibration loads on the riser brace will become higher. In particular, if the natural frequency of the riser brace leaves coincides with the vane passing frequency resulting in a resonance condition, the vibration levels in the riser brace leaves could exceed the allowable values and therefore must be evaluated. SIL 551, "Jet Pump Riser Brace Cracking" also addresses this issue of VPF and riser brace resonance.

In the MELLLA operating region, prolonged operation of the recirculation pump speed could happen near the expected resonance speed [[  
]]for some of the Dresden 2 riser brace leaves. Such prolonged operation near a resonance speed may result in significant fatigue usage factor accumulation. If the accumulated fatigue usage factor exceeds 1.0 by a significant amount, riser brace crack initiation may occur.

To understand the effects of vane passing frequency (VPF) on the jet pump riser braces at the D/QC plants, it is first necessary to compare the differences in the riser brace designs at these four plants. Table 3.1 describes the riser brace design configurations for the different Exelon BWR3 plants. [[

]].

**Table 3.1-1: Riser Brace Designs**

[[



For Quad Cities 1 and 2, the riser braces are much thicker [[ ]]when compared to the Dresden 2 riser braces and therefore have natural frequencies much higher than the maximum VPF. Thus, the QC riser braces are acceptable for EPU without any pump speed limitations.

Dresden 3 (D3) had significant cracking in the thinner two leaf riser brace. It is believed that the cracking was initiated by IGSCC or vibration fatigue. Subsequent propagation was due to vibration fatigue. However, the cracking did not present any structural safety concerns since D3 has a second redundant brace (thicker single leaf riser brace). The presence of the thicker brace at D3 means that the jet pump is still adequately supported even if all the thin riser leaves are broken. The thicker brace leaves at D3 are identical to the QC riser brace leaves in design. The thicker riser brace leaves natural frequency is well outside the range of the VPF and hence they will not go into resonance with the VPF. Thus, it is concluded that D3 riser braces are acceptable for EPU without any limitation on recirculation pump speed.

Dresden 2 (D2), on the other hand, has one thin double leaf riser brace and does not have the redundant thicker single leaf brace. The thin riser brace leaves have the possibility of resonance with the VPF. An inspection of the Dresden 2 jet pump riser brace leaves during the October, 2001 outage revealed a crack at the vessel end of the upper leaf of jet pump No. 9. This failure appeared to be due to high cycle fatigue. The safety aspect of operating with a cracked riser brace leaf at D2 was assessed, and it was shown that there were no safety concerns and that D2 can continue to operate for another cycle. The safety assessment was consistent with the conclusions of BWRVIP-06 and BWRVIP-28, both approved by the NRC. At the next outage, a repair clamp will be installed at jet pump No. 9. Recirculation pump speed restrictions were also put in place as a pro-active measure to avoid damage to other jet pump riser braces. At the upcoming outage, clamps will be installed on all jet pumps as a proactive measure.

### **3.1.1.2 Reactor Internal Components in Steam and Feedwater Flow Path**

In this section, the structural adequacies of reactor internal components in the steam and feedwater flow paths, subjected to flow induced vibration (FIV) loads, are assessed. For each component evaluated, the geometry of the component is first described. The method used to determine its lowest natural frequency, including any finite element model details, is then described. Finally, the FIV load is used to determine the structural adequacy of the component. In lieu of the above analytical evaluation, FIV test data, where available, is used to demonstrate the structural adequacy of the components in the steam or feed water paths. The adequacy evaluation for each component is described below.

#### **3.1.1.2.1 Feedwater Sparger**

The feedwater sparger is a non-safety component (BWRVIP-06). A typical feedwater sparger is shown in Fig. 3.1-2. In the early 1970's several BWRs experienced cracking of feedwater nozzles and spargers. These early failures were resolved by reducing the leakage of cold feedwater past the thermal sleeve to RPV nozzle safe end connection. Reducing the leakage of colder water eliminated the RPV nozzle blend radius rapid cycling fatigue cracking and the flow induced vibration observed in early BWR feedwater spargers. All the Dresden and Quad Cities feedwater spargers are of the improved interference fit sparger design with triple thermal sleeves installed in place of the original loose fit feedwater spargers. The improved sparger was tested extensively for flow induced vibrations, and shown to be acceptable for generic BWR application.

The main cause for the feedwater sparger vibration is the leakage flow past the gap between the safe end and the thermal sleeve. [[

]]Thus, it can be concluded that the feedwater sparger is structurally adequate for FIV based on a total FW viewpoint.

Finally, the NRC reviewed and agreed to the generic application of the improved sparger in NUREG-0619 (Ref. 3.1-10).

In addition to leakage flow induced vibration, consideration was given to the effects of feed water pump pressure fluctuations at the vane passing frequency (VPF) of the FW pump on the feedwater sparger vibration response. The FW pump is a multi-stage high

pressure centrifugal pump. Thus, the pressure fluctuations tend to have random and multiple peaks. Furthermore, the FW pumps are far from the reactor and the FW goes through FW preheaters on its path to RPV. Therefore, it is likely that the pressure pulsations at the VPF will be greatly diminished. Thus, any pressure pulsation effects at the VPF will be negligibly small.

In summary, test data for the improved feedwater sparger show that it is not likely to be affected by the flow induced vibration due to the higher flow rates resulting from EPU.

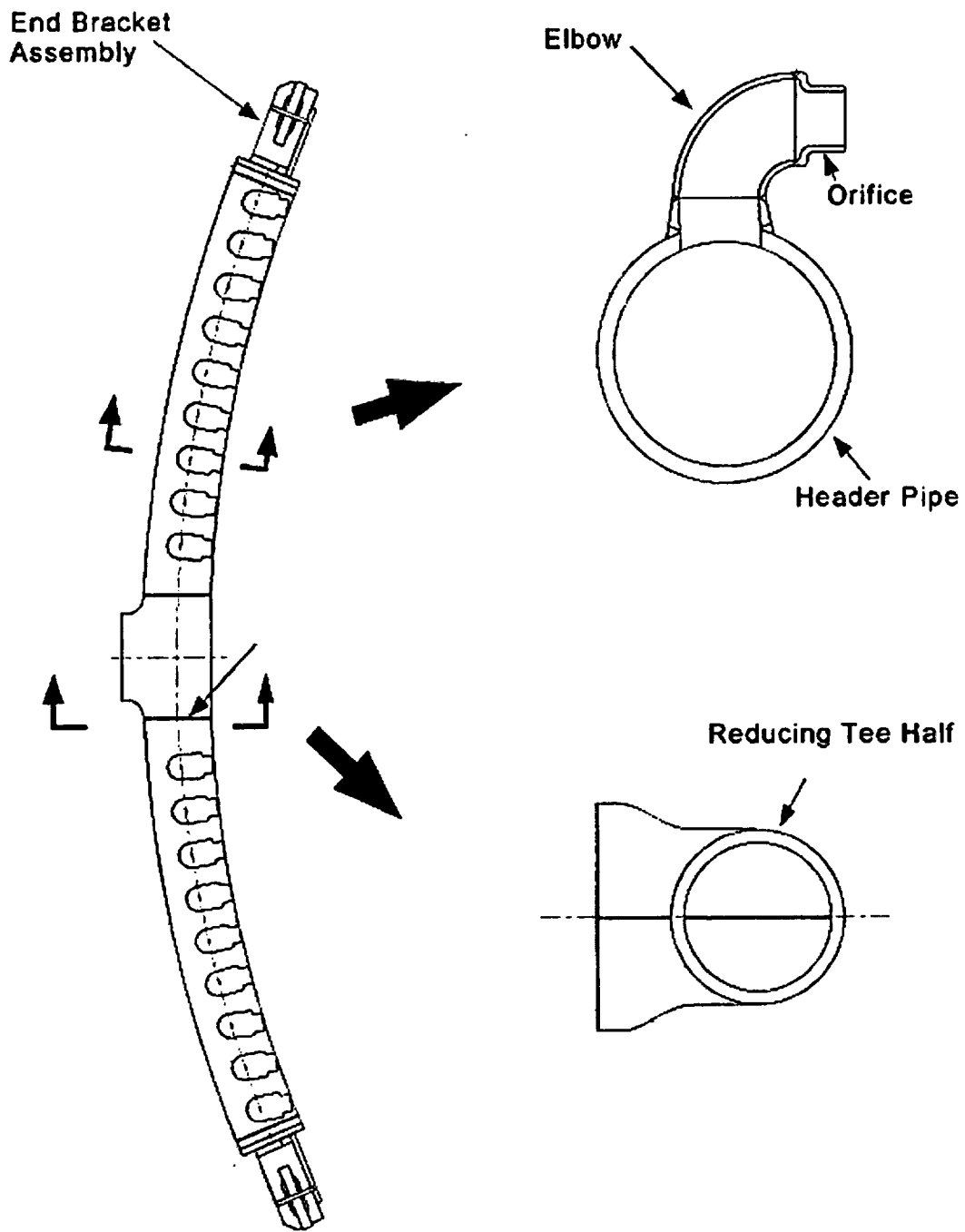


**Figure 3.1-2: Typical Feedwater Sparger**

### 3.1.1.2.2 Steam Dryer Guide Rods

The two steam dryer guide rods are mounted on brackets welded to pads on the RPV wall. The guide rods guide the travel of the steam dryer during removal and installation.

The steam dryer guide rods are fabricated from Type 304 stainless steel. Most of the length of each guide rod consists of a solid 3.0 inch diameter bar. The steam dryer guide rod has an unsupported length of approximately 181 inches. There are two steam dryer guide rods, which are located at 0 and 180 degree azimuth. Each guide rod is supported by two vessel brackets. Shown in Figures 3.1-3 and 3.1-4.

Assuming the guide rod has a fixed-end condition at the two support brackets, and using the material properties at 547°F, the calculated first mode natural frequency is [[ ]]. This frequency is calculated using a closed-form solution (Reference 3.1-11).

The guide rods for the steam dryer are in the regions of stagnant steam and water. The bottom of the guide rod is above the feedwater sparger, and water in this region has eddy flows, but no significant velocity. The mid section of the rod stays in the annulus formed by the dryer skirt and the vessel wall. In this region, there is no flow. The portion of the rod that is exposed above the steam dryer may experience some steam velocity, because the steam flow in the steam dome may not be symmetric all the time. The guide rods are at 0 and 180 degree azimuth locations and the steam outlet nozzles are near 90 and 270 degree azimuth locations. Therefore, theoretically at the 0 and 180 degree locations the expected steam velocity is zero. However, the turbulent flow in the steam dome would not allow such zero velocity points. The steam velocity is expected to be much lower than the other areas in the steam dome. A major portion of the guide rod is in the steam region, with the bottom of the rod above the feedwater sparger. These steam dryer guide rods are in the regions of stagnant steam and water. Thus, it is expected that the flow-induced vibration of the guide rod would be negligibly small.

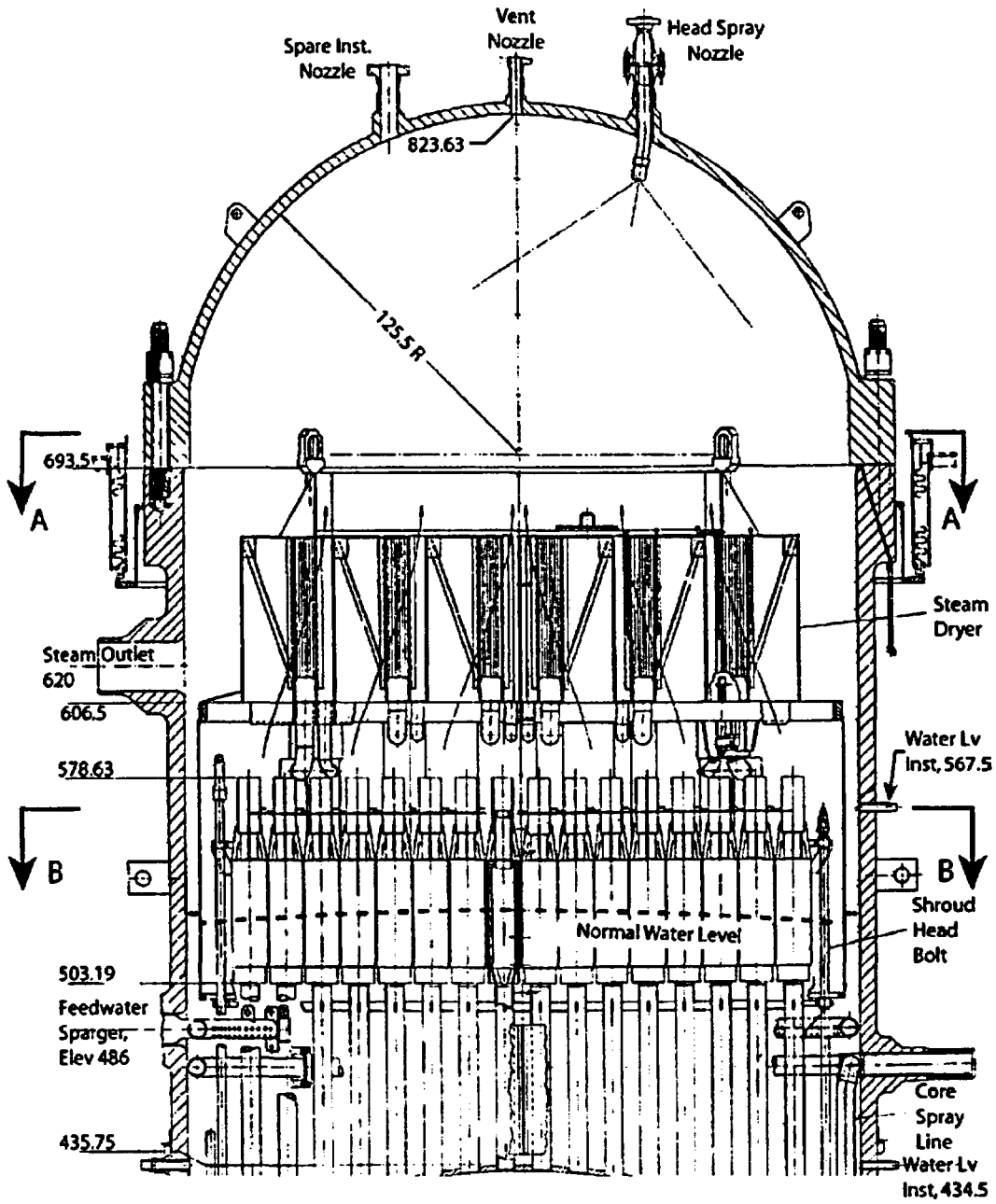


Figure 3.1-3: Upper RPV Region Showing Dryer Guide Rod

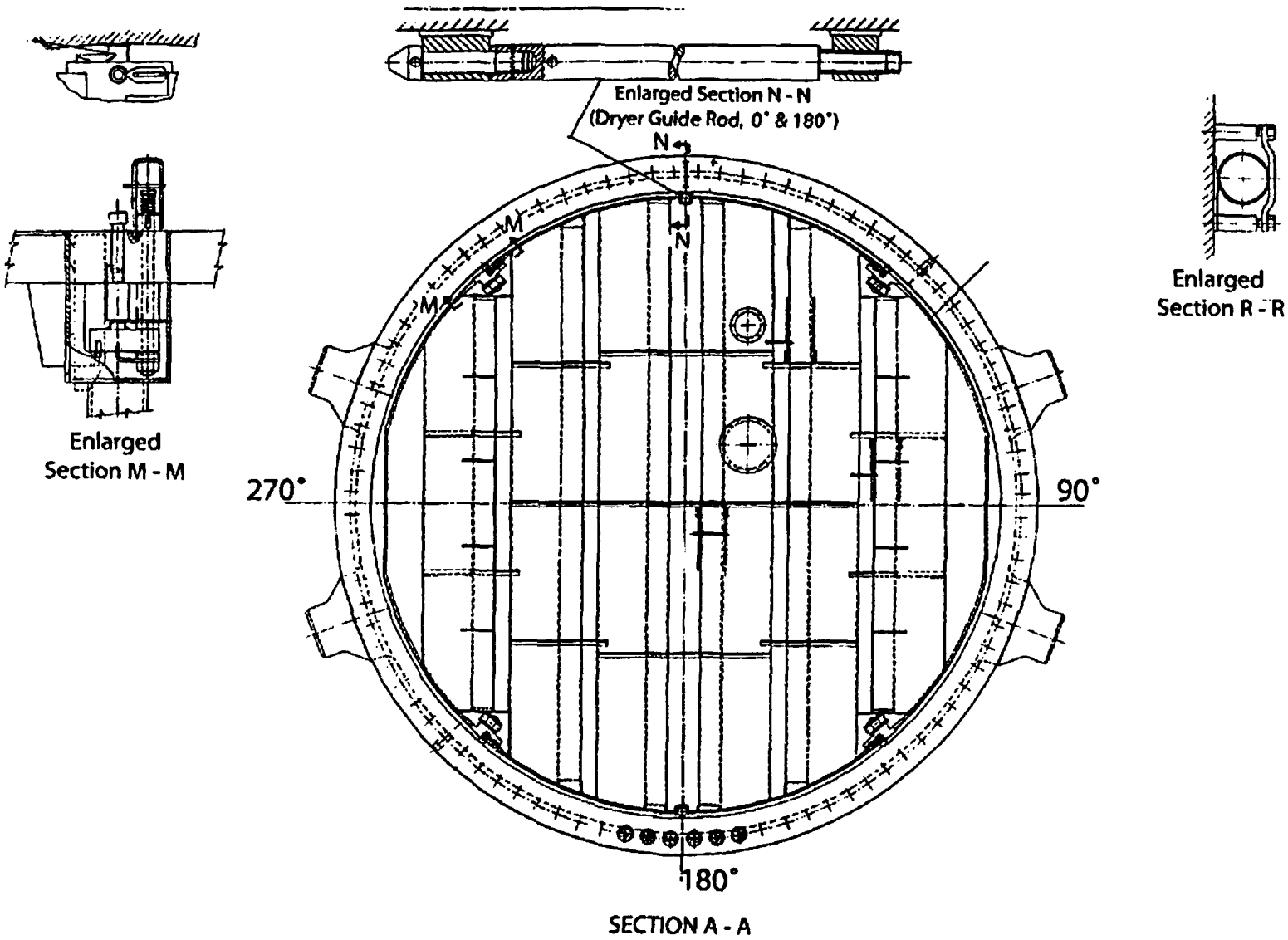


Figure 3.1-4: Dryer Guide Rod Azimuth Orientation

### 3.1.1.2.3 Shroud Head Guide Rods

The two shroud head guide rods guide the travel of the shroud head and separator assembly during removal and installation. The shroud head guide rods (see Figure 3.1-5) are each mounted on an upper bracket welded to a pad on the RPV wall, and on a lower bracket welded to the top of the shroud. The shroud head guide rods are fabricated from Type 304 stainless steel. Most of the length of each guide rod consists of a solid 3.0 inch diameter bar. The unsupported portion of the shroud head guide rod is about 89 inches. The major portion of the guide rod is below the water level.

To calculate the shroud head guide rod natural frequencies, the effect of the water on guide rod vibration is accounted for using the concept of 'hydrodynamic mass' (Reference 3.1-12). Assuming the guide rod has a fixed-end condition at the two support brackets, and using the material properties at 529°F, the calculated first mode natural frequency is [[ ]]. This frequency is calculated based on a closed-form solution (Reference 3.1-11).

The shroud head guide rods are in regions above as well as below the feedwater spargers. The flow condition in the region above the feedwater spargers is described above for the guide rods for the steam dryer. The flow in the region below the feedwater spargers increases when approaching the bottom of the rod, which is near the shroud head flange. Near the shroud head flange, the water velocity is calculated [[ ]]. As a result of EPU, [[ ]]. The core flow rate is unchanged for EPU conditions; however, the increased steam CU at EPU conditions may result in a slight increase in the water velocity. As a result of increased CU, the void occupied by the steam increase, [[ ]]. Using conservative assumptions. This conservatively calculated velocity is used for flow-induced vibration evaluation.

By conservatively assuming the [[ ]] flow velocity over the entire length of the guide rod, two bounding flow induced vibration evaluations are made: (a) cross flow induced vibration and (b) parallel flow induced vibration.

For the cross flow induced vibration evaluation, the vortex shedding frequency is calculated to be [[ ]]. Since the guide rod natural frequency [[ ]] is more than three times higher than the vortex shedding frequency, it is expected that the cross flow induced vibration will be small (Reference 3.1-13)

For the parallel flow induced vibration evaluation, the response equation as presented in Reference 3.1-14 (Burgreen equation) is used. The calculated maximum vibration stress is about [[ ]] which is small compared with the allowable of 10,000 psi (Reference 3.1-15).

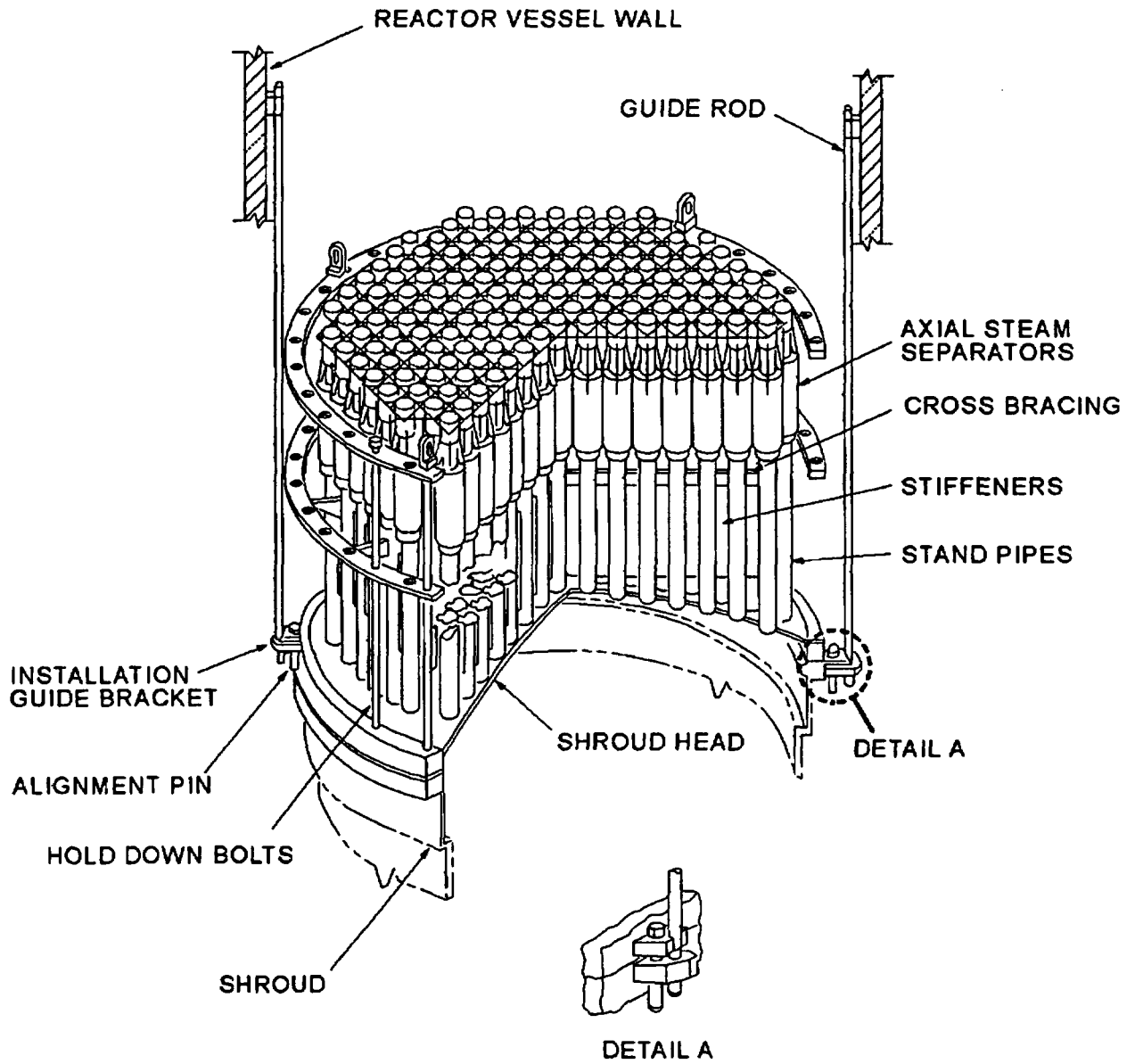


**Figure 3.1-5: Typical Shroud Head Guide Rod**

### 3.1.1.2.4 Top Head Instrument Nozzle

The spare top head instrumentation nozzle, shown in Figure 3.1-6, has a blank flange installed on the 6-inch weld neck flange.

The instrumentation nozzle is shown in Figure 3.1-6, which is located at zero degree of the RPV. The lowest natural frequency of the instrumentation nozzle is calculated to be [[ ]]. The dryer steam flow is towards the 90 degree and 270 degree section of the RPV. Therefore, theoretically the steam flow velocity at the instrument nozzle is zero. Thus, the stress due to flow induced vibration is deemed negligible.

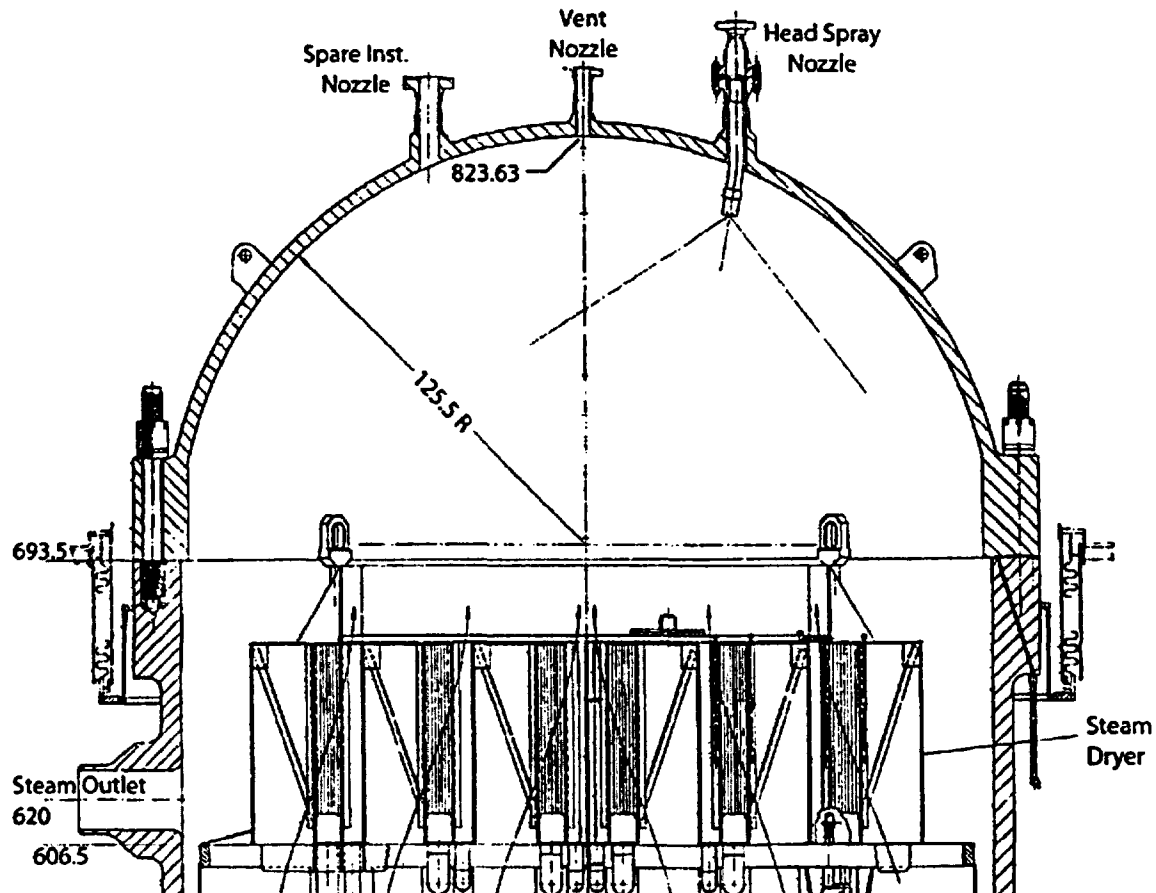


Figure 3.1-6: Top Head Nozzles

### 3.1.1.2.5 Head Spray Nozzle

The RPV head spray pipe and nozzle configuration prior to the removal of the head spray pipe is shown in Figure 3.1-6. The head spray pipe has been removed and the nozzle has a blank flange installed on the 6-inch weld neck flange. The head spray nozzle is located at 180 degree of the RPV. The lowest natural frequency of the head spray nozzle is calculated to be [[ ]]. The dryer steam flow is towards the 90 degree and 270 degree section of the RPV. Therefore, theoretically the steam flow velocity at the head spray nozzle is zero. Thus, the stress due to flow induced vibration is deemed negligible.

### 3.1.1.2.6 Top Head Vent Nozzle

Natural frequencies of the top head vent nozzle were calculated using a 3-D finite element model. The lowest natural frequency was [[ ]], and is higher than the FIV and acoustic loading frequencies from 0 to 230 Hz. Therefore, the top head vent nozzle will be structurally adequate from a vibration view point at EPU conditions.

### 3.1.1.2.7 Core Spray Sparger

The four core spray spargers' function is to provide a uniform distribution of core spray flow over all fuel bundles to assure long term core cooling. The core spray spargers are mounted on the inside of the upper part of the core shroud. The core spray sparger headers are 4.0 inch Schedule 40S pipe, fabricated from Type 304 austenitic stainless steel. Each header is equipped with a large number of stainless steel spray nozzles. Each header pipe is supported by brackets attached to the inner wall of the shroud, at approximate 35 degree increments.

The core spray spargers are off the direct flow stream from the core. Because of this, only secondary eddy flow may exist around the core spray spargers. Near the periphery of the core, the velocities of water and steam are much lower than the middle of the core. [[

]]After EPU, the core is managed to have less radial power peaking, and therefore the periphery has higher power, higher steam quality, and higher steam velocity. The core flow rate is unchanged at EPU conditions; however, the increased steam flow at EPU conditions may result in an increase in eddy flows.

When the above flow reaches the core spray spargers, the flow velocity magnitude is expected to be about [[ ]] of those quoted above. Except for the secondary flow induced by the flow in the periphery of the core exit, no other significant flow is expected in this area. The very low flow velocity indicates that FIV adequacy is assured during EPU operation.

### 3.1.1.2.8 Fuel Assembly

The basic mechanical design used for the fuel assemblies (fuel bundles and channels) is generic to all jet pump BWRs. The plant operating conditions used in the fuel assembly design are bounding for Quad Cities at EPU conditions because the generic design must be applicable to plants with higher core powers and core flows than Quad Cities. The bundle power is constrained by fuel rod thermal-mechanical limits and the bundle thermal-hydraulic characteristics. These constraints are independent of core power. Therefore, the maximum power that can be generated by the peak power bundle is unchanged for EPU and the flow conditions in the peak bundle are unchanged for EPU. The peak power bundle flow induced vibration conditions bound the other bundles with lower power.

The GE14 reference bundle was tested for flow induced vibration effects. The tests were conducted [[  
]]The FIV test program included three steady state test conditions as well as one flow sweep test.

[[

]]

The test results from GE14 were compared to a GE12 reference bundle FIV test. Based on this comparison the GE14 FIV performance was deemed acceptable.

In addition to the flow tests, which show the adequacy of the fuel assembly for EPU conditions, core design considerations also assure the FIV adequacy of the individual bundles. This is because the fuel assemblies are designed for plants with higher core flows than Quad Cities. The maximum power generated by the peak bundle is unchanged for EPU. Therefore, the FIV response in the peak bundle is unchanged with EPU. The peak bundle FIV bounds the other bundles with lower power per bundle.

### 3.1.1.2.9 Steam Separators

The fixed axial flow type steam separators have no moving parts and are made of stainless steel. In each separator, the steam-water mixture rising through the standpipe impinges on vanes which give the mixture a spin to establish a vortex where in the centrifugal forces separate the water from the steam in each of three stages. The steam leaves the separator at the top and passes into the wet steam plenum below the dryer. The separated water exits from the lower end of each stage of the separator and enters the pool that surrounds the standpipes to join the down comer annulus flow.

The Quad Cities shroud head and steam separator assembly uses 219 GE Model 65M axial flow steam separators. Each steam separator is mounted on a 6-inch schedule 40 stand pipe. The array of standpipes and steam separators are braced laterally. A typical shroud head and steam separator assembly is shown in Figure 3.1-5 and a typical steam separator is shown in Figure 3.1-7. The 65M separator has an inner barrel ([[ ]]), a middle tube with skirt ([[ ]]) and an outer tube ([[ ]]). At the top of the separator is the pre-dryer tube ([[ ]]). From the bottom of the skirt to the top of the pre-dryer is about [[ ]] in height. Because the GE Model 65M steam separators at the QC plants were judged to be structurally very robust, no vibration tests were performed on them. Only thermal hydraulic tests were completed during the steam separator development tests.

With the introduction of a smaller diameter and more flexible BWR/6 steam separators (Model AS2B), extensive vibration tests were conducted. The AS2B separator has an inner barrel ([[ ]]), and an outer tube with skirt ([[ ]]). From the bottom of the skirt to the top of the separator is about [[ ]]" in height. The results of the BWR/6 separator FIV testing (Ref. 3.1-17) has shown that the expected maximum flow induced vibration stress is around [[ ]] which is under GE allowable stress of 10,000 psi.

In order to calculate the flow induced vibration response of the Model 65M separator, the structural dynamic characteristics are established first and then they are compared with those of the Model AS2B separator. Structurally both steam separators are composed of a number of concentric cylinders with ring segments and radial struts. Finite element models using SAP4G07V beam element (Reference 3.1-16) are developed for both separators. [[ ]]

[[ ]]It is seen that first natural frequency of Model 65M separator is about two times higher than that of the Model AS2B separator. The finite element model predicted AS2B separator first model natural frequency [[ ]] is in very good agreement with the test measured first model frequency of [[ ]] (Ref. 3.1-17).

It is assumed that the turbulence flow induced forcing function established from the Model AS2B separator test condition is also applicable to the Model 65M separator. The magnitude of the forcing function is then adjusted according to the dynamic pressure head ( $\rho U^2$ ). It is noted that the steam/water velocity,  $U$ , inside the 65M separator is about [[ ]] of that inside the tested AS2B separator. The steam/water density,  $\rho$ , inside the 65M separator is about [[ ]] of that inside the AS2B separator. The analytic calculated peak stress response of the Model 65M separator is about [[ ]], much less than the conservative GE allowable stress of 10,000 psi. Thus, it can be concluded that the QC2 Model 65M separator FIV performance is acceptable during EPU conditions.

The steam separators are subject to temperature and flow mixing effects from the feedwater flow. The interior separators in the array will experience a lesser effect of mixing than the outer row of separators. With EPU, the feedwater flow and temperature increase results in a decrease in the surface temperature gradient in the standpipe. The change in the gradient could range from a potential decrease of approximately 16°F (assuming the feedwater impinges on the separator with no mixing) to an increase of approximately 2°F (assuming the feedwater completely mixes with the downcomer water before impinging on the separator). While the decrease in thermal gradient is beneficial from the point of view of secondary stresses, the effect of the minimal potential increase in temperature gradient is insignificant. Because of the increase in feedwater temperature at EPU conditions, the maximum temperature range for thermal oscillations due to turbulent flow and incomplete mixing is reduced with EPU operation. Also, the steam separators have no known structural problems related to temperature or flow effects in Quad Cities Unit 2 or in other plants of similar size with larger feedwater flow and power output. Thus, EPU is not expected to have any detrimental effect on the structural integrity and functionality of the steam separators.

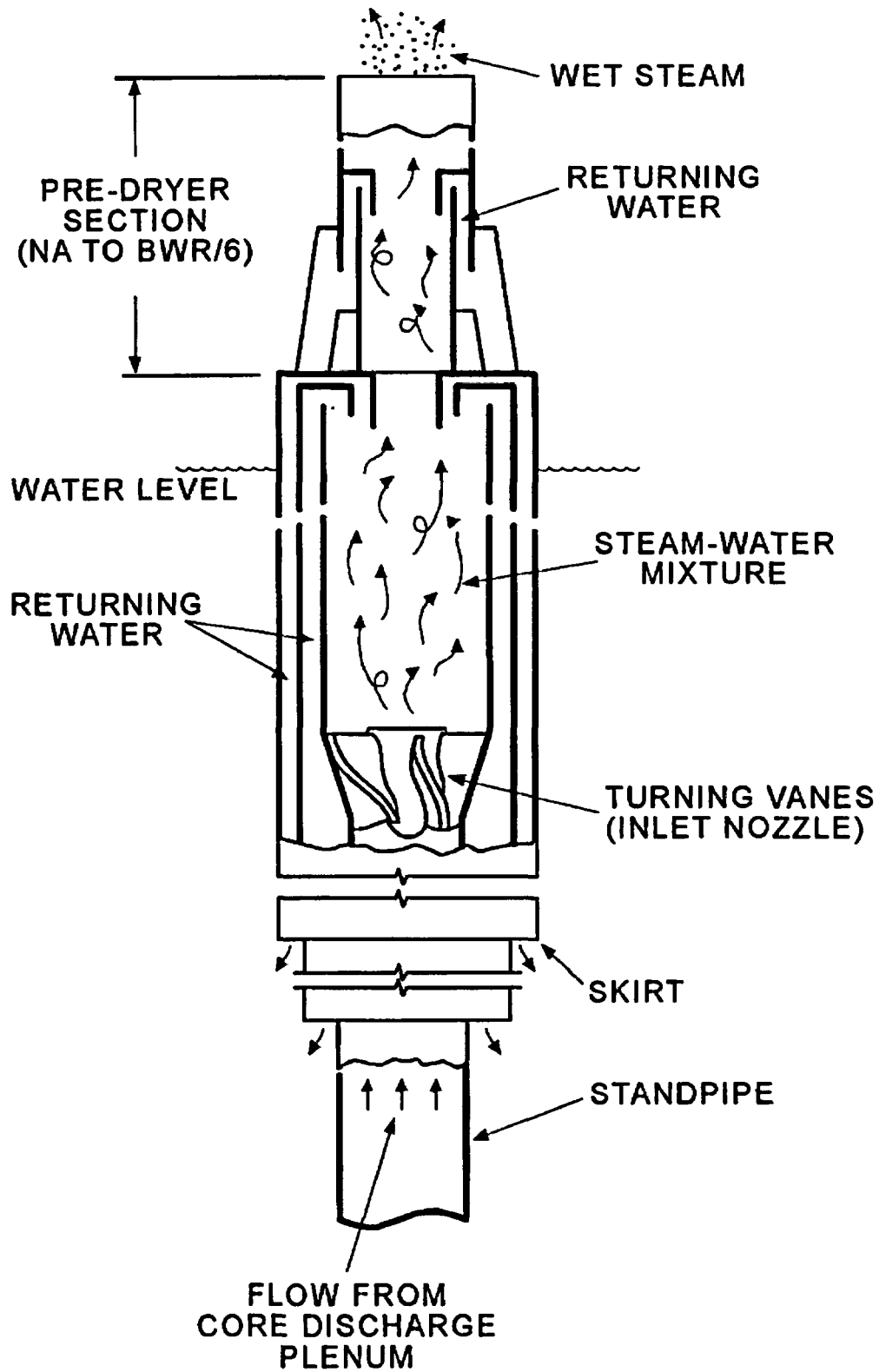


Figure 3.1-7: Typical Steam Separator

### 3.1.1.2.10 Shroud Head Bolt

The shroud head bolts have supports at three level: the upper bolt ring, the middle bolt ring and the shroud head flange. The length from the upper bolt ring to the shroud head flange is about 151 inches. On the outside of the bolt is a sleeve, which is made of 2.5 inch Schedule 160 type 304 stainless steel pipe. The feedwater sparger is situated at the middle section of the shroud head bolts and is about 4.6 inch away from the bolt.

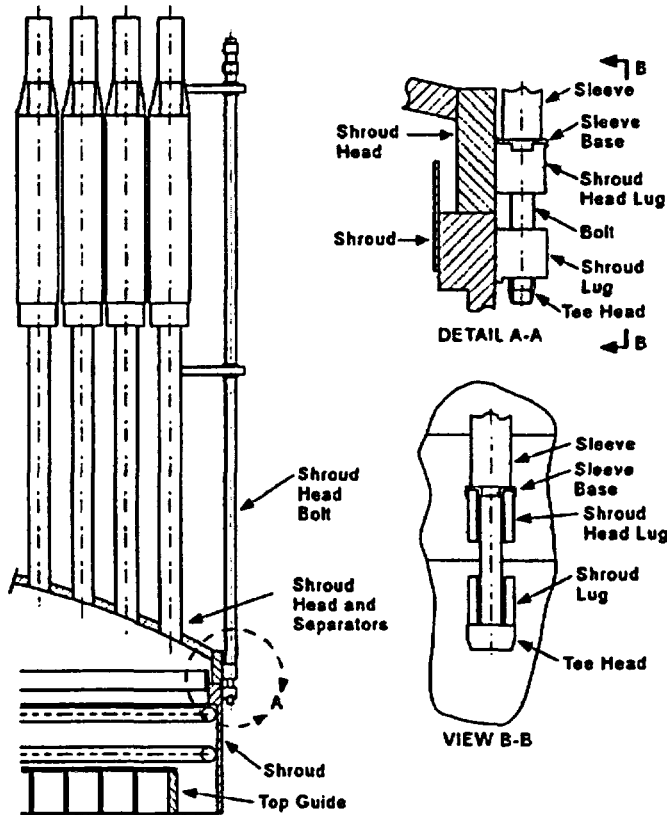


Figure 3.1-8: Typical Shroud Head Bolt

Jets issuing from the top mounted elbows of the feedwater spargers impinge upon the middle section of the shroud head bolts. The jet velocity at the feedwater sparger elbow exit is calculated to be about  $[[ \quad ]]$ . When these jets reach the shroud head bolts, which is about 4.6 inches away, the jet expands, and the velocities are reduced to  $[[ \quad ]]$  depending on the size of the orifice at the outlet of the top-mounted elbows. The larger orifice size provides higher velocity at the shroud head bolts. The jet velocity at the higher range of  $[[ \quad ]]$  is used for flow induced vibration evaluation.

Assuming a clearance at the middle bolt ring, and fixed-end conditions at the top bolt ring and shroud head flange support, the calculated first mode natural frequency is [[ ]]. This frequency is calculated using a SAP4G07 finite element model (Reference 3.1-16). This calculated frequency using a finite element model is in complete agreement with that calculated based on the closed-form solution (Reference 3.1-11). The effect of the water is accounted for using the 'hydrodynamic mass' (Reference 3.1-12). Also, structural material properties and water density at 529<sup>0</sup>F are used in this frequency calculation.

For the flow induced vibration evaluation, the procedure as established in Reference 3.1-13 is used with the upper bound flow impinging velocity of [[ ]]. [[ ]]

]]Due to the proximity of the cross flow vortex shedding frequency to the fundamental structural frequency of the shroud head bolt sleeve, the lock-in phenomenon is assumed to occur, and thus resonant vibration amplitude is used to calculate the cross flow induced vibration stress. The stress is calculated to be [[ ]].

The above calculated cross flow stress occurs at the vortex shedding frequency and is along the lift (perpendicular to the flow) direction. There is also an oscillating drag (in-line) force which occurs at twice the vortex shedding frequency and the magnitude of the oscillating drag force is about one-tenth of the oscillating lift force (Reference 3.1-13). [[ ]]

]]This total flow induced vibration stress is below the allowable stress of 10,000 psi. Thus, it is concluded the shroud head bolts are structurally adequate to withstand the effects of flow induced vibration at EPU condition. Please note that the above calculation uses the upper bound flow velocities and is thus conservative.

The shroud head bolts are preloaded predominantly by the differential thermal expansion between the Inconel and stainless steel components of the bolt mechanism. With EPU, the feedwater flow and temperature increase. The change in temperature that the shroud head bolts may experience due to EPU could range from a potential increase of approximately 16°F (assuming the feedwater impinges on the bolt with no mixing) to a decrease of approximately 2°F (assuming the feedwater completely mixes with the downcomer water before impinging on the bolt). While the potential increase in temperature is beneficial from the bolt preload point of view, the effect of the minimal potential decrease in temperature is insignificant. Because of the increase in feedwater temperature at EPU conditions, the maximum temperature range for thermal oscillations due to turbulent flow and incomplete mixing is reduced with EPU operation. Thus, the structural integrity and functionality of the shroud head bolts are maintained in the EPU condition.

### 3.1.1.2.11 Core Spray Piping

Two internal core spray piping runs connect the RPV core spray nozzle thermal sleeves with the core spray sparger ring headers located inside the core shroud. A typical arrangement of internal core spray piping is shown as Figure 3.1-9.

As described in Section 3.1.1.2.3, EPU conditions may result in a slight increase in the water velocity. The core spray pipe experiences a similar flow field as the shroud guide rods below the feedwater sparger. The maximum water velocity may increase from about 7[[ ]].

The Quad Cities 2 core spray pipe is 6 inch, schedule 40 pipe. The piping system is modeled using pipe elements. The weight of metal, enclosed water and hydrodynamic mass are included in the eigenvalue analysis. The piping system is assumed to be fixed at the vessel nozzle and at the shroud penetration. The calculated first mode frequency is [[ ]]. This natural frequency will be compared to the calculated vortex shedding frequency to assess structural adequacy from a vibration viewpoint. The vortex shedding frequency calculation begins with a Reynolds number calculation as follows:

[[

$$Re = \frac{U \times D}{\nu}$$

$$f_s = \frac{S \times U}{D}$$

]]

The calculated lowest natural frequency is [[ ]]. Thus, the lowest natural frequency is more than 3 times the vortex shedding frequency. Therefore, the FIV stress due to vortex shedding is minimal.

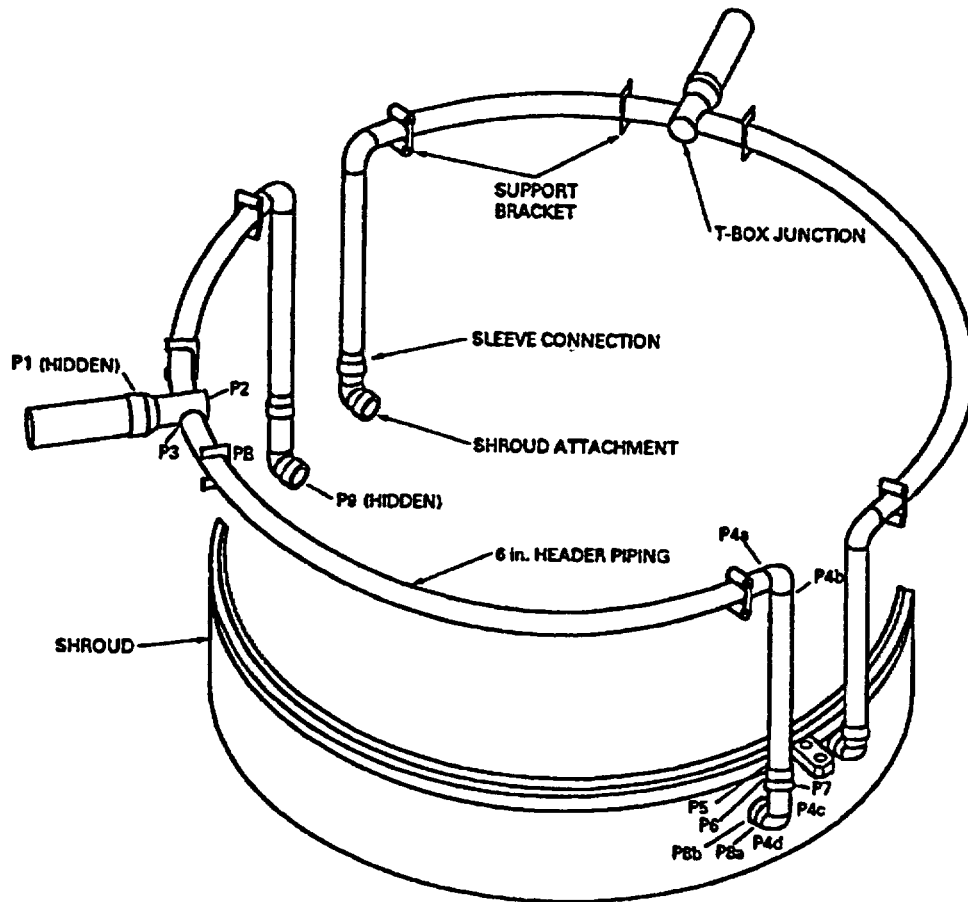


Figure 3.1-9: Typical BWR/3/4/5 Internal Core Spray Piping

### 3.1.1.2.12 Steam Line Nozzle

Natural frequencies of the steam outlet nozzle were calculated using a 3-D finite element model. The lowest natural frequency was [[ ]], and is higher than the FIV and acoustic loading frequencies from 0 to 230 Hz. Therefore, the steam line nozzle will be structurally adequate from a vibration viewpoint at EPU conditions.

### 3.1.1.2.13 Water Level Instrument Nozzle

The water level instrument nozzle is a partial penetration welded nozzle as shown in Figure 3.1-10. The diametric clearance between the nozzle body OD and the ID of the shell penetration is [[ ]]. For potential dynamic loadings this close fit will make the nozzle act as if it is supported through the full thickness, approximately

6-inches, of the RPV shell. Therefore, the water level instrument nozzle will have a very high natural frequency for any potential cyclic pressure loading from the vessel annulus.

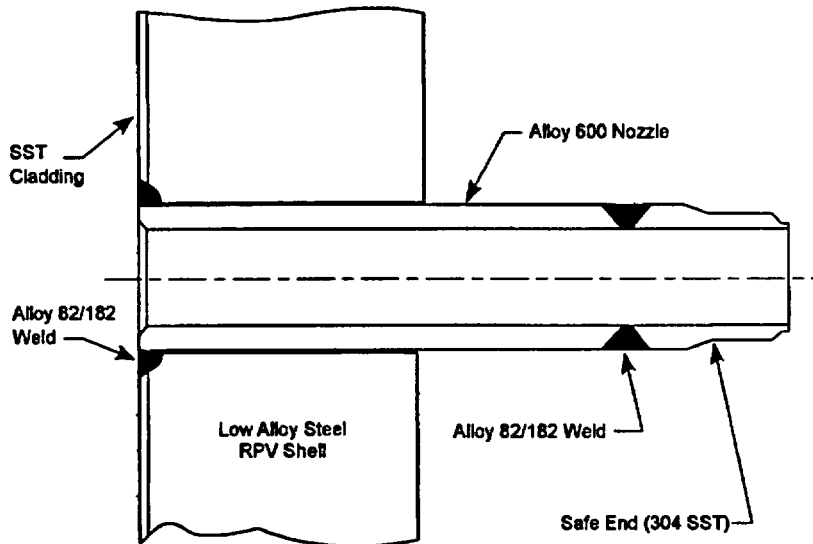


**Figure 3.1-10:Quad Cities 2 Water Level Instrument Nozzle**

The instrumentation nozzle connected to the steam leg is in the stagnant steam region, and is not affected by EPU.

The instrumentation nozzle connected to the reference leg of Narrow Range Reactor Water Level experiences similar changes as the lower part of the shroud guide rods or core spray pipe. See the sections above, describing the flow field.

The low flow velocities and the high natural frequencies of the water level nozzle assure that any FIV effects would be negligibly small.

#### **3.1.1.2.14 Dryer Drain Channels**

Cracks in steam dryer drain channels have been discovered in BWR plants under original licensed thermal power conditions. Drain channel cracking is discussed in detail in GE SIL No. 474. There is no steam flow inside the drain channels. The steam dryer drain channels may be susceptible to increased vibration during EPU conditions due to steam flow outside the drain channels. However, the drain channel cracking that has been observed so far has happened in drain channels, which were made of 1/8 inch thick plate with a 1/8" attachment fillet weld. The drain channels at Quad Cities 2 are inside the skirt and are much stronger design. They are made of 1/4 inch thick plate with a 1/4 inch fillet attachment weld. The Quad Cities 1/4 inch thick drain channels are formed arc

sections with a radius of 5 inches that results in a much stiffer member than the larger span 1/8 inch thick BWR/4/5/6 drain channel design. Hence, they are judged to be better able to withstand the FIV forces.

### **3.1.1.2.15 Dryer Support Bracket**

Dryer rocking is believed to be the cause of dryer support bracket cracking. The propensity for dryer rocking is increased in EPU conditions. To increase the reliability of the steam dryer support bracket, the potential for dryer rocking needs to be minimized. To this end, procedures for assuring firm contact between the dryer and its supports have been implemented at the QC 2 plant as part of the original dryer design. Quad Cities 2 dryer has leveling screws at each of the four support points, which were adjusted during the initial installation to assure firm and uniform contact between the dryer and its supports.

### **3.1.1.3 Evaluation of Mitigating Features**

The following mitigating features were evaluated for flow-induced vibration during operation in the extended power uprate region.

Shroud Repair: Shroud hold-down tie rods were installed at D2, D3, QC1 and QC2. Flow induced vibration evaluation of the tie rods was performed prior to the shroud repair work. The evaluation was based on the vortex shedding frequency and the natural frequency of the tie rods. Since the cross-flow velocity does not increase during power uprate, there is no concern for tie rod vibrations due to power uprate. The shroud repair at Dresden and Quad Cities included replacing a welded access plate with a bolted access plate that has an identified leakage. Replacing the welded access plate with the bolted access plate will have negligible effect on the FIV of this component.

Core Plate Wedges: Core plate wedges were installed to provide an alternate load path to the shroud and vessel. FIV of reactor internal components are not affected.

Jet Pump Riser Clamps: At QC1, cracks occurred in the riser pipes at jet pump riser brace yoke attachment of jet pumps #5/6 and #7/8. Mitigation clamps were installed at the crack locations. Flow induced vibration evaluation of the clamps were performed prior to the clamp installation. Since the jet pump flow velocity does not increase significantly during power uprate, there is no concern for vibrations due to power uprate

Feedwater sparger: Feedwater spargers for all four plants were changed to the triple thermal sleeve design. There has been no flow-induced vibration problem with the feedwater spargers with the triple thermal sleeve design, and this modification will have insignificant effects on the vibrations.

**D3 Core Spray Riser Clamp:** To mitigate cracking in the D3 vertical pipe near the lower elbows at azimuths 110° and 290°, deflection-limiting bolted clamps were installed at the sparger elbows, one on each loop. FIV of the core spray riser clamp is influenced by annulus flow. Since the annulus flow velocity is not increased during power uprate, there is no concern for core spray riser clamp vibrations due to power uprate

**Quad Cities Unit 1 Core Spray T-box Repair:** To mitigate cracking in the QC1 core spray T-box, a repair clamp was installed on the lateral pipe in the annulus between the shroud and vessel at azimuth 185°. FIV of the core spray piping and T-box is influenced by annulus flow. Since the annulus flow velocity is not significantly increased during power uprate, there is no concern for the core spray piping and T-box vibrations due to power uprate (see Section 3.1.1.2.11).

[[

]]

#### **3.1.1.4 Evaluation Conclusions**

Flow induced vibrations of reactor internals during EPU were evaluated to support operation up to 117.8% of the original licensed core thermal power level (2957 MWt). These evaluations concluded that the previous EPU component analyses remain valid and that Quad Cities 2 can operate at EPU conditions without exciting the key internal components above their established vibration criteria limits.

With the possible exception of D2 jet pump riser brace and some D/QC JPSL's, there is no resonance problem due to vane passing frequency excitation at EPU conditions.

The D2 riser brace leaves can be in resonance with the recirculation pump VPF at certain pump speeds. An inspection of the Dresden 2 jet pump riser brace leaves during the October, 2001 outage revealed a crack at the vessel end of the upper leaf of jet pump No. 9. The safety aspect of operating with a cracked riser brace leaf at D2 was assessed, and it was shown that there were no safety concerns and that D2 can continue to operate for another cycle. At the next outage, a repair clamp was installed at jet pump No. 9. Recirculation pump speed restrictions were also put in place as a pro-active measure to avoid damage to other jet pump riser braces. At the upcoming outage clamps will be installed on all jet pumps as a pro-active measure.

JPSL analysis [Ref. 3.1-8] shows that some lines at D2, D3, QC1 and QC2 units have the potential for resonance in the current operating speed range. Operating at higher pump speed will move the VPF away from the natural frequencies of some JPSL's and closer into the second mode natural frequencies of other JPSL's. The results indicate that only JPSL's 1/11, 2/12, 3/13, and 10/20 for all four plants have the potential for resonance with the VPF of the recirculation pumps. JPSL clamps have already been installed at Quad Cities 2 to mitigate this problem.

JPSL cracking does have economic impact, but does not directly affect safety. Failure of a sensing line can be detected and thus no specific consideration of the sensing line is necessary from a plant safety viewpoint.

All the components in the main steam and feedwater flow paths were evaluated and found to be acceptable for EPU operation.

### **3.1.2 Reactor Internal Pressure Differences**

The CFD analysis in Section 2.5 identified that the static pressure load distribution across the dryer hood varied in magnitude over the surface area, with some regions showing a higher load during steady-state operation than what is calculated in the normal reactor internal pressure difference (RIPD) analysis. This assessment reviewed the RIPD load definitions for the reactor internals for similar situations where the RIPD load definitions at EPU conditions could potentially be higher based on a more detailed consideration of the flow field.

In the typical structural analysis, the RIPDs are calculated across the following major components:

- Core Plate and Guide Tube
- Shroud Support Ring and Lower Shroud
- Upper Shroud
- Shroud Head
- Top Guide
- Steam Dryer
- Fuel Channel Wall

The increased RIPD loading on the steam dryer is due to the high velocity of the steam flow across the hoods and accelerating into the steam piping. The high velocity region is on the low pressure side of the dryer hood. Since the velocity effect reduces the pressure on the hood, this effectively increases the pressure difference across the hood. This velocity term has not been included in the RIPD analyses.

The velocity term will increase the previously calculated component RIPD values if the high velocity field is on the low pressure side of the component boundary. For components in the core flow path inside the core shroud, the high velocity field is on the high pressure side of the component boundary. Accounting for the velocity term will not increase the RIPD across the component boundary. For the components listed above, the core shroud is the only component where the high velocity field is on the low pressure side of the boundary (in the downcomer region). Using the flow velocity in the downcomer region of [[                    ]]

would increase the pressure difference across the core shroud by [[ ]]to a value of [[ ]]at EPU conditions. This increased value remains within the margin available in the design loads used for the original shroud repair stress analysis. Since adequate margin exists for the increased loading, the shroud remains qualified for EPU conditions.

## **3.2 Components in Steam Path External to the Reactor**

This section evaluates the Main Steam (MS) piping and associated components from the vessel to the turbine including attached small-bore lines for potential vulnerabilities to the vibrations that affected the dryer. The main steamline piping is addressed in Section 3.2.1. Main steamline components such as MSIVs and SRVs are addressed in Section 3.2.2.

### **3.2.1 Steamline Piping**

A vibration monitoring plan for the main steamline piping was developed and implemented as part of the test plan for EPU implementation. The vibration monitoring plan and evaluation results are described below.

#### **3.2.1.1 Background**

Because of EPU, MS system steam flows increased. This flow increase was expected to result in increased levels of vibration to connected components. Similar to start up testing a vibration monitoring plan was developed and implemented to ensure that vibration levels would not cause piping degradation or failure. The acceptance criteria were based on displacement limits. These limits were derived from the stress criteria of the ASME OM report (Section 3.2.1.2 (b) of Ref. 3.2-1). The method for deriving the displacement limits is described in Ref. 3.2-2. The piping analysis was utilized to choose accelerometer locations that were representative of the highest dynamic displacements as well as locations that were accessible for the installation of the accelerometers utilized for data collection.

#### **3.2.1.2 Testing Methodology/Process**

The power ascension test program, implemented by procedure TIC-321 for Quad Cities Unit 2, included the vibration monitoring locations and acceptance criteria. The plan consisted of vibration readings taken at 26 locations on Main Steam, Feedwater and EHC piping. Data was collected at approximately 40%, 60%, 75% and 85% to establish baseline information as 85% power represents pre-EPU 100% power of 2511 MWth.

During EPU power ascension, vibration data sets were gathered at every 3% power increase until testing was completed at approximately 97% thermal power, 100% rated

electric of 912 MWe. After each data set was obtained, the values were then compared to the acceptance criteria to determine if piping would remain at acceptable levels, prior to allowing further power ascension. Acceptance criteria were utilized based on infinite service life, at any frequency.

### **3.2.1.3 Results**

At each power level of data collection, the observed values were found acceptable and met the acceptance criteria for infinite service life during plant operation. For any discrepancies that were found during any step, including such items as failed accelerometers; the test discrepancy was evaluated by engineering and approved by the test director and Operations Senior Reactor Operator, prior to authorizing continuation of power ascension. Discrepancies consisted of loss of vibration measurements in several locations due to accelerometer failures and attachment problems. There were no recorded values outside of the acceptance criteria for unlimited plant operation.

### **3.2.1.4 Additional Evaluations**

Post EPU power ascension, in early April 2002, one MS low point drain line failed due to vibration-induced fatigue. This failure was evaluated under CR 102091 with a root cause and piping vibration analysis studies. The root cause was determined to be a failure of the vibration-monitoring program due to personnel errors. This error occurred by insensitivity to an incipient resonance condition that was not appropriately understood during initial power ascension. Details of this event and causes can be found under AT 102091-08 (Reference 3.2-4).

The results of the additional studies are detailed in References 3.2-1 through 3.2-4. The studies included assessment of other lines for potential small bore problems and evaluation of any potential high frequency vibration impact to piping. No further potential problems were found. Corrective actions from this event were applied to the other two units, which resulted in no additional problems due to piping vibration issues.

## **3.2.2 Steamline Components**

The MSIVs, PORVs, thermowells, and HPCI and RCIC isolation valves were evaluated for acoustic vibrations at EPU conditions in Reference 3.2-5. The following sections review the evaluations for these components considering the lessons learned from this failure evaluation.

### 3.2.2.1 MSIVs

Reference 3.2-5 identified that the MSIV main disk was free to move and may be susceptible to the pressure pulsations due to flow-induced vibrations and acoustic vibrations. The disk movement may result in excessive wear in the valve guide that could prevent the valve from closing on demand. The disk movement can also lead to stem failure. SIL 568 (Reference 3.2-8) describes the effect of flow-induced vibration on the disk and valve guide and provides recommendations for a partial stroke test to confirm MSIV operability. The full-stroke test recommended in Reference 3.2-5 is not required provided the partial stroke test valve travel is greater than the free disk travel. SIL 473 (Reference 3.2-9) describes the conditions that may lead to stem failure and provides recommendations for reducing or eliminating the fatigue loading on the stem.

SIL 568: Recommendations from this SIL were focused on providing periodic testing that provides assurance that the main disk is free to move and will therefore close upon demand. This can be accomplished through the quarterly MSIV closure testing, performed under QCOS 0250-01, provided the percentage of closure represents sufficient travel to ensure main disk movement. For the Quad Cities valves, manufactured by Crane, this is accomplished by movements greater than 1/2". Procedure QCEM 0600-07 is performed every refuel outage to check both as found and as left limit switch settings that establish the amount of movement when performing the quarterly stroke test. The results of the most recent performance of this activity have been reviewed for both Quad Cities units. This review confirms that there is sufficient movement during the 10% stroke test to demonstrate that the main disk is free to move, i.e. no groove has been formed to restrict movement and the valve will close upon demand. No further actions are required to ensure valve acceptability. The full-stroke test recommended in Reference 3.2-5 is not required because the partial stroke test valve travel is greater than the free disk travel.

SIL 473: this SIL was dispositioned in 1988 when it was issued. The disposition remains valid in that the type of valve discussed in the SIL is a different manufacture than the valves utilized at Quad Cities. Specific OPEX searches were conducted at that time to ensure that the Crane 20" valves used by Quad Cities were not subject to the same failure mode. No evidence was found of similar problems with the Crane valves.

As part of the environmental qualification for the MSIVs, the MSIV actuators were seismically tested (Reference 3.2-6). The protocol used to vibration age the specimen prior to testing subjected the actuator to an acceleration of [[ ]] over a frequency range of 5 Hz to 200 Hz. This aging protocol bounds the steamline vibration observed during EPU operation. Following the testing for upset and faulted events, the test specimen was examined for signs of damage. There was no visible evidence of physical damage to the test specimen resulting from the seismic tests. Therefore, the MSIVs continue to be acceptable for plant operation at EPU conditions.

### **3.2.2.2 PORVs**

Reference 3.2-5 also identified that flow induced vibration can cause the pilot valve for a PORV to leak. Main Steam line vibrations/harmonics can be transmitted down the pipe to the PORVs. Based on the frequency of this acoustic vibration, it may induce a sympathetic vibration in the pilot valve and cause the pilot valve seating surface to wear. Leakage past the pilot valve seat could then increase until it would vent the over-pressure on the main disc and cause the PORV to self-actuate open.

On March 14, 2002 Main Steam line "B" vibration levels were measured at EPU conditions. These measurements were taken approximately 4 feet downstream of the 3B PORV at thermal power level of 2825 MWth. The only significant vibrations occurred at approximately 160 Hz and 321 Hz. These measured frequencies do not coincide with the valve natural frequencies as determined in EASI 2073.0000.00, which assessed the Target Rock PORV main disc and spring's susceptibility to vibration. This evaluation determined the main disc and spring natural frequency to be less than 3 Hz and the main body and actuator natural frequency to be approximately 103 Hz. In addition, the natural frequency of the pilot valve assembly and spring was calculated to be 209 Hz. Based on the significant differences in the natural frequencies of the valve body, main disc and spring, and pilot valve assembly and spring as compared to the measured Main Steam line vibrations, it can be concluded that the operating vibrations are not likely to have caused the 3B PORV failure. Based on the above, the recommendations and conclusions for the relief valves in Reference 3.2-5 remain valid.

### **3.2.2.3 Thermowells**

The thermowells and sample probes in the steamlines were extensively analyzed in Reference 3.2-7 for susceptibility to flow induced vibration at EPU conditions. These analyses remain valid in light of the dynamic loads defined for the dryer in Section 2.5.3. In addition, the acoustic loads from the steamlines (Section 2.5.3.4) have long wavelengths relative to the size of the thermowells (7 feet and longer compared to the probe diameters of less than two inches); therefore, the pressure amplitude experienced by the probe is only a fraction of the wave amplitude. Therefore, the thermowells and the sample probes in the steamlines continue to be acceptable for plant operation at EPU conditions.

### **3.2.2.4 HPCI/RCIC Isolation Valves**

Reference 3.2-5 determined that there was minimal concern for FIV or acoustic impacts on the HPCI and RCIC isolation valves because of the location of the valves out of the main steam flow path and the reduction in pipe cross sectional area. The basis for this assessment remains valid in light of the dynamic loads defined in Section 5.2.3. Therefore, the HPCI and RCIC isolation valves continue to be acceptable for plant operation at EPU conditions.

### **3.2.3 Conclusions**

The steamline piping and components in the steam flow path were evaluated in light of root cause of the dryer failure. Since the cause of the dryer failure was attributed to high cycle fatigue, detailed evaluations were performed for the main steam piping and components to determine their susceptibility to flow induced vibrations at EPU conditions. These evaluations concluded that the steamline components are acceptable for plant operation at EPU conditions.

### **3.3 Extent of Condition Conclusions**

The reactor internal components and components in the steam flow path were evaluated in light of the dryer failures. Since the cause of the dryer failures was attributed to high cycle fatigue, detailed evaluations were performed for these components to determine their susceptibility to flow induced vibrations at EPU conditions. These evaluations concluded that the previous EPU component analyses remain valid and that Quad Cities 2 can operate at EPU conditions without exciting the key internal components above their established vibration criteria limits.

## 4. Dryer Repair Assessment

As part of the root cause evaluation, a detailed evaluation was performed in order to more thoroughly understand the pressure loads acting on the dryer. Since the dryer repair design preceded this evaluation, the repair design was assessed against the static and dynamic loads developed in this evaluation in order to confirm the adequacy of the repair. The repairs installed on the outer hoods at the 90-degree and 270-degree sides consist of:

1. Gussets connecting the hood front plates to the cover plates.
2. 1-inch replacement plates for the top portions of the hood front plates and the front portions of the hood top plates.
3. Addition of stiffeners to reinforce the horizontal welds between the hood front plates and top plates.
4. Addition of angle irons to reinforce the vertical welds at the corners of the hood front plates.
5. Addition of angle irons between the 45-degree vertical plates and top plates.

In addition, angle irons were added to reinforce the vertical welds at the back corners of the 45-degree vertical plates on the hood at the 90-degree side.

Analyses of the repaired configuration showed that all stresses after repair were within allowable limits.

1. The repairs increase the outer hood plate frequencies from [[ ]] removing the susceptibility to flow turbulence loads which were determined to be the root cause of the hood failure.
2. Since the lowest natural frequency of the repaired hood is outside the low frequency excitation range (0 – 50 Hz.), the dynamic response would be insignificant.
3. The repair analyses with and without the vertical and diagonal braces showed that the maximum stresses were essentially the same.
4. A comparison of the results of the finite element analysis plate stresses due to a 1 psi static load shows that after the repair, the peak normal operation stress in the outer hood top plates decreased to [[ ]], or 20% of the peak stress of [[ ]] before repair. Peak normal operation stress in the front plates decreased to [[ ]], or 29% of the peak stress of [[ ]] before repair. The actual stress reduction would be considerably larger since the dynamic response at [[ ]] to the 0-50 Hz load would be much smaller than the static load response.

5. A comparison of the results of the finite element analysis plate stresses shows that after the repair, the peak PORV event stress in the outer hood top plates decreased to [[                    ]], or 22% of the peak stress of [[                    ]]before repair. Peak PORV event stress in the front plates decreased to [[                    ]], or 38% of the peak stress of [[                    ]]before repair.

#### **4.1 Hood Frequencies**

The dryer analysis model was updated to add the repair components and remove the diagonal braces and appropriate vertical braces. Frequency calculations were limited to the outer hood region extracted from the full dryer model. The outer hood model and the mode shapes calculated for the outer hood using the model are shown in Figure 4.1-1. The hood fundamental frequency of [[                    ]]places the repaired hood out of the flow turbulence excitation range.

[[

**Figure 4.1-1: Repaired Hood: Frequencies**

]]

## 4.2 Hood Stresses

Stress analyses were performed for the normal operation flow turbulence loads and combined normal operation pressures and PORV loads based on simultaneous PORV events on all steam lines. The loads were applied as static loads with the results used with a dynamic amplification factor when necessary. Stress distributions for the normal operation pressure load are shown in Figures 4.2-1 and 4.2-2. Stress distributions for the normal operation pressure and PORV loads are shown in Figures 4.2-3 and 4.2-4.

Figure 4.2-5 compares the hood stresses before the hood failure with the stresses in the repair hood assuming the normal pressure load distributions based on the pre-failure analyses. Actual stress reduction would be larger than indicated in the figure because the frequency shift out of the 0-50 Hz range would decrease the dynamic load amplification in the repaired hood design.

[[

]]

**Figure 4.2-1: Repaired Hood Plate Stresses: Normal Operation Pressure Load**

[[

]]

**Figure 4.2-2: Repaired Component Stresses: Normal Operation Pressure Load**

[[

]]

**Figure 4.2-3: Repaired Hood Plate Stresses: PORV and Normal Operation Pressure Loads**

[[

**Figure 4.2-4: Repaired Component Stresses: PORV and Normal Operation Pressure Loads**

]]

[[

**Figure 4.2-5: Stress Reduction With Repair: Normal Operation Pressure Load** ]]

### 4.3 Loss of Braces

Both diagonal braces and one vertical brace were lost or removed during repair for the 90-degree side and the 270-side hoods of the dryer. The hood stresses without these braces are acceptable as discussed in Section 4.2.

The vertical braces also support the dryer banks against gravity and pressure loads. The loads act on the drain trough plates at the same locations as the braces. Conservative analyses were performed to determine the effect of loss of braces on these components to show acceptability of operation without replacing the lost braces.

**Deadweight:** Analyses were performed for a 1200-lb unit load 1) with intact vertical braces and assuming that both diagonal braces have broken off, and 2) assuming the two diagonal and all the four vertical braces have broken off. The analysis results in Figure 4.3-1 show that the peak stresses in the trough would increase to [[ ]] for the 1200 lb applied load. For the dryer bank weight of 3000 lb, the peak stress value will be [[ ]] The [[ ]] stress without the braces is well within the stress limits for static loads.

**Pressure:** Analyses were performed for a 1200-lb unit load 1) with intact vertical braces and assuming that both diagonal braces have broken off, and 2) assuming the two diagonal and all the four vertical braces have broken off. The pressure was assumed to apply on the exit side plate of the trough and the 1½-inch dryer retaining plate at the top end. The analysis results in Figure 4.3-2 show that the peak stresses in the trough plate will actually decrease slightly with the removal of the trough. Therefore, operation without the braces is acceptable.

[[

**Figure 4.3-1: Effect of Vertical Braces on the Dryer Vane Support Structure:  
Deadweight Load**

]]

[[

**Figure 4.3-2: Effect of Vertical Braces on the Dryer Vane Support Structure:  
Pressure Load**

]]

## **5. Assessment for Other Units**

The root cause evaluation in Section 2 identified routine low frequency high cycle fatigue as the primary cause of the dryer failure at Quad Cities 2 that occurred in May 2003. A review was performed to determine if there were any identifiable differences between Quad Cities 2 and the other three units that may account for the dryer failures observed in Quad Cities 2. This section also identifies recommended actions for monitoring, inspection, and repair for all four units.

### **5.1 Significant Differences Between Units**

The root cause evaluation in Section 2 identified that a contributing factor to the high cycle fatigue is the steamline geometry. This geometry is common to all four units.

A review was performed to determine any identifiable differences between Quad Cities 2 and the other three units that may account for the dryer failures observed in Quad Cities 2. Of particular interest are differences between Quad Cities 2 and Dresden 2 since Quad Cities 2 experienced failures shortly after EPU operation while Dresden 2 has operated for almost a complete cycle with no indication of any problem. This review focused on the geometry and structure of the vessel, steamlines, and internals, the plant operating conditions, and significant events experienced by the units.

All four plants have basically the same structure and geometry. The significant geometry differences identified were the lower cover plate on the steam dryer, the relief valve inlet geometry, the steamline flow limiter, and the main steamline piping length.

- On Dresden 3 and Quad Cities 1, the original lower cover plate was replaced with a 1/2" thick plate before EPU operation. This may have reduced the stresses on the dryers for those units.
- Quad Cities 2 has one relief valve inlet that has an acoustic resonance near the natural frequency of the lower cover plate, which may have lead to the failure observed in 2002. The acoustic resonances for the relief valve inlets at the other units do not coincide with the natural frequencies of the dryer components.
- The main steamline piping between the equalizing header and the turbine is significantly longer at the Dresden units. This may alter the pressure amplitudes generated by the steamlines.
- The steamline flow limiter at Dresden 2 has a smaller throat area than the limiters at the other units. The smaller area may tend to inhibit the pressure load transmission through the steamline piping to the hood in Dresden 2. The Dresden 2 dryer may therefore be experiencing a lower loading.

In addition to the known geometry differences, minor variations in dryer materials and construction can result in differences in the natural frequencies of the dryer components. The main steamlines and equalizing headers also may have different as-built dimensions, which could result in differences in pressure loading on the dryer. These differences may be enough to account for variations in the stresses experienced by the dryers.

All four plants operate at the same EPU conditions. The main steamline high frequency vibration response at Quad Cities 2 shows a significant increase at EPU conditions. This vibration appears to be related to the relief valve inlet geometry.

The Dresden 2 dryer has operated at EPU conditions with the original 1/4" cover plate for almost a full cycle while the Quad Cities 2 cover plate failed after only a few months. Based on the root causes identified for the 2002 and 2003 dryer failures, the most significant differences between the units are the relief valve inlet geometry at Quad Cities 2 and the smaller flow limiter area at Dresden 2. These differences may account for the successful dryer operation at Dresden 2.

## **5.2 Recommended Actions**

Based on the root cause investigation of the Quad Cities Unit 2 dryer, the following long-term actions are recommended for monitoring, inspection, and repair of the Dresden and Quad Cities steam dryers.

### **5.2.1 Monitoring**

The following parameters should be monitored in order to detect signs of structural failure in the steam dryer. Appropriate action levels should be defined for the monitored parameters.

#### **Main Steam Line Moisture Content**

- Na-24 Samples should be obtained at a frequency of at least once a week and following rod pattern exchanges. Based on this information, a baseline and expected range of normal variation of MSL moisture content for the plant should be established. Relaxation in the sampling frequency can be considered after a baseline has been established.
- Na-24 samples also should be taken following any transient that may induce pressure loads on the dryer.
  - These samples should be taken as soon as possible after the event allowing time for conditions to stabilize.
  - Daily samples should be taken until it can be established that the dryer has sustained no damage (as indicated by an unexplained increase in moisture

content). Once it has been established that the dryer has sustained no damage, routine sampling can resume.

### Other Process Parameters

If an unexpected increase in moisture content occurs, reactor water level, reactor pressure, and individual steamline flows should be evaluated for variation from an established baseline. Establish baselines and expected range of variation for each parameter monitored. Record indications on plant process computer to aid in analyzing data.

### Action Levels

Action thresholds should be established for moisture content deviations from the baseline which specify actions appropriate to the indication such as:

- Detailed engineering evaluation of indications
- Power reduction
- Plant shutdown

The appropriate action should consider the degree of variation in moisture content, potential impact on steam line component contamination, indication of lost parts, and previous operating experience.

## **5.2.2 Inspections**

At each refueling outage or a forced outage due to unexplained high moisture content, perform a complete visual inspection of all external and internal dryer surfaces for indication of cracking.

- Inspect the underside of all dryer hoods and cover plates.
- Remove trapped bubbles to ensure complete coverage.
- Thoroughly inspect areas of high stress concentration (e.g. internal brackets on outer dryer hoods)

## **5.2.3 Repairs**

Since a growth rate for the observed cracks cannot be established because it can be affected by transient events, fatigue damaged components must be repaired. Therefore, if the inspection identifies a dryer component that shows fatigue cracking or damage, the damaged component must be repaired prior to restarting the unit.

Based on the root cause investigation for Quad Cities Unit 2, the following preemptive repairs are recommended for Dresden 2/3 and Quad Cities 1:

**Dresden 2**

1. Perform the complete visual inspection before performing any modifications or repairs. This will allow in situ evidence to be documented and used to support the Quad Cities 2 root cause investigation and dryer repair basis.
2. Stiffen the lower cover plates on the outer hoods. Replace the 1/4" plate with 1/2" plate. Add gussets between outer hood vertical plate and lower cover plate.
3. Reinforce horizontal and vertical plates on outer hood

**Dresden 3, Quad Cities 1**

1. Add gussets between outer hood vertical plate and lower cover plate.
2. Reinforce horizontal and vertical plates on outer hoods.

## 6. Conclusions

The cause of the dryer failure is postulated to be high cycle fatigue resulting from low frequency pressure loading on the outer hoods during normal operation. The pressure loading is thought to be amplified by the geometric configuration of the main steamlines. The cracks in the hoods and braces are most likely to have been initiated during steady-state EPU power operation. The cracks continued to grow until the transient pressure loads from the stuck open relief valve and subsequent manual valve openings opened the cracks through-wall, leading to the increased steam moisture content. The previous cover plate failure in 2002 subjected the dryer structure on the 90° side to significant additional loading.

The reactor internal components and components in the steam flow path were also evaluated in light of the dryer failures. Since the cause of the dryer failures was attributed to high cycle fatigue, detailed evaluations were performed for these components to determine their susceptibility to flow induced vibrations at EPU conditions. These evaluations concluded that the previous EPU component analyses remain valid and that Quad Cities 2 can operate at EPU conditions without exciting the key internal components above their established vibration criteria limits.

The adequacy of the dryer hood repair design was evaluated for the more detailed static and dynamic loads developed during this root cause evaluation. Based on the results of this evaluation, the dryer hood repairs were determined to be adequate for EPU operation.

## 7. References

- 2.4-1. Bathias and Pelloux: Metallurgical Transactions, 1972.
- 2.5-1. GE-NE-A22-00103-05-01, “Dresden and Quad Cities Extended Power Uprate, Task T0303: RPV Internals Structural Integrity Evaluation,” October 2000.
- 2.5-2. US Plant Steam Dryer Vibration Steady State and Transient Response, MDE #199-0985, October 1985.
- 2.5-3. Stress Analyses for the Quad Cities Unit 2 Steam Dryer Repair, GENE-0000-0018-0985-01, June 2003.
- 3.1-1. GE Nuclear Energy, “Generic Guidelines for General Electric Boiling Water Reactor Extended Power Uprate,” Licensing Topical Reports NEDC-32424P-A, Class III (Proprietary), February 1999; and NEDO-32424, Class I (Non-proprietary), April 1995.
- 3.1-2. GE Nuclear Energy, “Generic Evaluations of General Electric Boiling Water Reactor Extended Power Uprate,” Licensing Topical Reports NEDC-32523P-A, Class III (Proprietary), February 2000; NEDC-32523P-A, Supp 1, Supplement 1 Volume I, February 1999; and Supplement 1 Volume II, April 1999.
- 3.1-3. Dresden-3 Vibration Measurements, 384HA148, May 15, 1974 Class-II
- 3.1-4. Dresden-2 Hot Vibration Tests, 383HA537, March 17, 1971.
- 3.1-5. Quad Cities Station Units 1 and 2, Amendment 19 to Final Safety Analysis Report, Docket Nos. 50-254 & 50-265, March 1, 1971
- 3.1-6. ASME Section III, Division 1, Appendix I, Figure I-9.2.2, Design Fatigue Curve for Austenitic Steels.
- 3.1-7. GE Report, NEDO-20554, “feedwater Sparger Cold Flow Vibration Test,” by M. R. Torres, Class I, June 1974 (See § 4.7.2 and Figures 4-8 and 4-10)
- 3.1-8. GE Report, NEDE-21821-02, “Boiling Water Reactor feedwater Nozzle/Sparger Final Report,” by H. Watanabe, Class III, August 1979 (See § 4.1)  
Exelon (QC and D) EPU Task Reports
- 3.1-10. NRC Report, NUREG-0619, “BWR feedwater and Control Drive Return Line Nozzle cracking,” Office of Nuclear Reactor Regulation, NRC, November 1980 (See Appendix C, § 4.1)
- 3.1-11. “Formulas for Natural Frequency and Mode Shape”, R. D. Blevins, Van Nostrand Reinhold Company, 1979.
- 3.1-12. “Hydrodynamic Masses and Hydrodynamic Moments of Inertia”, Kurt Wendel, Hamburg, Germany, Translation 260, July 1956.

- 3.1-13 ASME Pressure Vessel Code, 1998, Section III, Division 1, Appendices, N-130
- 3.1-14 "Vibration of Rods Induced by Water in Parallel Flow", D. Burgreen, J.J. Byrnes, and D.M. Benforado, Transactions of the ASME, July, 1995
- 3.1-15 GE Document "Fatigue Design Criteria" 409HA105, Rev. 1, November 1974
- 3.1-16 SAP4G07 User's Manual, GE NEDO-10909, Revision 7, December 1979
- 3.1-17 Letter K. S. Ananth to Martin Torres, "FIV Testing – BWR/6 Steam Separators" September 9, 1975.
- 3.1-18 H. L. Hwang, "Dresden 2- Evaluation of Recirculation Pump Speed Effect on Jet Pump Riser Brace and Sensing Line" GE-NE-189-24-0591, May, 1991.
- 3.2-1 ASME OM-S/G-1997. Standards and Guides for Operation and Maintenance of Nuclear Power Plants.
- 3.2-2 Steady State Vibration Acceptance Criteria for Quad Cities 2, issued June 15, 2001, revised February 15, 2002, by Stone & Webster.
- 3.2-3 TIC-321, Temporary procedure to provide instruction in carrying out the start-up test program for extended power uprate (EPU), dated 3-1-02. "Quad Cities Unit 2 EPU Power Ascension Test".
- 3.2-4 Root Cause Report for MS piping low point drain line failure, April 2, 2002, Quad Cities Unit 2, AT 102091-08.
- 3.2-5 GENE 0000-0008-1763-01, "Dresden Units 2 and 3, Quad Cities Units 1 and 2, Assessment of Acoustic Vibrations on MSL Components," October 2002.
- 3.2-6 NEDC-31886P, "Quad Cities Nuclear Power Station Units 1 & 2, Environmental Qualification Report," December 1990.
- 3.2-7 GE-NE-A22-00103-30-02, "Dresden and Quad Cities Extended Power Uprate, Task T0316: NSSS Piping Thermowell and Sample Probe Flow Induced Vibration Evaluation," September 2000.
- 3.2-8 SIL 473, "Atwood and Morrill MSIV Stem Failures," October 11, 1988.
- 3.2-9 SIL 568, "MSIV Guide Rib Wear," August 10, 1993.